International Journal of Material Forming (2025) 18:72
https://doi.org/10.1007/s12289-025-01928-1

RESEARCH

ESAFORM benchmark 2024: study on the geometric accuracy of a complex shape with single point incremental forming

Marthe Vanhulst[1] · Youngrok Lee[2] · Dennis Steinfels[3] · Thomas Bremen[3] · Konrad Perzyński[4] · Hans Vanhove[1] · Giuseppina Ambrogio[5] · Radu-Eugen Breaz[6] · Gianluca Buffa[7] · Romina Conte[5] · Liugi De Napoli[5] · Livan Fratini[7] · Xiao Da Terrence Fu[9] · Francesco Gagliardi[5] · Margarida Gralha[10] · Putong Kang[8] · Łukasz Kuczek[11] · A. Senthil Kumar[9] · Andreas Kunke[12] · André Leonhardt[12] · Yanle Li[13] · Zhuoer Li[2] · Roberto Licari[7] · Hui Long[14] · Darren Wei Wen Low[9] · Sever-Gabriel Racz[6] · Peter Scholz[15] · M. Beatriz Silva[10] · Shaoqi Song[13] · Dieter Weise[15] · Krzysztof Żaba[11] · Hui Zhu[14] · David Bailly[3] · Mihaela Banu[2] · Lukasz Madej[4] · Joost R. Duflou[1]

Received: 28 March 2025 / Accepted: 3 July 2025 / Published online: 11 August 2025

Abstract
The benchmark 2024 project on Incremental Sheet Forming (ISF), involving 15 research institutes in 13 experimental contributions, provided a unique opportunity to compare experimental outputs from various setups and forming strategies in ISF. This collaboration led to the development of uniform data exchange formats, measurement guidelines, and standardized nomenclature, fostering efficient future collaborations. The project addressed challenges in geometric accuracy when forming a relatively large part (400×400 mm) using Single Point Incremental Forming (SPIF) and focused on multiple common pitfalls in ISF, in particular the tent effect and pillow effect. Additionally, some experiments have been conducted using Two Point and Double Sided Incremental Forming (TPIF and DSIF). By combining the knowledge and experience of all participating institutes, this project aimed to provide insights into effective parameter choice and toolpath strategies, and shows the importance of multi-stage processes to increase the geometric accuracy. Despite the theoretical simplicity of SPIF setups, such multi-stage toolpath strategies directed toward improved geometric accuracy also add some new challenges. The study highlighted the need for multi-stage strategies that focus on local effects, as well as geometric compensation techniques to enhance ISF's industrial applicability. Alternative process variants like TPIF and DSIF, showed promising results, but they also had limitations and presented challenges, emphasizing the importance of predictive simulation tools to further increase geometric accuracy. The scalability of ISF experiments remains a significant challenge, necessitating further research into scale laws for process optimization.

Keywords Single point incremental forming · Geometric accuracy · Benchmark

Introduction

Incremental sheet forming (ISF)

Incremental sheet forming (ISF) has been the subject of rather intensive research for more than two decades, driven by the seemingly low complexity of this flexible forming technology [1]. In its most primitive form of implementation, known as Single Point Incremental Forming (SPIF), the limited hardware requirements can easily create the impression that the process can be accommodated without substantial investments while entirely avoiding workpiece-specific tooling costs. Over the past two decades, moreover, many of ISF's initial limitations have been rectified: contributions like multi-stage forming allowed to extend the process window, enabling the capacity to create steep forming angles, while heat-supported process variants facilitated forming of materials with limited strainability at room temperature [2]. Remaining process limitations in terms of geometric shape complexity and achievable workpiece accuracy, however, have tempered the enthusiasm for exploring the limited complexity of the applied hardware configurations. In response, many complex variants that facilitate counter pressure, either by using well-designed static support structures (Two Point Incremental Forming, TPIF) or additional programmable tool capabilities (Double Sided Incremental

Extended author information available on the last page of the article

Forming, DSIF), have been conceived and demonstrated. The original attractiveness of the low cost, low complexity of the pure SPIF implementation is, however, largely lost in these developments, and the question is often raised whether a well-optimized use of smart SPIF toolpaths could obviate the need for new and sophisticated hardware configurations. The attractiveness of low-cost hardware requirements and the absence of workpiece-specific tooling are obviously major advantages of SPIF that should be considered in a possible trade-off with the superior process control capabilities of the TPIF and DSIF variants. The complexity of the process planning efforts required to optimize the output of SPIF in terms of shape complexity and workpiece accuracy is an important consideration in such a trade-off exercise.

This study aims to conduct an in-depth exploration of the capabilities and limitations of SPIF as a versatile forming process according to the present state of knowledge. For this purpose, a challenging workpiece geometry has been identified that is impossible to produce in a straightforward way with conventional toolpath strategies. A broad international team of researchers with expertise in ISF has been invited for this in-depth benchmark exercise. They have contributed by exploring the limited degrees of freedom of SPIF through well-optimized process planning strategies and imagining different approaches. To ensure a systematic comparison of the effectiveness of the respectively proposed approaches, the same grade, thickness, and sizes of the sheet material, as well as well-documented and reproducible toolpath specifications and standardized measuring procedures, have been applied. This effort has resulted in a valuable repository of process data and derived measurement results that are reviewed in this benchmark report. The major aim of this joint effort by 15 participating institutes contributing to 13 experimental inputs, see Table 1, is to assess the state-of-the-art in mastering the versatility of SPIF as a seemingly simple ISF process variant. In addition to reporting the results obtained from a wide variety of processing strategies, the authors also have the ambition to derive conclusions and recommendations with respect to advisable process planning strategies and toolpaths for a broad spectrum of possible geometries to be produced with this flexible forming process.

Goal of the benchmark study

ISF knowledge building

The flexibility of ISF is one of its key advantages. However, this advantage is unfortunately challenged by its inherent complexity. The process has a multitude of degrees of freedom in process control and encompasses a vast range of potential component geometries. However, the accumulated process understanding and empirical knowledge are still insufficient, especially for geometrically complex components. Preventing undesired geometric deviations requires considerable process planning and often numerous trial-and-error tests. This is particularly detrimental in low-volume production, where the planning and testing costs can only be allocated to a small number of components. If a fast and economical pathway is to be realized, from a designed component to an as-specified sheet-metal part, it will emerge by systematically gathering knowledge and experience about the ISF process, especially regarding the large number of possible component geometries as well as possible process setups and parameter settings. Because individual research teams struggle to build up this broad knowledge and experience on their own, a collaborative learning approach was chosen. The idea was to use an online database for an international knowledge exchange between the world's leading research teams and ISF users.

Table 1 Overview of the participating institutes and their acronyms used in this work

	Participating institutes	Role	Acronym
1	AGH University of Krakow	Organizing committee	AGH Krakow
2	Fraunhofer IWU and Chemnitz University of Technology	Participant	Fraunhofer IWU
3	KU Leuven	Organizing committee	KUL
4	Lucian Blaga University of Sibiu	Participant	LBUS
5	National University of Singapore	Participant	NUS
6	Northwestern University	Participant	Northwestern
7	RWTH Aachen	Organizing committee	RWTH
8	Shandong University	Participant	SDU
9	University of Calabria	Participant	UNICAL
10	University of Lisbon	Participant	ULisboa
11	University of Michigan	Organizing committee	UMICH
12	University of Palermo	Participant	UNIPA
13	University of Sheffield	Participant	TUOS

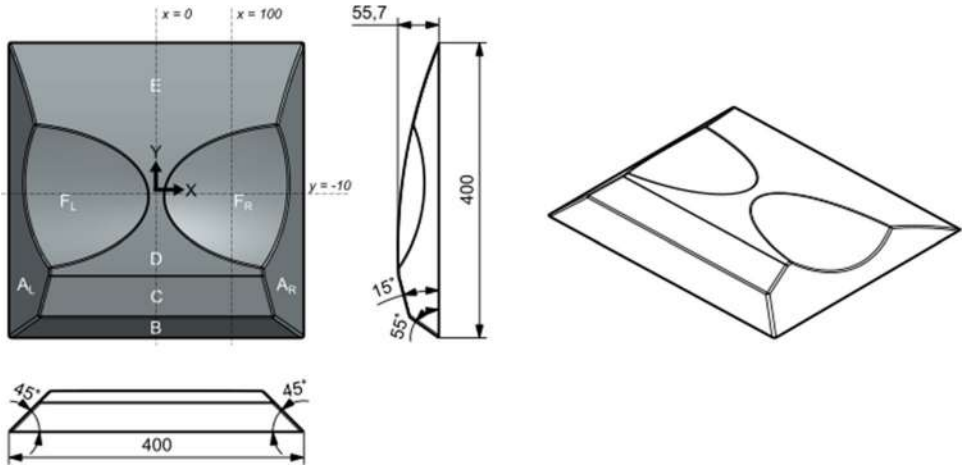

Fig. 1 The different zones of the benchmark workpiece, its dimensions [mm], and its orthogonal and isometric projections

ISF database platform

The documentation of experience requires the systematic and comprehensive collection of data regarding the components, corresponding processes and process results. Experiments and processes must be recorded in a structured manner to ensure their reproducibility by other ISF researchers and users. The shared data indicate which components have been successfully manufactured and which process parameters were instrumental in achieving this. In addition, the aim is also to document which components could not yet be produced and, ideally, to identify the underlying reasons for this.

In order to collect and exchange knowledge and experience on a very large scale with many ISF users, a web-based database[1] [3] has been developed to facilitate the documentation of users'own component and process data, the analysis of data from other users, and the comparison of different experiments in an accessible and systematic manner. The database enables the structured and visually responsive processing of documented data. A major challenge in the optimization of ISF is the complexity of the input and output variables inherent in the process. The part geometry, toolpath, and resulting accuracy are complex three-dimensional data that cannot be simplified to individual parameters without a significant loss of information. This issue is not exclusive to process optimization; it even poses a challenge in the pure documentation of processes. Other complex parameters include the (partial) supporting dies and the occurrence of intermediate geometry data in multi-stage processes and potential preliminary process steps. All of these need to be documented as three-dimensional data.

The database and the integrated forum function allow for an efficient and accurate exchange of knowledge and experience between researchers and end users, where the data can also be directly referenced in discussions. This collaborative exchange platform tool can bridge the gap between different research teams and PhD research generations. The database can also be used to systematically document and moderate benchmark studies, such as the study described in this paper. Such benchmark studies are a perfect trigger for collaborative learning and help to effectively advance the process knowledge. Regarding the prevailing development of data-driven methods, the described detailed collection of process data and annotated metadata can enable machine learning to extract process boundaries for a wide range of geometry-material combinations. Ultimately, the shared ISF data on the platform will be used to generate novel insights into the underlying causes of geometric deviations and potential compensation measures.

Approach of the benchmark study

Benchmark part

A single benchmark geometry, identified by consensus among the organizing committee members, provides an excellent way to combine the research experience built-up in incremental forming over the last two decades. This geometry is shown in Fig. 1 and contains a combination of features that proved to be challenging in ISF. The geometry consists of four flat surfaces with a discrete angle change, a slightly curved area with a low wall angle, and a small waist section between two ellipsoidal segments, which is prone to instability in larger constructs. The geometry is provided to the participants in different data formats (STL, IGES, STP, and PRT), and can be downloaded from https://www.isf-exchange.com/aboutEsaformBenchmark/.

The designed geometry looks simple, but it has been shown to present five critical challenges:

[1] https://www.isf-exchange.com

- **Tent effect**. A zone of discrete angle change (Fig. 1 between flat zones B and C) leads to underforming of the surface prior to the angle change (B) when processing the area after the angle change (C). This effect is called the tent effect and has been extensively studied [4] and is discussed in Sect."Geometric accuracy". Common remedies for this inaccuracy are to compensate for the expected deviations prior to forming or to employ a die support through two-point incremental forming.
- **Wall angles.** A wall angle reaching the forming limit of the material (zones A and B). High wall angles are associated with severe sheet thinning or even fracture. Designing a part with wall angles close to the maximum achievable wall angle limits the solution space for compensation when the part is underformed due to the tent effect. Also, flat areas with large wall angles are prone to inward bulging (see Sect."Geometric accuracy").
- **Pillow effect**. Shallow angled areas (zones C, D, E) are susceptible to the pillow effect, where the material in the center of the designed part bulges upwards due to compressive strains in the sheet.
- **Instability at the waist.** The narrow waist in zone D can cause instability in the sheet during forming. Especially in large parts, the sheet will tend to rotate around this small waist as the tool moves around the sheet.
- **Residual stresses.** A part with relatively low geometric stiffness, due to the size and the limited curvatures in the part, is particularly sensitive to elastic deformation due to residual stresses released during unclamping.

Materials and methods

The part is made **of Aluminium 5754 (AA5754), an alloy commonly used in automotive applications, with the blank sheets having a thickness of 1.5 mm.** The benchmark dimensions are chosen to be $400 \times 400 \times 55.7$ mm, which are as large as possible while being manufacturable by most of the benchmark consortium members, so that the deviations are clearly visible and the differences between the forming strategies are clearly distinguishable. The exact computer-aided design (CAD) files are available on the ISF database platform described above. The sheet metal was purchased at KU Leuven and distributed to all participating institutes, to ensure the same material properties for all experiments.

In this work, the main forming side of the shape is referred to as the front side. In SPIF and DSIF, this corresponds to the interior of the part, see Fig. 2, even if some backside forming steps (see Sect."Reducing overforming in concave areas") are applied. In TPIF, however, the forming side is flipped, hence, the exterior shape is called the front side (see Sect."Two Point Incremental Forming").

The challenging benchmark CAD geometry has been provided to the participating institutes with as objective to form the target geometry as accurately as possible. To ensure comparability of the results and to provide a common basis for exchanging experiences, the process boundary conditions have been fixed for the first round of experiments. In this first"**basic trial,**"only SPIF was allowed for forming, without the use of additional (supporting) tools or heat, except for a suitable backing plate to clamp the contour of the part. In addition, no post-treatment other than the trimming process was allowed before the resulting part was uploaded to the database. Many other platform and process parameters remain open for optimization, as shown in Fig. 3. Here, the parameters marked in yellow have been fixed for the basic trial.

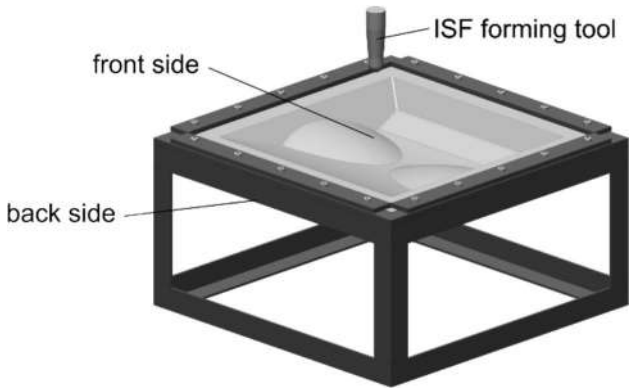

Fig. 2 ISF setup for this benchmark study

In a second "**open experiment,**" the participants were free to choose the boundary conditions and forming strategies according to their individual preferences for the best possible results. The only remaining requirement was the use of Incremental Sheet Forming as the main forming operation.

A detailed set of measurement guidelines was drafted for the participants to ensure the same modus operandi, as the alignment parameters and comparison parameters between CAD and measured part greatly influence the results. These guidelines are available in Online Resource 4 and summarized here:

- The parts are intended to be measured after forming while still clamped.
- Alignment to the CAD is performed using the rigid clamping system as it is not deformed. Compared to, for example, a best-fit approach, this type of alignment typically results in relatively high observed deviations but provides the ground truth of the forming accuracy and allows to study over- and underforming.
- The comparison between the CAD and the measured part is made as the deviations along the normal from the CAD towards the measured data.

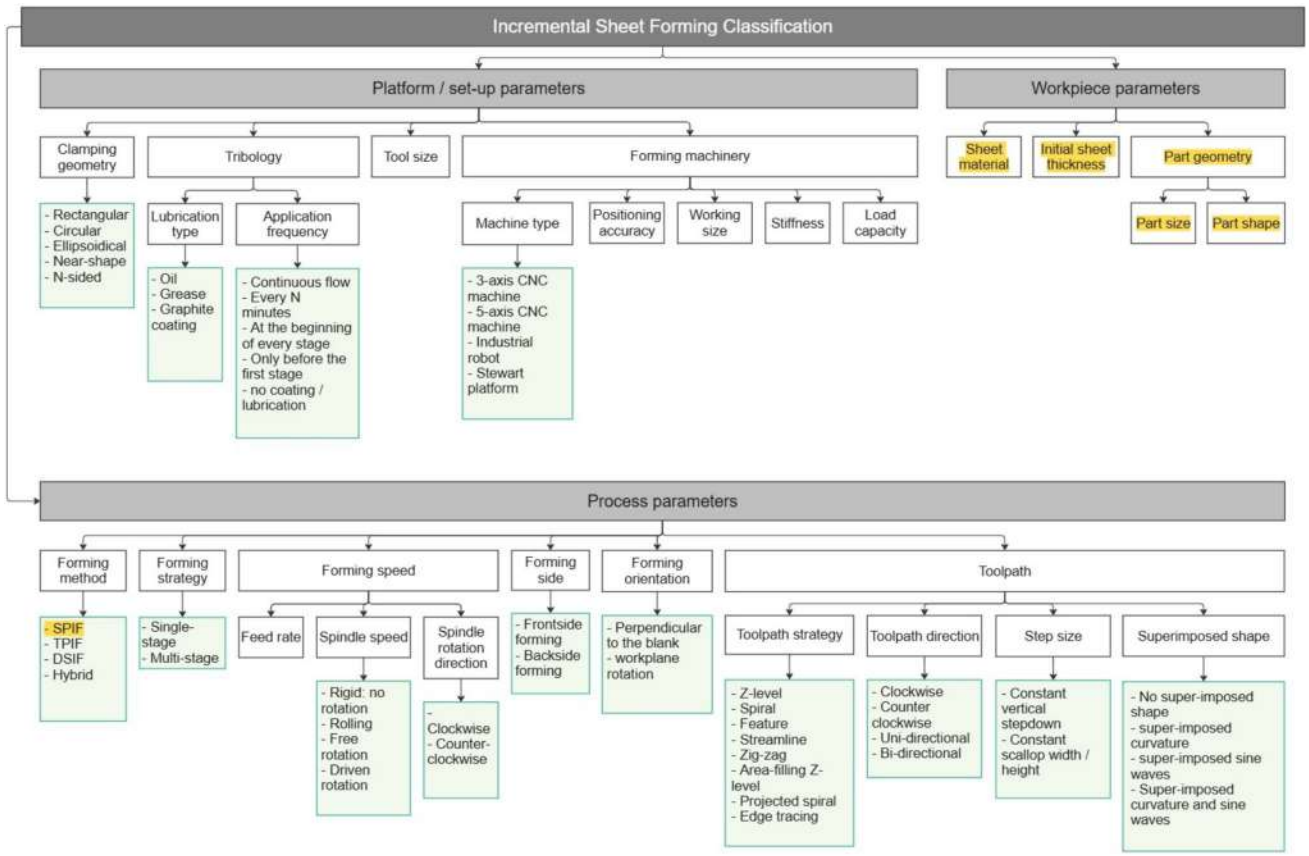

Fig. 3 Classification of Incremental Sheet Forming parameters. The white boxes are independent parameters that can be combined. The yellow-colored parameters were fixed for this benchmark study

- Sectional views are taken in the vertical direction at the center of the geometry (x = 0 mm, see Fig. 1), within the concave areas at one-quarter of the geometry's width (x = 100 mm) and in the horizontal direction at the narrowest point of the waist (y = −10 mm).

Incremental sheet forming: status quo

ISF processes

ISF is a category of flexible manufacturing processes determined by a small deformation zone travelling along a predefined path on a metal sheet, superimposing deformations until a final shape is created [5]. The key benefits of ISF have been described in a review by Gatea et al. [6] and include (1) low setup costs and high flexibility, as the process requires only a machine tool equipped with computer numerical control (CNC) and an adaptable machine part program; (2) improved formability compared to conventional processes such as stamping; and (3) a small contact surface, resulting in low forming forces. These advantages make ISF particularly suitable for rapid prototyping and the production of replacement parts without the need for costly dies and tooling. Despite its high potential and two decades of research, ISF has not yet been adopted by industry on a large scale. Unfortunately, due to the difficult nature of these processes, numerous challenges inhibit broadening the application range. These challenges are further discussed in Sect."ISF Challenges".

Within the ISF process category, three main forming methods can be distinguished, as illustrated in Fig. 4 and the ISF classification scheme in Fig. 3: Single Point Incremental Forming (SPIF), Two Point Incremental Forming (TPIF) and Double Sided Incremental Forming (DSIF). Each of these methods is based on a different working principle and offers unique advantages and limitations. **SPIF** involves a single tool that follows a predefined toolpath, with no support on the opposite side of the sheet, apart from the clamping and backing. This lack of support simplifies the setup, reduces tooling costs, and increases flexibility. This makes SPIF particularly well-suited for producing complex shapes, low-cost prototypes, and custom parts without the need for specialized tooling [1]. However, the lack of sheet support also leads to challenges in achieving geometric accuracy and controlling elastic

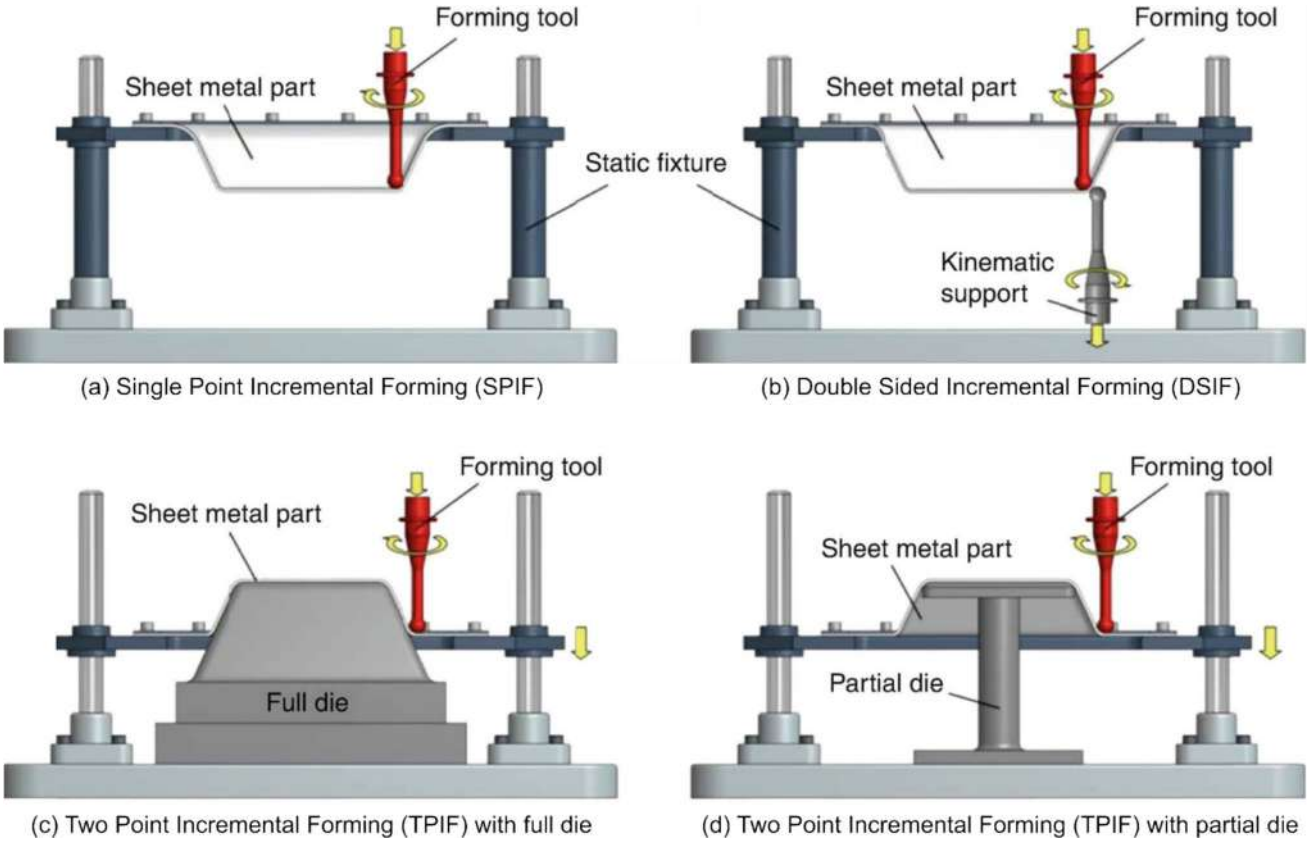

Fig. 4 Schematics of (**a**) SPIF, (**b**) DSIF and (**c**, **d**) TPIF [9]

springback. **TPIF** incorporates a full or partial supporting die at the back side of the sheet, which serves as a supporting structure and increases the forming stability [7]. This allows for greater control of the final geometry and improves the geometric accuracy. However, the main drawback of TPIF is that it requires a (semi-)custom-made die and thus leads to increased setup costs and efforts, which make it less flexible than SPIF. **DSIF** uses two dynamic tools operating simultaneously on both sides of the sheet. This dual-tool approach offers improved control over the forming process, thereby increasing the geometric accuracy compared to SPIF while eliminating the need for custom made dies typical for TPIF. However, DSIF requires a more complex setup than SPIF and precise synchronization of the two forming tools to prevent collisions and to ensure uniform deformation. To this point, Lu et al. [8] conclude that DSIF offers better formability than SPIF for cones and pyramids with variable wall angles, but with greater operational complexity and programming requirements to prevent the tools from colliding or penetrating the sheet.

This study primarily focuses on SPIF due to its superior flexibility, ease of setup, and cost effectiveness. This makes it an ideal choice for applications that require rapid adaptation and low production volumes.

ISF challenges

Five critical challenges in ISF were considered in the design of the chosen benchmark shape. According to Gatea et al. [6], the most significant drawbacks of ISF include (1) insufficient accuracy due to unwanted elastic and plastic deformations, (2) forming limits making it difficult to produce parts with wall angles close to 90 degrees, (3) local material thinning, and (4) poor surface finish. Ajay and Mittal [5] also highlight (5) low productivity as one of the challenges. The following section addresses geometric accuracy (Sect."Geometric accuracy") followed by forming limits and material thinning (Sect."Formability"), as these two aspects are closely related.

Geometric accuracy

Achieving sufficient geometric accuracy in SPIF-manufactured parts is a major challenge [1]. The nature of superimposing local deformations in combination with the absence

of a supporting die results in undesired deformations such as under- and overforming, defined as the deviations between the produced part and the desired CAD model. Several deformation mechanisms contribute to these issues, including springback, bulging, the pillow effect and the tent effect.

Springback occurs upon removal of the external load: the geometry of the formed region undergoes deformation due to the redistribution of residual stresses [10]. Three types of springback occur: (1) the local springback immediately after the forming tool passes, which occurs during forming, (2) the springback after unclamping, and (3) the springback after trimming. Various methods have been proposed to counteract springback. Zhang et al. [11] investigated the influence of the clamping system on the springback after unclamping by focusing on stress annealing and concluded that a roller clamping system reduces this springback compared to commonly used fixed clamping systems. Patel et al. [12] state that five parameters influence the springback significantly: the sheet thickness, feed rate, spindle speed, tool size, and step size. Oleksik et al. [13] showed that a decrease in tool diameter, step size, or initial sheet thickness results in increased springback. Li et al. [10] found increased springback in multi-stage forming compared to single-stage SPIF and attributed it to the accumulation of residual stresses in each forming stage.

The **bulging effect**, another common undesired deformation in ISF, involves local outwards or inwards curved displacement from the target geometry (Fig. 5 (**a**). The **pillow effect**, a specific type of bulging occurring in flat areas, typically at the bottom or base of a formed sheet part (Fig. 5 (**b**), results from sheet bending due to in-plane stresses, as noted by Isidore et al. [14]. They state that the material is largely deformed in the transverse direction, which is in the XY-plane perpendicular to the toolpath, within the tool vicinity, where the material is pushed towards the center of the sheet, thereby causing the formation of a pillow-like bulging effect. This pillow can be reduced by decreasing the step size [15] or hardening exponent [16], increasing the tool radius [14, 16], or using a flat-end tool instead of a hemispherical one [14]. According to Hussain et al. [16], it is particularly pronounced at smaller wall angles. The pillow effect can be influenced in the following ways:

The **tent effect** occurs at discrete changes in wall angle (Fig. 6). Guzmán et al. [4] studied this by forming and

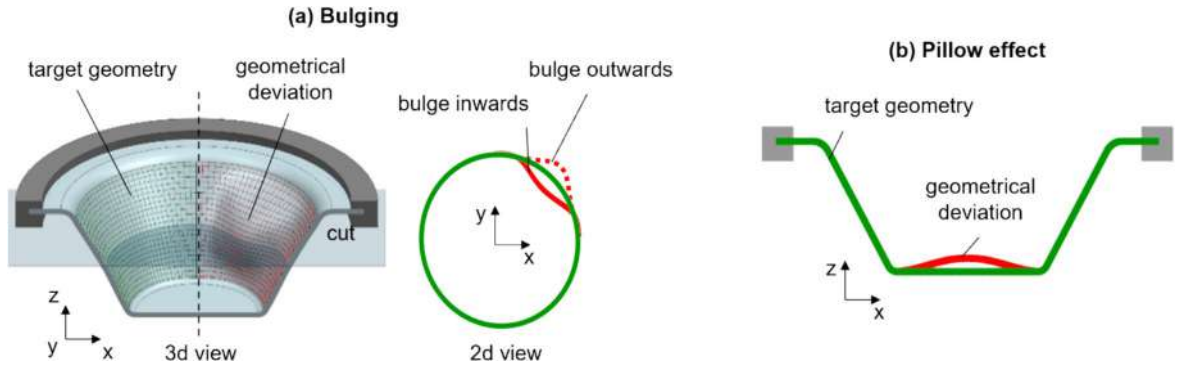

Fig. 5 (**a**) Bulging and (**b**) pillow effects in ISF

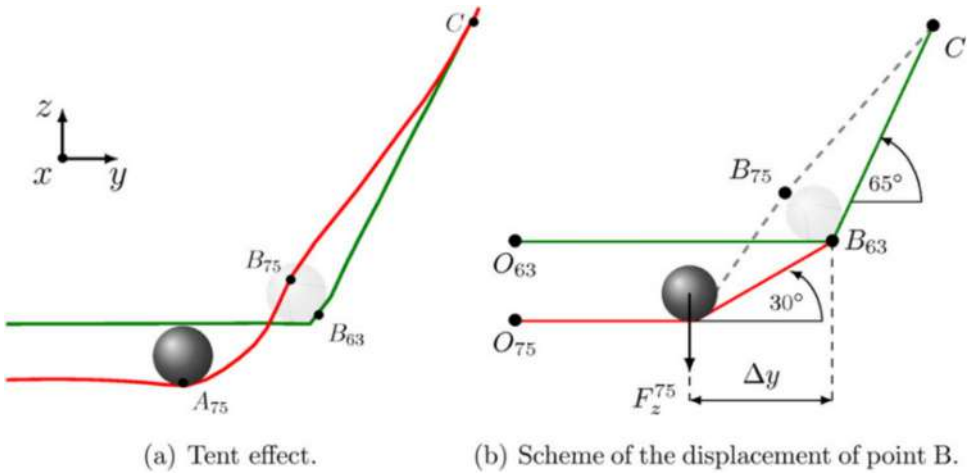

(a) Tent effect. (b) Scheme of the displacement of point B.

Fig. 6 The tent effect after a discrete change of wall angle [4]

simulating a two-sloped pyramid and observed that these deviations occur due to both plastic deformation outside the tool/sheet contact zone and stress release triggered by new boundary conditions after the discrete change in angle. According to Behera et al. [17], its magnitude depends on the wall angles and on the difference between them.

Although the authors of this study experienced a difference in geometric accuracy when scaling geometries to larger dimensions, to the best of their knowledge, no systematic studies have been conducted to investigate the **scale effect** in larger-scale geometries, despite limited studies comparing micro- and macro-scale ISF [18]. Although larger workpieces, like automotive component prototypes [19], have been investigated, no direct analysis of the scale effects on geometric accuracy has been reported.

Formability

Compared to conventional forming limit diagrams, the material fracture strain limits observed in SPIF are considerably higher [2]. Montanari et al. [20] identify failure mechanisms in SPIF, attributing failure to extensive thinning before necking. Strategies to enhance the process window include heat-assisted SPIF, which increases formability [21]. Heating methods include laser-assisted, joule heating, and friction heating. Other strategies to overcome the forming limits include increasing the initial blank thickness or redistributing the material [22]. In single-stage forming, thinning can be approximated by the sine law, where steeper wall angles lead to more thinning [23]. Consequently, the maximum formable wall angle of a given material and sheet thickness can be determined through a cone test [1]. While parameters such as tool diameter and step size [24] can slightly influence this limit, increasing the initial sheet thickness is another option. However, to further extend the maximum wall angle, material redistribution is necessary, which can be achieved through a multi-stage approach [23]. In multi-stage forming, the use of preshapes helps equalize strain distributions across the sheet surface by creating high strains in areas of the intermediate shape that have low strains in the final geometry, and vice versa [1]. This technique reduces localized thinning and thereby extends the forming limits. Because failure in SPIF is closely related to uneven thickness distributions and excessive thinning in critical areas [25], accurately predicting and optimizing thickness distributions – or the minimum thickness of formed parts – is crucial for process optimization [26]. Multi-stage forming as an important strategy in this respect is further discussed in Sect."Multi-stage SPIF".

Single-stage SPIF

The challenges discussed in the previous section can be addressed by adapting the SPIF process. This can be accomplished by modifying the ISF parameters, applying compensation strategies, or using multi-stage forming to obtain better results. This section, based on the prevailing literature, focuses on improving single-stage SPIF by adjusting process parameters and applying compensation. According to Ajay and Mittal [5], ISF parameters can be categorized in three groups: (1) workpiece parameters, (2) machine parameters, and (3) process parameters. An elaborate schematic has been constructed for this study and is discussed above, in Sect."Materials and methods". This literature study focuses mainly on the state of the art regarding process parameters, as workpiece parameters are kept constant in this benchmark study and machine parameters depend on the hardware facilities available in the institutes conducting the experiments. An overview of the machine parameters per institute can be found in Online Resource 1. Sect."Process parameters"concentrates on process parameters such as tool diameter, step size, and rotational speed. Sect."Toolpath strategies"delves into different toolpath strategies described in literature and their influence on the geometric accuracy of the formed part. Sect."Compensation strategies"discusses compensation strategies.

Process parameters

This section does not aim for exhaustive coverage of all possible process parameters but highlights the most intensively researched ones, as considered relevant to this project.

The **tool diameter** has a significant effect on geometric accuracy and thickness distributions, as it affects the forming forces. As discussed in Sect."Geometric accuracy"on the geometric accuracy, an increased tool size reduces the unwanted deformations caused by springback [13]. The forming limits are also influenced by the tool size. Kim and Park [27] assert that a larger tool increases the deformation zone, leading to lower strains and hence the possibility to achieve a higher critical wall angle before failure [12]. Mirnia and Dariani [28] conclude that a smaller tool diameter increases tangential stresses, causing more thinning. Additionally, Echrif and Hrairi [29] conclude that a larger tool results in an improved surface finish. Li et al. [30] suggest selecting a tool diameter as large as possible. While a smaller tool allows producing parts with higher resolution (features with small radii of curvature), a larger tool is better for a more homogeneous thickness distribution, requiring a trade-off. One option is multi-stage forming, where a larger tool is used initially for better thickness distribution and formability, followed by a smaller tool for finishing or reaching zones with low radii of curvature features [31].

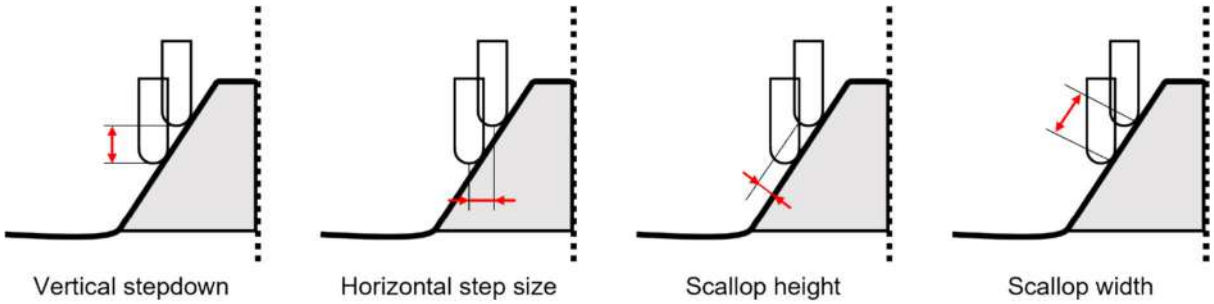

Fig. 7 Parameters describing the step size between different tool contours

The **step size** represents the distance between each toolpath contour and can be defined in several ways: One approach is using a constant vertical stepdown or horizontal step size, see Fig. 7. Another approach is maintaining a maximum scallop height or width, also referred to as stepover in computer-aided manufacturing (CAM) software, to keep the surface roughness constant. Since many different terms have been used in literature to refer to these step sizes, the terminology used in Fig. 7 is proposed to avoid confusion. Studies show that larger step sizes result in increased residual stress, pillow effect, and springback, hence a lower geometric accuracy [15, 32–34]. Honarpisheh et al. [35] and Attanasio et al. [36] found that a smaller stepdown or scallop height results in less thinning. Additionally, a toolpath with a small and constant scallop is best for a high surface finish, but this choice increases the forming time [37].

While lower friction, which can be achieved by strategic tooling-material combinations and proper lubrication, typically improves the formability, elevated temperatures are often used to improve sheet formability [27, 38]. A higher **spindle speed** can induce elevated temperature via contact-friction heat generation, resulting in increased ductility and lower forming forces [5]. Apart from the rotation, the forming speed, or **feed rate,** also has an influence. High-speed incremental forming raises the sheet temperature as well, yielding a higher formability while also lowering process times. Additionally, in materials with a negative strain rate sensitivity, the formability benefits even more from high feed rates [39]. Conversely, a lower feed rate can benefit the process window and geometric accuracy as well [27, 34].

Toolpath strategies

As the final shape in incremental forming is dictated by the toolpath, slight alterations in toolpath strategies directly impact the geometric accuracy. Different terms are often used to describe the same toolpath principles, often depending on the software used to construct them. To establish a clear and uniform terminology, this section provides definitions and defines unambiguous labels for different key toolpath strategies.

In a **Z-level toolpath** (Fig. 8 (a)), the CAD model is sliced into constant Z-levels based on a chosen scallop or stepdown. The tool forms the outline of the shape at each level, connecting to the next contour either by following the shape until the next Z-depth is reached or by lifting the tool and starting at the next contour. Z-level toolpaths can be unidirectional or bidirectional. In the second case, the tool changes direction at the beginning of each level. The **spiral toolpath** (Fig. 8 (b)) is a continuous variant of the regular Z-level toolpath, where the path is interpolated between two contour starting points, providing smoother transitions between levels.

Feature toolpaths, unlike the previous 2D-based tool contours, maintain a constant surface finish by keeping the scallop constant at all times. Carette et al. [41] described

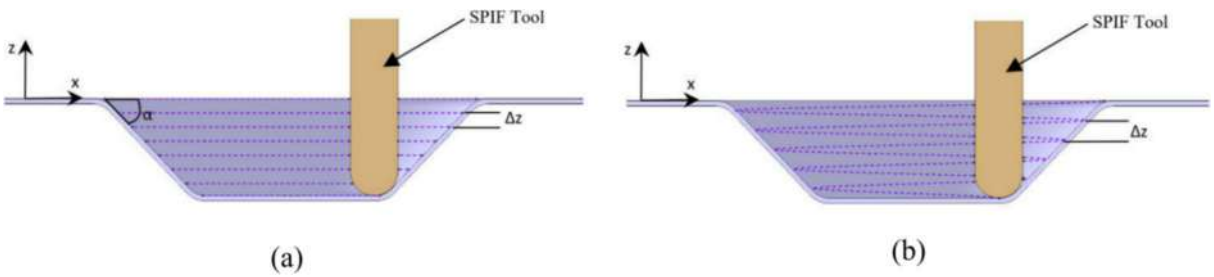

Fig. 8 (**a**) Z-level and (**b**) spiral toolpath as the most basic toolpath strategies for ISF [40]

the feature toolpath, which starts from the outer edges of the desired geometry and offsets along the part geometry to keep the *scallop width and height constant at all times*, resulting in non-planar tool contours, also called equipotential lines by Lu et al. [42]. This toolpath strategy is particularly suitable for forming geometrical features in a multi-stage approach Fig. 9.

Streamline toolpaths are generated based on a set of guiding curves or surface features to achieve smooth, continuous motion with consistent stepover or scallop width. Unlike Z-level toolpaths, which follow the outline of the geometry at a certain Z-depth, streamline toolpaths cover the full surface. This distinction is especially noticeable on horizontal surfaces, that are covered by streamline toolpaths but not with Z-level or spiral ones. **Zig-zag toolpaths** correspond to streamline toolpaths with alternating tool directions [43] (Fig. 10) and are mostly used for non-closed forms [42]. Lu et al. [44] utilized a zig-zag toolpath to form a groove. Ben Said [45] compared unidirectional and bidirectional Z-level toolpaths to zig-zag toolpaths, finding that Z-level toolpaths result in lower forming forces and stress distributions, while zig-zag toolpaths offer higher productivity in terms of demands on a computer's central processing unit (CPU), particularly important when running and evaluating simulations.

Bremen et al. [43] introduced adding a curvature to streamline or zig-zag toolpaths. This **convex or concave curvature** has a certain amplitude and follows the CAD surface around the zig-zag lines (Fig. 11). The curvature is added to prevent the local bending moments from being parallel to each other. This way, an accumulation of bending moments around the same axis is prevented, as the bending moments of the different zig-zag lines reduce the effects of the other lines instead of amplifying them. Additionally, they studied **superimposed wave shapes** on both linear and curved zig-zag paths, finding that convex toolpaths with superimposed waves performed best in terms of geometric accuracy, by significantly reducing deviations and springback.

Another approach to improve the geometric accuracy or thickness distribution is a **workplane rotation**. Rotating an asymmetric workpiece to minimize the wall angles relative to the toolpath results in more uniform thickness distributions [22, 46]. This can be achieved by starting

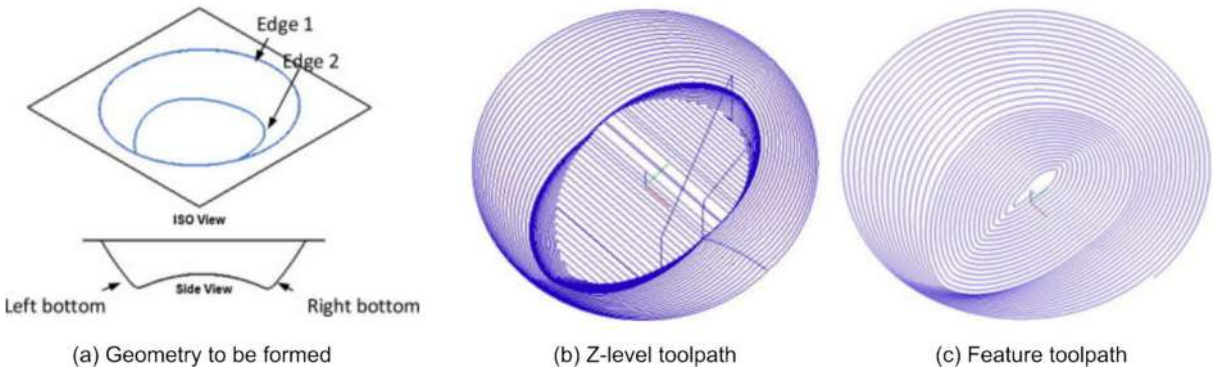

Fig. 9 Feature toolpath compared to the conventional Z-level toolpath [42]

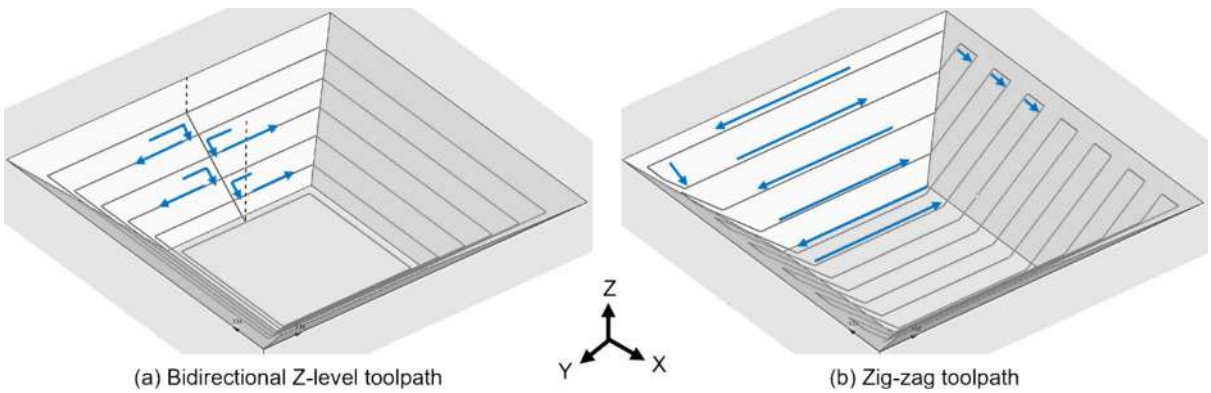

Fig. 10 Comparison between the (**a**) bidirectional Z-level and (**b**) zig-zag toolpath

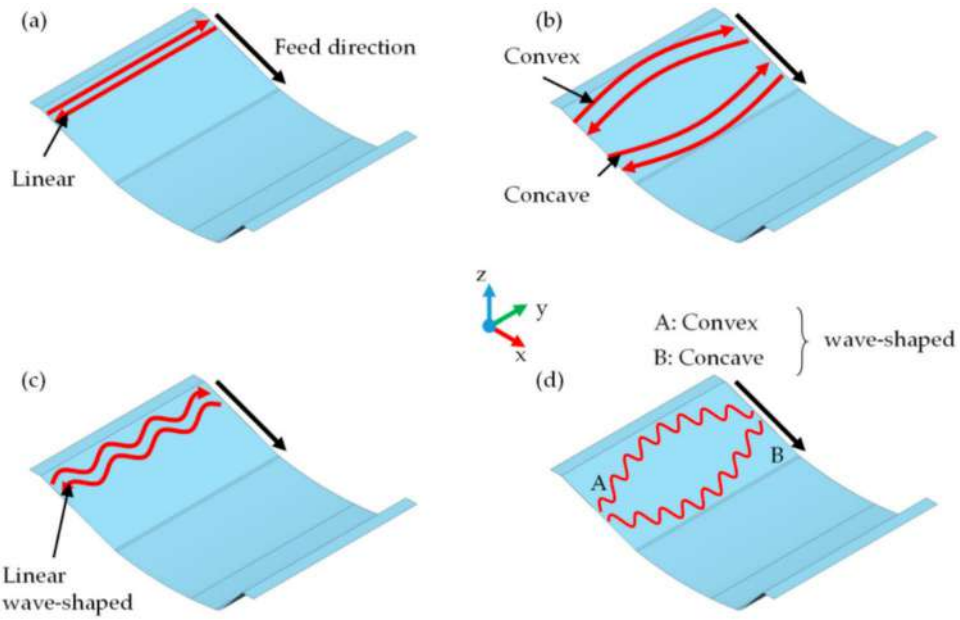

Fig. 11 (**a**) Regular or linear zig-zag toolpaths versus (**b**) convex and concave zig-zag toolpaths and (**c**, **d**) superimposed wave shapes [43]

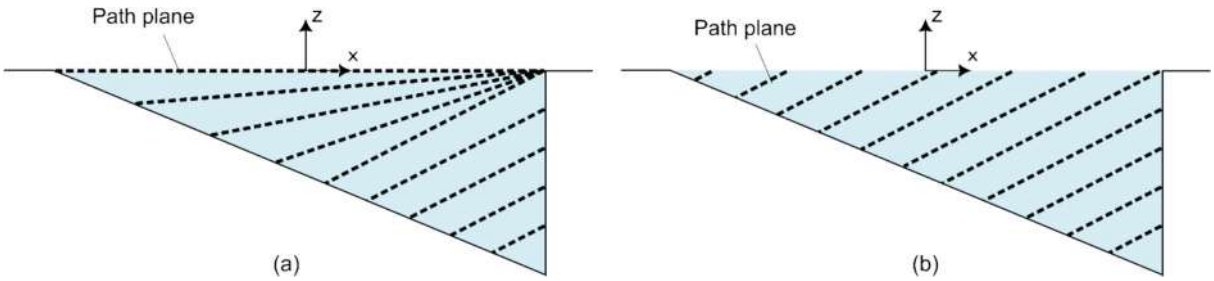

Fig. 12 Workplane rotation for a pyramid with a single vertical wall by (**a**) tilting the toolpath in each contour and (**b**) rotating the entire toolpath. This figure is based on [46]

from the XY-plane and tilting the toolpath incrementally in each contour (Fig. 12 (**a**), or by tilting the entire toolpath, e.g., in a multi-stage approach (Fig. 12 (**b**).

Compensation strategies

Even though some of the toolpath strategies specified above already contribute to improving the geometric accuracy, achieving industrial qualification levels requires techniques such as compensation based on the deviations to the CAD model [47]. Often, the compensation is applied by shifting all target geometry points with the measured deviation, calculated perpendicular from the target geometry, in the opposite direction. This method is also known as mirror compensation [48] and can be applied based on measured or predicted deviations. Even though compensation significantly increases the geometric accuracy, the compensated geometry still results in new unwanted deformations. Hence, mirror compensation alone does not yield optimal results and necessitates multiple iterative steps. Consequently, consecutive experiments and iterative compensation steps are often used. Recent research developments have explored the use of machine learning models to predict these deviations, enabling compensation strategies without unnecessary experiments [49]. Behera et al. [50] were among the first to study compensation strategies and developed a prediction model based on features and their interactions. Ren et al. [51] introduced an in-situ springback compensation method based on online force measurements, leading to continuous toolpath modifications during forming. However, their proposed combination of offline preparation and online compensation was unable to compensate for the pillow effect, as it is unrelated to springback. Mollensiep et al. [52] propose a regression-based compensation method to predict the deviations after SPIF, which are then used to adapt the toolpath based on mirror compensation. Carette et al. [53] also propose a prediction framework that applies multiple compensation steps to account for additional unwanted deformations

on the modified predicted geometries. Praveen et al. [54] studied mirror compensation of springback for DSIF, based on predictions of tool deflection using an empirical model and sheet deflection using both membrane theory and small-deflection theory. Bonnardot et al. [55] applied mirror compensation based on measured deviations directly on the toolpath, rather than adjusting the CAD model and applying a toolpath on it.

Multi-stage SPIF

Multi-stage forming is a type of ISF where a single tool incrementally reshapes a sheet throughout multiple sequential passes. While classifying an ISF forming strategy as single-stage or multi-stage is usually straightforward, ambiguity can sometimes arise. Therefore, in this study, experiments where at least one area of the sheet is formed more than once are classified as multi-stage experiments. Multi-stage SPIF has been intensively investigated as a way to improve the process window [23], but it can also be used to enhance the geometric accuracy [56]. This section divides the strategies found in literature into shape-altering and toolpath-altering categories. The first category involves forming pre-geometries or intermediate stages before forming the target geometry, while the second alters the toolpath shape or process parameters, such as tool size and step size, without modifying the geometry. These two categories can also be combined.

Shape-altering multi-stage strategies

Forming a workpiece in multiple stages is one way to enhance the process limits and exceed the material-specific critical wall angle. Multi-stage forming was first proposed by Verbert et al. [57] and Duflou et al. [23] to extend the process limits. The authors formed truncated cones with vertical walls by creating intermediate cones with increased wall angles in each step. Subsequent research focused on improving this approach by designing intermediate geometries with a smaller base diameter combined with progressively increasing wall angles [58–60] and by adjusting the depth of intermediate shapes to compensate for rigid body motion [61]. Combining these strategies has also been explored [58, 62], as well as using parabolic shapes instead of straight walls for intermediate geometries [63].

Tanaka et al. [46] offer a strategy to form a square prismatic part by segmenting the part into a square pyramid (Fig. 13) and progressively forming the four walls using workplane rotation (see Sect."Toolpath strategies").

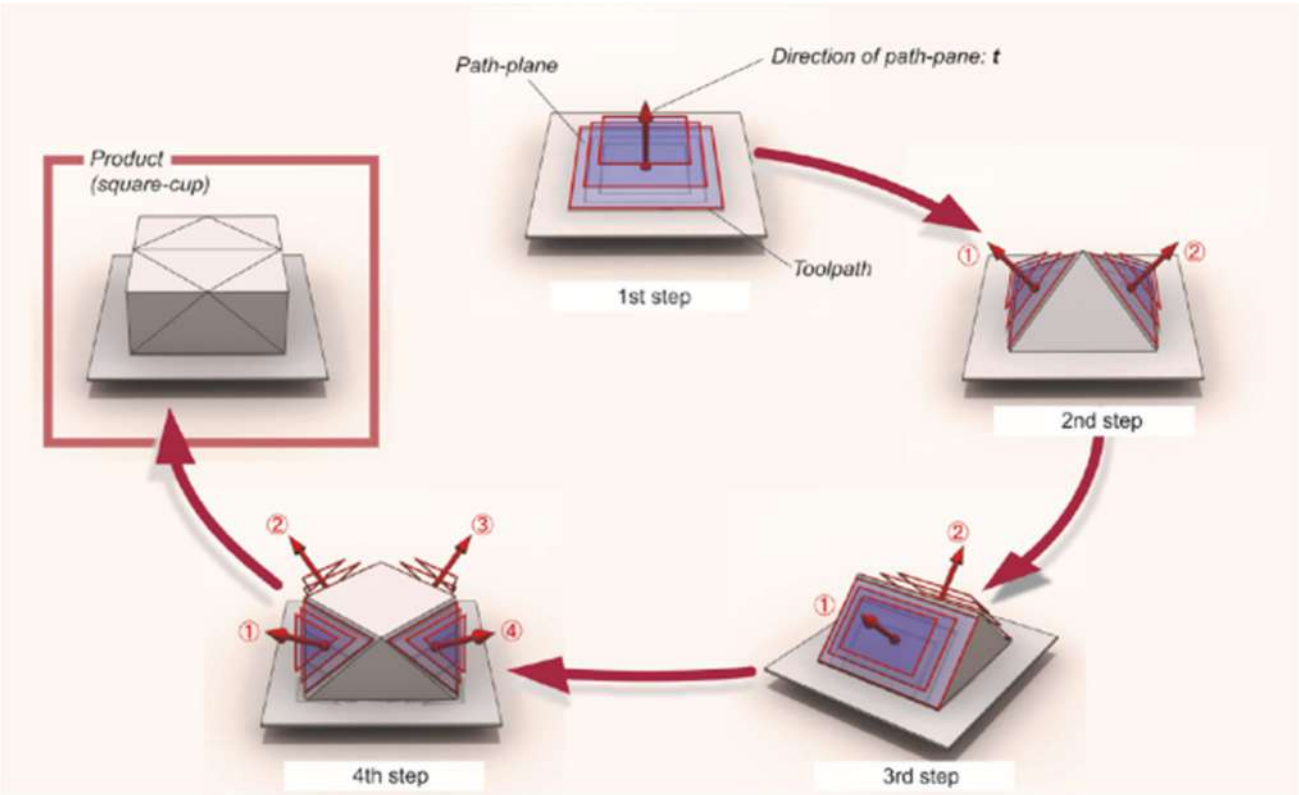

Fig. 13 Multi-stage strategy to form a square prismatic part by segmenting the geometry [64], as first described in [46]

Forming more complex geometries with multi-stage forming has been studied as well. Gupta et al. [65] used intermediate shapes with lower wall angles to form an aerospace component with steep sides. The authors used measurements to compensate for the rigid body motion but could not avoid it in the final stage. Li et al. [66] studied forming a car taillight and concluded that traditional single-stage or two-stage forming led to failure. Instead, they propose a multi-stage strategy that splits the workpiece into different areas and uses backside forming for concave areas that were overformed in a previous step.

Other applications where the design of intermediate geometries has been studied include medical implants. The strategies proposed for these shapes include double curved surfaces [67, 68]. However, multi-stage forming does not automatically result in more uniform thickness distributions, and it can even lead to increased thinning in critical areas [56, 61]. Hence, careful design of intermediate shapes and toolpaths is essential.

Compensation strategies for multi-stage forming build on such strategies used in single-stage forming, which have been thoroughly researched. For example, compensating stepped features induced by rigid body motion when forming a vertical-walled cup have been studied and predicted [61]. Dai et al. [69] added an additional forming step after multi-stage forming a complex cavity part with stepped features based on measured deviations to the CAD model, thereby increasing final geometric accuracy. However, combining compensation of the full geometry with multi-stage forming adds complexity, as altering intermediate toolpaths also affects the final outcome by introducing additional unwanted deformations. To the best knowledge of the authors, no systematic strategies to overcome this complexity have been reported yet.

Toolpath-altering multi-stage strategies

Not only can intermediate shapes be modified, but toolpaths can also be adjusted. Similar to adjustments in single-stage forming, process parameters and toolpath strategies can be adapted to increase geometric accuracy and enhance the process window. Skjoedt et al. [63], for example, compared conventional downwards (D) or out-to-in (OI) toolpaths on intermediate shapes with upwards (U) or in-to-out (IO) toolpaths. Malhotra et al. [70] combined IO and OI forming within one stage by splitting the path into upward and downward movements. Toolpath-altering strategies mostly focus on different process parameters, reforming specific areas, and applying backside forming [66].

Simulation of SPIF: finite element modeling

Finite element (FE) simulations of sheet metal forming processes have achieved high precision in process modeling [71]. High-fidelity FE models have significantly improved the understanding and predictive accuracy of SPIF through extensive experimental validation. Due to the highly nonlinear nature of SPIF, achieving accurate numerical predictions requires careful selection of numerical parameters. This section outlines critical factors, including integration schemes, material models, and element formulations, that influence numerical accuracy. The modeling work for the benchmark is detailed in Sect."Simulations".

For SPIF numerical modeling, equilibrium equations can be solved using either implicit or explicit methods, as the process is quasi-static. Explicit methods are widely adopted for efficiently handling large deformations, with time increment adjustments through mass scaling to maintain practical computational costs [72, 73]. While many studies favor explicit schemes for SPIF simulations [74–79], some researchers have explored implicit approaches [80–85]. The NUMISHEET SPIF benchmark [86], which focused on simulating a 45° cone, found no clear preference for implicit or explicit methods. Instead, accuracy and computational cost depend significantly on factors such as the material model and element type chosen.

The choice of material model is crucial for accurate SPIF simulations, particularly for predicting tool-load history during forming [81]. The isotropic von Mises and Hill 1948 yield functions [87] have been extensively used for SPIF modeling and remain popular in commercial FE codes due to their simplicity and ease of parameter identification. More advanced 3D yield functions, such as Barlat's Yld2004-18p [88], have been developed to capture the complex stress states in SPIF and have been examined in recent studies [77]. Esmaeilpour et al. [89] compared von Mises, Hill 1948, and Yld2004-18p functions in Abaqus/Explicit for simulating a 67° conical geometry of AA7075-O. Notably, Yld2004-18p required significantly higher computational resources, with CPU times of 101 h compared to 74 h for Hill48 and 72 h for von Mises (using 24 CPU cores). The influence of these yield functions on forming force predictions was further validated experimentally by Betaieb et al. [90]. Their study found that Hill's 1948 yield function, calibrated using tensile and shear tests, achieved accuracy comparable to Yld2004-18p and even provided better force predictions at high wall angles.

Hardening laws play a key role in defining material behavior in the plastic regime. Henrard et al. [80] emphasize that hardening law selection has a more pronounced impact on forming force prediction than the choice of yield function. Voce-type and Hockett-Sherby [91] isotropic hardening models, which incorporate saturating formulations, are particularly effective for aluminium alloys [92–95]. Meanwhile, kinematic and mixed hardening models (isotropic-kinematic) have been explored in multiple studies to better account for the complex strain paths inherent in SPIF [80–82, 84, 96].

Given the localized plastic deformation inherent to incremental forming, element formulation greatly affects both computation time and result fidelity. Solid elements are often preferred for capturing thickness variations and localized strain gradients, as demonstrated in earlier studies [74, 77, 78, 85, 90]. However, their high computational cost has led some researchers to explore shell elements as an alternative [80–82]. Solid-shell elements have emerged as a hybrid solution, balancing computational efficiency and predictive accuracy. These elements effectively predict thickness variations and forming forces while significantly reducing simulation time [94, 97, 98]. An adaptive mesh refinement strategy, which refines the mesh near the tool, was introduced by Hadoush and van den Boogaard [99] and Lequesne et al. [100]. De Sena et al. [85] further confirmed the benefits of this strategy, demonstrating significant reductions in CPU times.

From state of the art to benchmark testing

The state of the art in SPIF has been taken into account as a starting point for the experimental comparative benchmark exercise reported in the remainder of this report. The chosen benchmark geometry was designed to contain the known challenges in terms of geometrical accuracy, as summarized in this section. By involving a broad team of contributing research institutes, it could be assured that the available experimental infrastructure would be compatible with the most advisable process strategies as explored in literature, effectively allowing an in-depth verification of the SPIF process capabilities anno 2025.

Single-stage SPIF

In single-stage SPIF, the entire benchmark shape is formed in a single pass, with no area of the sheet undergoing multiple forming steps. This strategy is both straightforward and efficient in terms of productivity, as the entire part is formed through a continuous toolpath without revisiting previously formed areas. The following sections present key observations from the baseline experiments in single-stage forming and highlight challenges encountered by multiple institutes. Strategies to address these challenges, including adjustments to process parameters and toolpath strategies, are discussed. These challenges and insights from single-stage SPIF highlight the need for multi-stage SPIF, which is discussed in detail in Sect."Multi-stage SPIF".

Observations from baseline experiments

As mentioned, baseline trials of the single-stage strategy were conducted by various research groups to evaluate the geometric accuracy of the proposed benchmark part. The detailed process parameters and toolpath strategies are listed in Online Resources 2 and 3, respectively. All the experiments discussed in this section follow the part dimensions described in Sect."Benchmark part"to ensure a consistent basis for comparison. As it was not possible for all institutes to align the measurements based on the clamping rig, a best-fit approach using GOM Inspect 2019 was employed to ensure comparability of the results. Ideally, measurements should be performed in the clamped state for accurate comparison. However, due to limitations of the experimental stand, some measurements were taken in the unclamped state (e.g., UNIPA EXP #1, ULisboa EXP #1), as illustrated in Fig. 14. The high deviations at the shallow wall area (zone E) in Fig. 14 (d) and (e) are caused by residual stress releasing during unclamping.

As briefly discussed in Sect."Benchmark part", the benchmark shape presents several challenges, particularly high deviations in critical regions (Fig. 14). This section provides a detailed discussion of some of the dominant inaccuracies observed in different zones of the benchmark workpiece. Additionally, strategies to mitigate these inaccuracies, such as adjustments to process parameters and toolpath strategies, are explored in Sect."Influence of process parameters"to improve geometric accuracy within the single-stage forming approach.

Reducing the tent effect

In all single-stage baseline experiments, the tent effect was observed in zones B and C, particularly at the transition point where a discrete wall angle change occurs (see Fig. 15 (a)).The steeper wall in zone B resulted in a noticeable geometric deviation near the transition region that emerged after passing of the tool. This effect typically develops when the tool processes the lower plane following an angle transition [4], preventing the toolpath from accurately capturing the intended angle change between zones B and C. This effect is pronounced in single-stage forming, as no compensation or multi-step strategies were applied to mitigate these deviations. Figure 15 (b) presents the baseline results from different institutions, aligned using a best-fit approach to ensure comparability.

Additionally, zones B and C are particularly susceptible to excessive thinning or even fracture, as their wall angles approach the forming limit of the material (Fig. 16).

Designing a part with a steep wall angle of 55° (see Sect."Benchmark part"), which approaches the material's forming limit threshold, restricts the solution space for a single-stage strategy, making it quite challenging to compensate for geometric deviations in these areas. One solution to mitigate these inaccuracies is to form

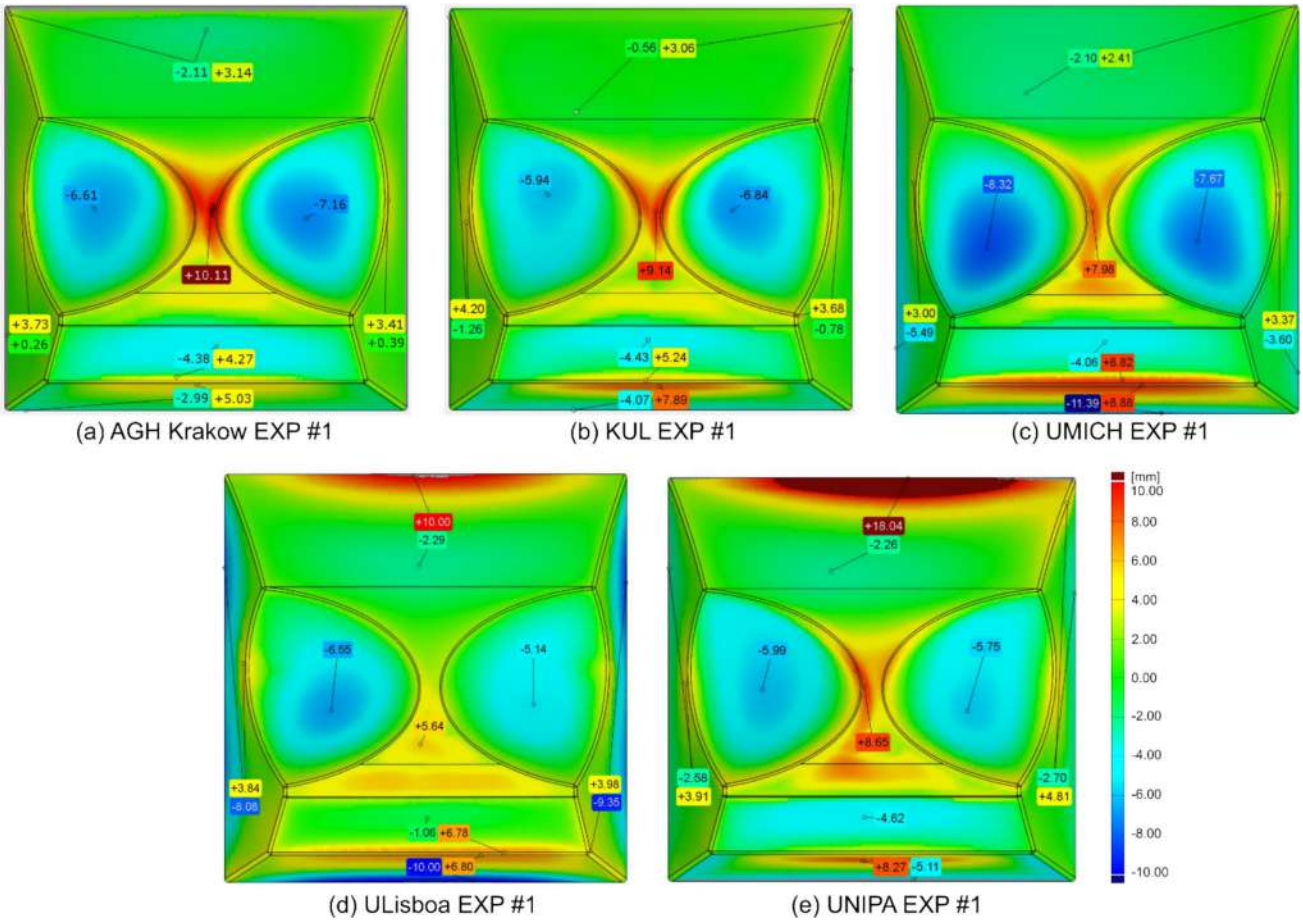

Fig. 14 Surface deviation comparison of baseline single-stage experiments against the target CAD model, aligned using the best-fit approach in GOM Inspect 2019

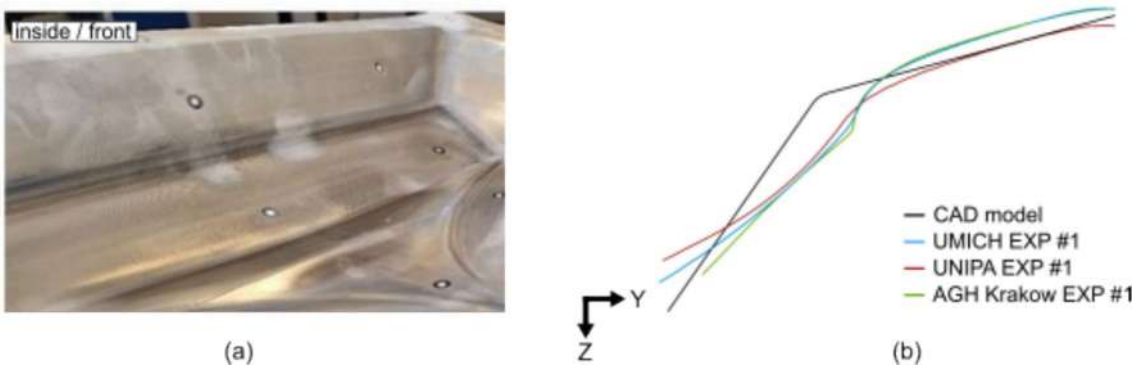

Fig. 15 (**a**) Formed part highlighting the transition region with an angle change. (**b**) Cross-sectional profile comparison (x = 100 mm) between baseline experiments and CAD model

these two walls separately in a multi-stage procedure in sequential steps (see Sect."Reducing the tent effect"). Another common remedy is using die support through TPIF to enhance shape control and minimize deviations (see Sect."Other ISF techniques"). However, even within a single-stage process, modifying key process parameters can help mitigate these issues, which is further discussed in Sect."Influence of process parameters".

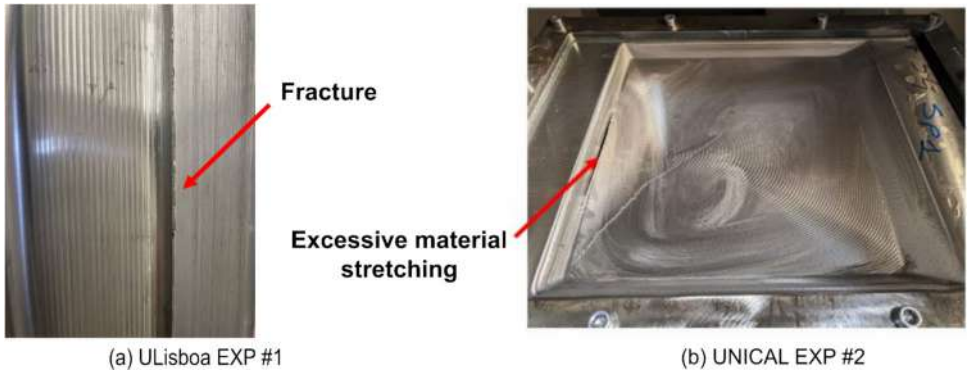

Fig. 16 (**a**) Fracture at the transition zone between steeper (zone B) and shallow wall angle (zone C). (**b**) Severe sheet thinning in zone B leading to failure

Fig. 17 The pronounced pillow effect observed in the flat waist area (zone D)

Reducing the pillow effect and corner folds

Another distinct defect observed was the pillow effect in the flat waist area, attributed to the accumulation of compressive stresses during forming. This localized material buildup occurs in the forming direction, whereby the material moves inward, resulting in a spatial curvature or pillow-like distortion of surfaces that are supposed to be flat (Fig. 17).

As mentioned previously, in single-stage forming, the entire part is formed through a continuous toolpath without revisiting previously formed areas, and this approach limits the ability to compensate for inaccuracies that may arise during the process. As a result, the compressive stresses generated during forming can propagate directly into unformed areas, such as the flat waist section (zone D), compromising the part's overall geometric accuracy. This challenge resulted in one of the highest deviations observed across the baseline experiments. According to the state of the art, the **pillow effect** can be mitigated by adjusting process parameters such as tool diameter or step size. Studies have shown that the pillow effect decreases with an increase in wall angle or tool diameter [16, 101]. In this benchmark study, however, the wall angle remains fixed unless multi-stage forming using a preshape is utilized. Similarly, reducing the step size helps minimize the pillow effect, while materials with a lower hardening exponent tend to show less pillow effect [8]. Since the material choice is predetermined in this benchmark, the primary focus is on process, not material, modifications to mitigate this issue.

Another distinctive defect observed in the middle of the waist section is a fold-like deformation that appears at the edge between the concave and narrow flat areas, propagating across the flat region. The phenomenon of sharp edges folded inwards has also been observed at the edges of a pyramid by Hussain et al. in [16] and [102]. They introduced these observations as corner folds. In this study, the term **corner fold** is used to describe all fold-like deformations observed after forming, even though the underlying cause might not be the same for all cases. The corner fold in Fig. 18 primarily results from material accumulation in the transition zone between these areas. The sharp change in geometry causes excess material to build up, leading to buckling or folding when reaching an edge or sharp change of direction. Additionally, high machine compliance (i.e., low stiffness) may further contribute to this defect. As the tool reaches the final stage of forming the narrow waist area, deflection can occur due to the restricted geometry, introducing localized distortions that exacerbate this issue. In severe cases, this deformation can cause surface fracture or chipping, as seen in Fig. 18.

Reducing overforming in concave areas

In the process of single-stage forming, some of the most significant deviations were observed in the concave areas (zones F_L and F_R), as shown in Fig. 19. While these large deviations were somewhat unexpected, they proved to be one of the most challenging aspects of forming this benchmark workpiece using single-stage SPIF. This difficulty arises from the distinct curvature transitions in these regions compared to their surroundings. As the lower adjacent sections are progressively formed, the concave areas

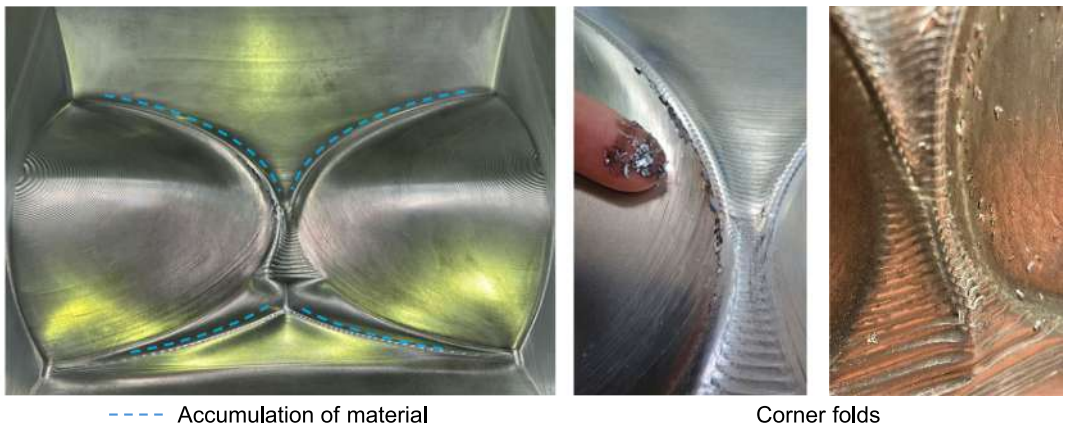

Fig. 18 Corner folds and chipping due to material accumulation

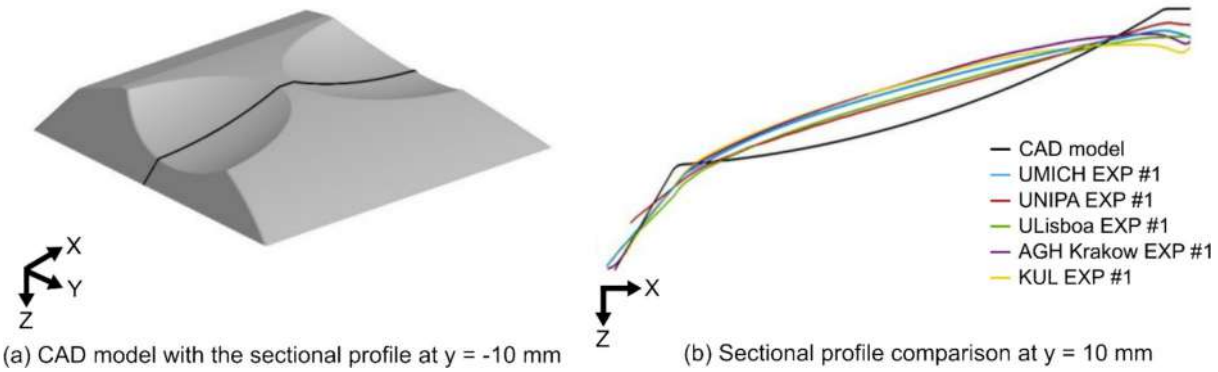

Fig. 19 Comparison of sectional profiles at $y = -10$ mm between baseline experiments and the target CAD model, highlighting inaccuracies in the concave zones. The alignment is done with a best-fit

have a tendency to flatten out or even bulge outwards, preventing them from fully conforming to the intended geometry.

In the baseline experiments, Z-level and spiral toolpaths were employed, but these strategies did not adequately adapt to the nuanced curvature transitions in the concave regions, indicating the need for improved toolpath adaptation to better accommodate concave geometries. As compensation methods, based on the measured deviations, result in too steep wall angles that exceed the maximum wall angle, this approach is not possible in a single-stage approach without invoking failure. Another possibility can include feature-separation-based toolpaths, where regions are identified and formed separately to better accommodate their unique geometric requirements. However, even with such adaptations, achieving the desired precision might necessitate multi-stage forming or additional reprocessing steps, allowing for more controlled refinement and adjustment of the intricate details found in concave areas.

Influence of process parameters

This section focuses on the effect of process parameters in single-stage SPIF. The influences of tool diameter, step size, feed rate, and spindle speed were investigated to establish guidelines for selecting process parameters to improve geometric accuracy. The findings help address inaccuracies discussed in previous sections, such as the tent effect and pillowing. Additionally, some institutions explored modifications to toolpath strategies within single-stage SPIF, providing insights that could provide input for future developments in multi-stage forming strategies.

Tool diameter

As discussed in Sect."Process parameters", the tool size is a key process parameter in SPIF. While all teams were restricted to the available tool size in their laboratories (see Online Resources 2 and 3), baseline tests were conducted

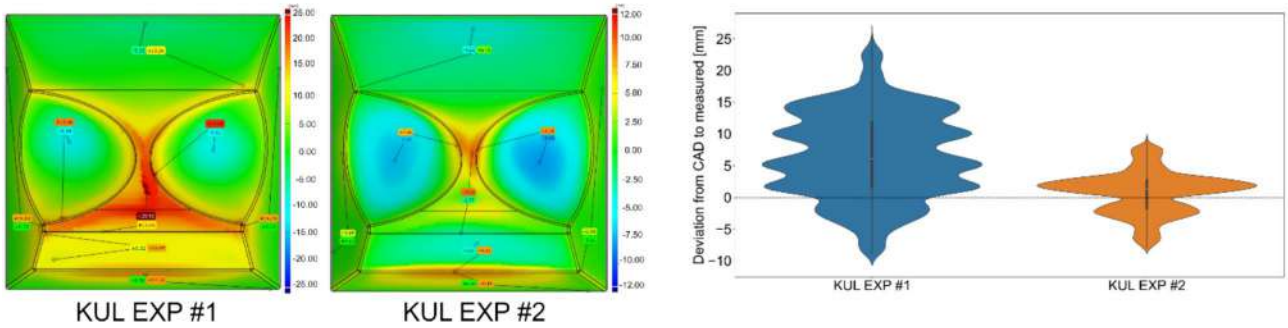

Fig. 20 Resulting surface deviations from the CAD geometry and corresponding violin plots for the single-stage EXP #1 and EXP #2 from KU Leuven, conducted with tool diameters of 10 mm and 25 mm, respectively. The alignment is based on the clamping rig

Table 2 The calculated maximum and minimum deviations from KUL EXP #1 and KUL EXP #2, with respectively tool diameters of 10 and 25 mm

Experiment name	Max positive dev. [mm]	Max negative dev. [mm]	Dev. Interval width [mm]
KUL Experiment 1	25.50	−9.04	34.54
KUL Experiment 2	9.24	−8.05	17.29

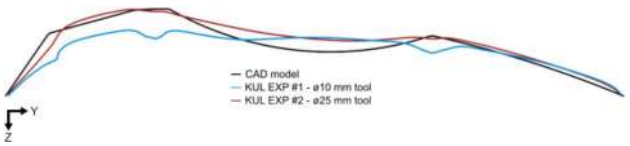

Fig. 21 Comparison of the cross-sectional profile at x = 100 mm for KUL EXP #1 and KUL EXP #2, showing the tent effect between zones B and C. The alignment is based on the clamping rig

with tool diameters of 10 mm and 25 mm in KUL EXP #1 and KUL EXP #2, respectively. The results highlight key insights into the influence of tool size for the benchmark geometry and serve as a basis for evaluating its impact on geometric accuracy. The surface comparisons from the measurement to the CAD model, along with deviation distributions in the form of violin plots, are shown in Fig. 20.

The overall geometric accuracy across the formed part, including the critical zones mentioned in the previous section, is significantly improved in KUL EXP #2. The maximum and minimum deviations are calculated and listed in Table 2. The deviation interval width of the entire part decreased by 46.76% when the larger tool of 25 mm diameter was tested. Specifically, the tent effect was greatly reduced, with the deviation in zone B decreasing from 17.29 mm to 8.14 mm. Figure 21 compares the cross-sectional profiles and further illustrates this benefit.

In addition to the accuracy improvement on the discrete angle change, the overall benefit of using a larger tool can be

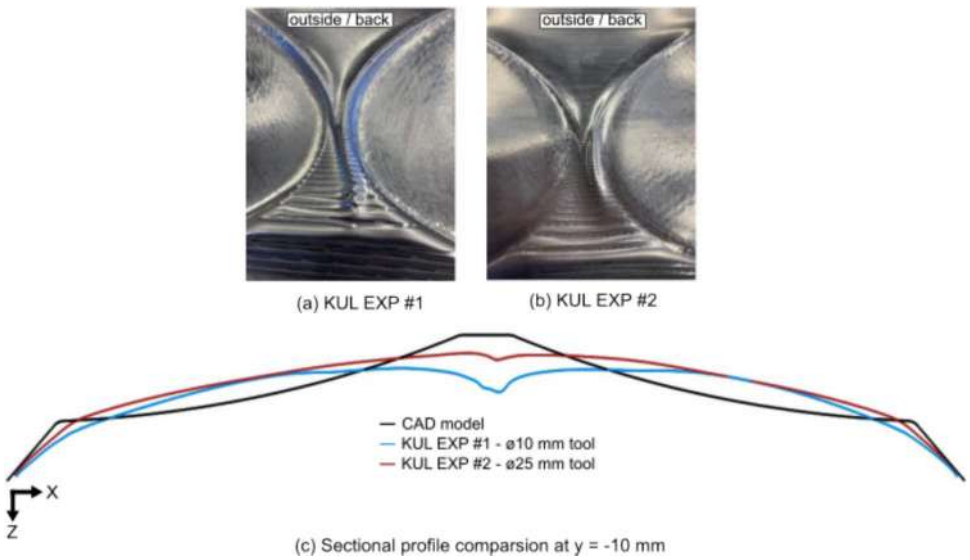

Fig. 22 Pillow effect in the flat waist area of the formed part for (**a**) KUL EXP #1 and (**b**) KUL EXP #2 and (**c**) cross-sectional comparison at y = −10 mm. The alignment is based on the clamping rig

directly observed through the improved surface and pillow effect at the flat waist area. The maximum deviation – after alignment based on the clamping rig – in this area (zone D) was 25.50 mm in KUL EXP #1 and reduced to 9.24 mm in KUL EXP #2. The highlighted view from the backside of the formed part from each experiment is shown in Fig. 22 (a) and (b), with cross-sectional profiles compared in Fig. 22 (c).

Based on the results of this systematic comparison, using a larger tool is recommended to limit ironing effects in zones sensitive to bulging and to improve geometric accuracy. Additionally, the measured minimum thickness of the formed part increased from 0.58 mm (KUL EXP #1) to 0.77 mm (KUL EXP #2), indicating that a larger tool diameter results in less thinning and may contribute a more uniform thickness distribution, helping to prevent fracture.

In summary, the tool size directly impacts the geometric accuracy of the benchmark in a single-stage forming strategy. Using a larger tool is advantageous for minimizing pillow effects in zones prone to bulging, as well as to achieve a more uniform thickness distribution and improved geometric accuracy. However, the tool size did not significantly affect the accuracy in the two concave regions studied (see Fig. 22 (c)). This indicates a need for more refined process parameters, such as toolpath strategies, to improve precision in these ellipsoidal segments. While a larger tool generally improves geometric accuracy in single-stage forming, smaller tools may still play a role in refining specific features after the overall shaping, allowing better control over fine details, particularly in a multi-stage strategy.

Step size

Another significant process parameter in ISF is the step size. As described in Sect."Process parameters", it can directly impact surface finish, processing time, and geometric accuracy (bulging). The surface finish was found to be improved with a decrease in step size, as this minimizes the scallops created when the tool locally deforms the sheet. Scallops represent the residual ridges left behind after each pass of the tool, and the step size directly influences their height. With a smaller step size, the tool makes finer passes, which smoothens these ridges and results in a superior surface finish, as can be seen in Fig. 23. However, reducing the step size increases the processing time and may induce excessive strain hardening, leading to potential fracture.

A set of experiments were conducted to investigate the influence of the step size on geometric accuracy and surface finish. The benchmark shape was formed in the ULisboa experiments using a Z-level toolpath with a ø12 mm tool and a constant vertical stepdown (Δz) of 0.5 mm, 0.7 mm, and 1.0 mm (EXP #1, EXP #2, and EXP #3, respectively). The smaller values tend to mitigate the pillow effect. However, no distinct trend was found regarding the independent impact of the step size on geometric accuracy (Fig. 24). Furthermore, fractures were observed in all three experiments in the transition between the high wall angle (zone B) and shallow wall angle (zone C), as shown in Fig. 25. This suggests that its effect may vary depending on other process parameters (e.g., tool diameter, toolpath) and material behavior. Therefore, an additional experiment was conducted with a modified strategy with a larger tool diameter of 25 mm.

Based on the observation, a follow-up experiment was conducted to assess the combined effect of step size and tool diameter. In ULisboa EXP #4, a larger tool with a 25 mm diameter was used, maintaining a constant scallop height 0.2 mm in a spiral toolpath. The results were compared with ULisboa EXP #1, which utilized a 12 mm tool diameter and a 0.5 mm stepdown in a Z-level contour toolpath (Fig. 26).

The measurements were performed in an unclamped setup; therefore, comparing the minimum/maximum deviations is challenging. While the overall deviation

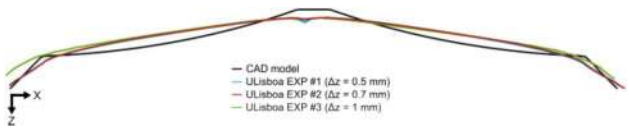

Fig. 24 Sectional comparison at y = −10 mm of the influence of step size on geometric accuracy for the first three single-stage experiments of ULisboa. The alignment is done with a best-fit on unclamped measurements

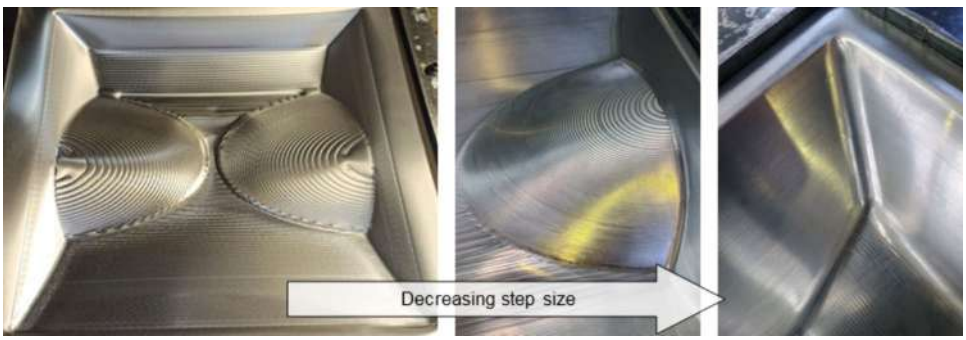

Fig. 23 The influence of the step size on the surface finish of the benchmark geometry. Decreasing step size leads to improved surface finish

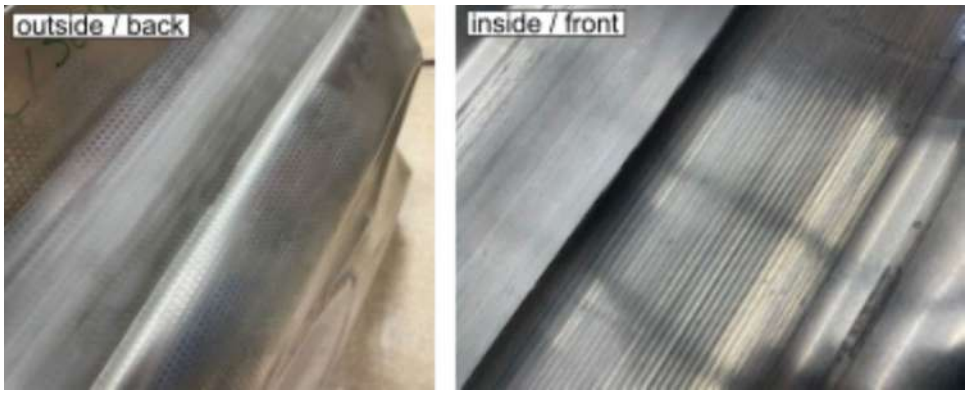

Fig. 25 Fracture (ULisboa EXP #1) observed at the discrete angle change between walls B and C, shown on the outside (left) and inside (right) of the formed part

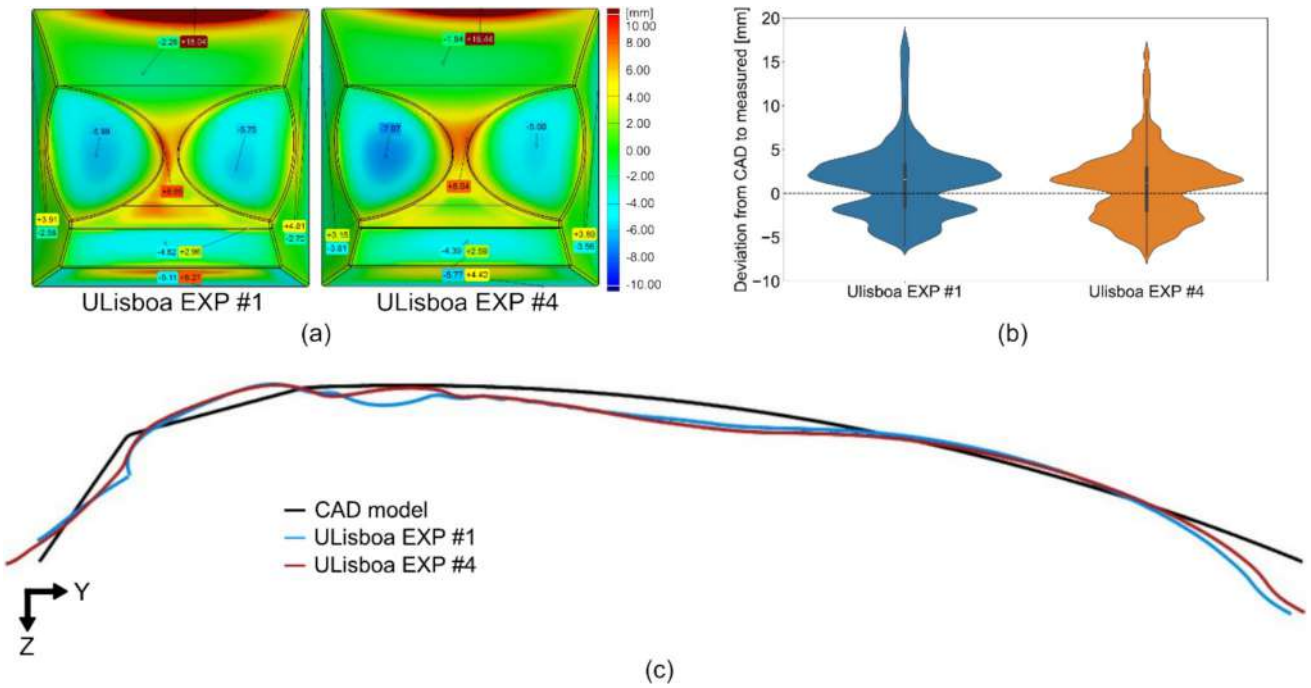

Fig. 26 (**a**) Resulting surface deviations to the CAD and (**b**) violin plots for ULisboa EXP #1, the experiment with a ø12 mm tool following a Z-level toolpath with constant stepdown of 0.5 mm and ULisboa EXP #4, 25 mm tool diameter with a constant scallop height of 0.2 mm following a spiral toolpath. (**c**) Cross-sectional profiles drawn at x = 0 mm compared to CAD. The alignment is done with a best-fit on unclamped measurements

Fig. 27 Pronounced pillow effect with visible toolpath marks (left) and fracture at the discrete angle change (right). Results from ULisboa EXP #1

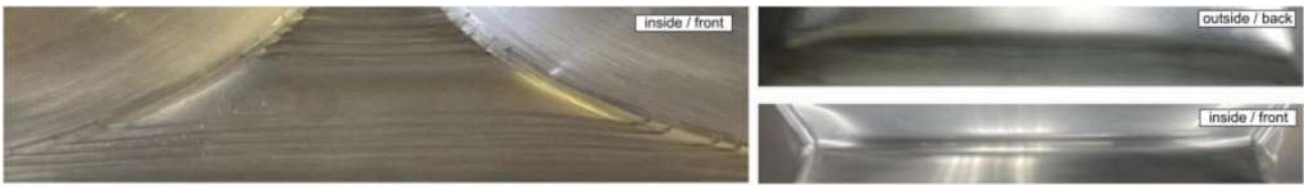

Fig. 28 Reduced pillow effect (left) without fracture at the discrete angle change (right). Results from ULisboa EXP #4

from CAD to measured geometry appears to be similar (Fig. 26), the pillow effect was significantly reduced in ULisboa EXP #4 compared to ULisboa EXP #1 (see Fig. 27 and Fig. 28). The smaller stepover used in the spiral toolpath with constant scallop width reduced indentation between parallel passes and led to less pronounced pillowing with improved surface finish. Additionally, the use of a larger tool helped prevent fracture in the transition at the angle changes (zones B and C) and alleviated the tent effect, as observed in the previous section. This approach highlights that the smaller step size can be combined with a larger tool diameter to prevent pronounced deviation in the critical zones while obtaining a superior surface finish.

In conclusion, a smaller step size minimizes scallop height and improves surface smoothness quality, but it increases processing time and may induce excessive strain hardening, leading to potential fractures. The absence of a universal trend in geometric accuracy suggests that step size must be optimized in conjunction with other process parameters to strike a balance between quality and efficiency.

Feed rate and spindle speed

As discussed in the state of the art overview in Sect."Process parameters", spindle speed directly impacts the final part's dimensional accuracy and surface quality. In this set of experiments, the influence of spindle speed with a different

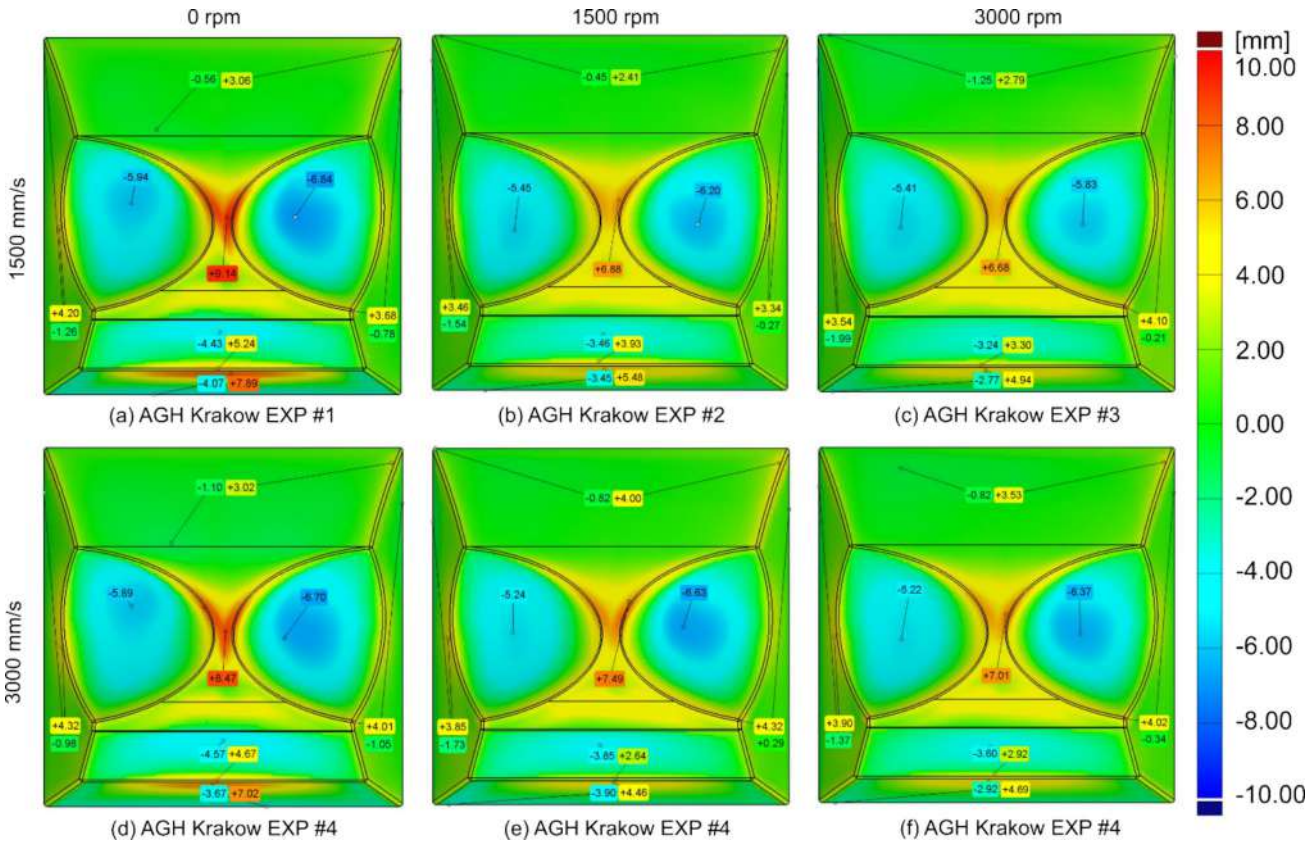

Fig. 29 Surface comparison on CAD geometry for AGH Krakow EXP #1 – EXP #6 with feed rates of 1500 mm/s and 3000 mm/s at spindle speeds of 0 rpm, 3000 rpm, and 6000 rpm. The alignment is done with a best-fit

feed rate was investigated for six case studies (AGH Krakow EXP #1 – EXP #6). The feed rates of 1500 mm/s and 3000 mm/s were tested in combination with spindle speeds of 0 rpm, 3000 rpm, and 6000 rpm after applying Teflon grease (PTFE) spray and lubricating with oil, prior to forming. The geometrical accuracy results, compared with the defined CAD geometry, are presented in Fig. 29.

As spindle speed increased from 0 to 3000 rpm, the inaccuracies in the critical zones, as highlighted in Sect."Process parameters"., were significantly reduced for both feed rates (1500 mm/s and 3000 mm/s). However, when the spindle speed further increased to 6000 rpm, the reduction in deviation was much less pronounced than the improvement observed between 0 and 3000 rpm. Additionally, the increase in linear velocity from 1500 mm/s to 3000 mm/s resulted in more significant overall deviations. The corresponding surface quality images for the same selected area are shown in Fig. 30.

In summary, both feed rate and spindle speed must be carefully selected to avoid extreme behavior. A feed rate of 1500 mm/s with a spindle speed of 3000 rpm showed improved dimensional accuracy and surface quality for this benchmark study by reducing friction and minimizing tool marks. For the specific size of the formed part used in this benchmark, heat effects appeared to be negligible during forming. However, these effects could become more significant in smaller parts or with different material systems.

Toolpath strategies

The definition of single-stage forming leaves some degrees of freedom for strategy optimization, as long as the entire benchmark shape is formed in a single pass, with no region of the sheet undergoing multiple forming steps, as shown in Fig. 31.

One common limitation of the conventional Z-level toolpath is its insufficient engagement in the waist region (zone D). Since the Z-level toolpath follows constant-height contours, it does not effectively process the horizontal surfaces in this region, leading to increased geometric deviations

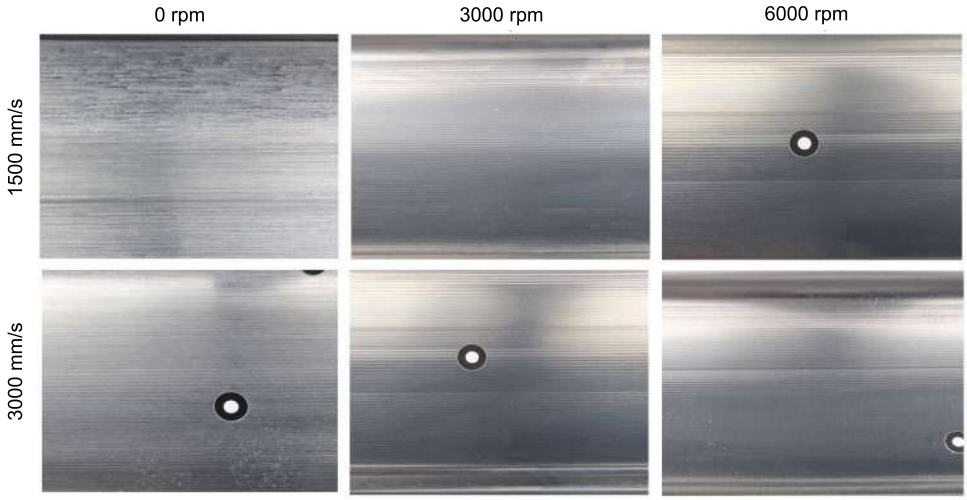

Fig. 30 Surface roughness for feed rates of 1500 mm/s and 3000 mm/s at spindle speeds of 0 rpm, 3000 rpm, and 6000 rpm

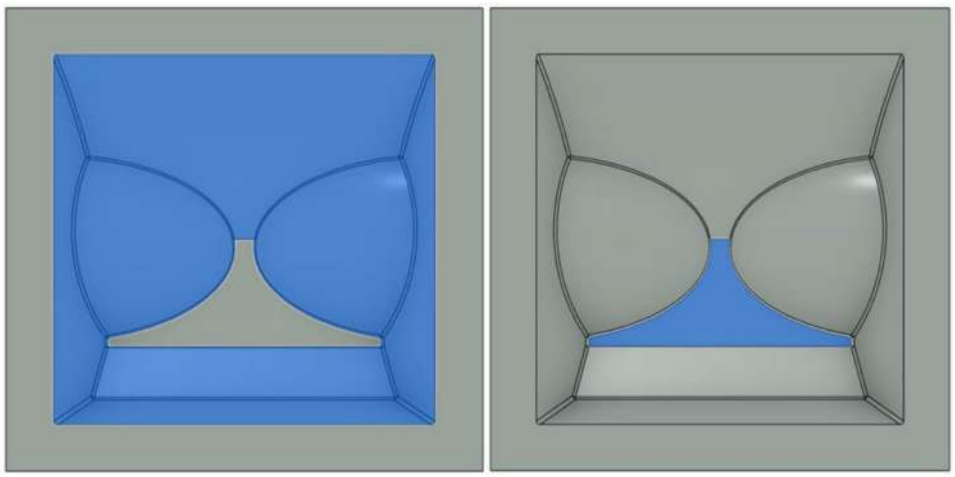

Fig. 31 Toolpath generation scheme of TUOS EXP #2 based on the differentiated features: Z-level toolpath for the non-flat area region combined with feature toolpath for the flat region

as result of the pillow effect. A comparative experiment was conducted to address this issue, where a conventional Z-level toolpath with a constant vertical stepdown of 0.2 mm (TUOS EXP #1) was compared with a modified strategy that splits up the toolpath depending on geometric features. In the modified approach, the entire geometry, except for the horizontal regions in zone D, was first formed using a Z-level toolpath with a constant stepdown of 0.2 mm. Afterwards, a feature toolpath with a constant scallop width of 1 mm was applied to form the horizontal area in zone D. The forming dimensions were scaled down to 260 mm × 260 mm to accommodate the experimental setup. The final formed parts and geometric deviations are compared and their cross-sectional profiles shown in Fig. 32.

The modified strategy not only reduced the inaccuracies in the critical zones but reduced the overall maximum and minimum deviations across the part, as can be seen in Fig. 33. This indicates that toolpath modification is more effective for achieving geometric accuracy than adjusting process parameters. Notably, this modification also introduced a star-shaped deviation in the flat area due to corner folds caused by the feature toolpath. These findings combined suggest that, while toolpath modifications can enhance geometric accuracy in critical regions, they may also introduce unintended shapes or distortions, requiring further refinement of the toolpath strategy. An alternative approach to mitigate this issue could be using a zig-zag toolpath instead of one that follows the outer boundary of the flat

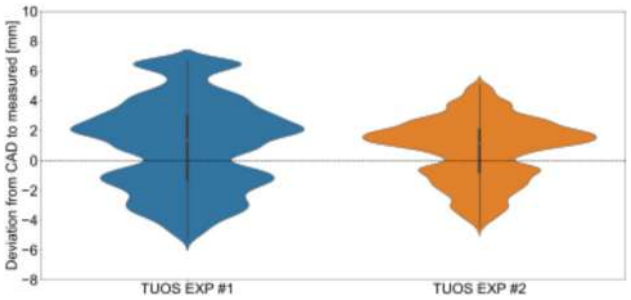

Fig. 33 Deviation distribution between CAD and measured geometry for TUOS EXP #1 and TUOS EXP #2. The alignment is done with a best-fit

area (see Sect."Toolpath strategies"). Due to the limitation of a single-stage strategy to address these issues, a more advanced approach through a multi-step strategy or another process variant is relevant and is detailed in Sect."Multi-stage SPIF".

Conclusion: single-stage SPIF

Multiple single-stage SPIF strategies were systematically tested and used as a baseline approach for forming the benchmark shape. Forming the workpiece in one stage enhances efficiency and simplicity, eliminating the need to revisit previously formed regions. However, as demonstrated by experiments across multiple institutions, persistent

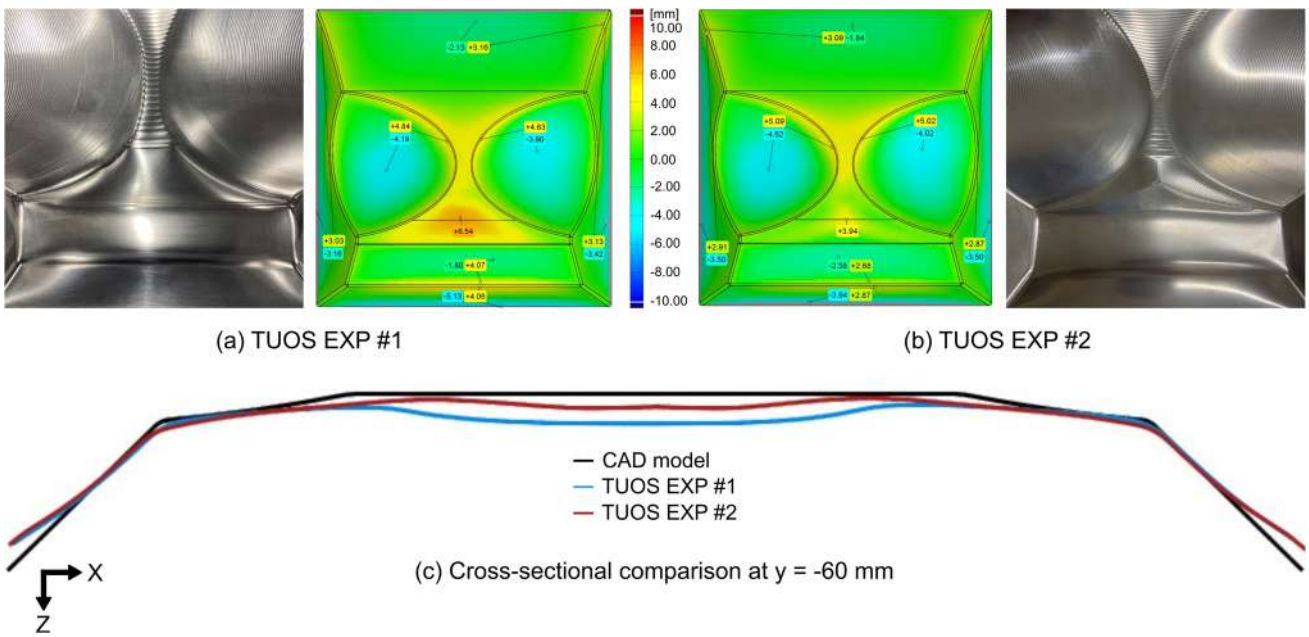

Fig. 32 (**a**) Formed part with resulting deviations to the CAD using a Z-level toolpath for the whole given geometry (TUOS EXP #1). (**b**) Formed part with resulting deviations using a modified strategy: Z-level toolpath applied to non-horizontal regions, with a separate toolpath adjusted for the horizontal area in zone D (TUOS EXP #2). (**c**) Cross-sectional profiles drawn at x = −60 mm compared to CAD. The alignment is done with a best-fit

Table 3 Summary of the observations in the single-stage SPIF baseline experiments conducted for this benchmark study

Effect to be reduced/improvement goal	Location	Observations
Tent effect	At discrete changes of wall angles (the transition zone between zones B and C)	Zone B and the transition with zone C is very susceptible to excessive thinning, even fracture occurred in some experiments
Pillow effect	At areas with low wall angles (zones D and E)	Due to the buildup of compressive stresses during forming, a bulge or pillow arises in areas that are supposed to stay (almost) flat
Inaccuracies at the edges	At the edges	A fold-like deformation arises at the edges between concave and convex areas. These corner folds are also a result of material accumulation and can be propagated across the waist section
Overforming	At concave areas (zone F) or close to the backing plate, at low curvatures and wall angles (zone E)	• The concave areas have the tendency to flatten out or even bulge outwards • Z-level and spiral toolpaths were not sufficient for countering this effect, so adaptive toolpaths might be needed
Increasing the overall geometric accuracy	Full geometry	Applying compensation was not possible, as this results in too steep wall angles that exceed the maximum wall angle, which results in failure

geometric inaccuracies remain, particularly in the concave zones where overforming poses a significant challenge. These issues highlight the limitations of a single-stage approach, where the absence of additional forming steps restricts corrective measures. A summary of the observations for some of the effects in these baseline experiments is provided in Table 3.

While modifications to process parameters such as tool diameter, step size, and spindle speed have led to improvements in geometric accuracy and surface quality, these adjustments alone are insufficient for addressing all deviations in the critical zones across the part. Toolpath modifications, including splitting up the toolpath and adjusting parameters based on geometric features, such as distinguishing between horizontal and non-horizontal areas, addressed some local inaccuracies but still fell short of achieving full geometric fidelity across the part. The influence of these process parameters on the observed outcomes is summarized in Table 4.

The primary goal of this benchmark study is to collect and share knowledge on optimizing geometric accuracy through testing various strategies. The findings emphasize

Table 4 Summary of the observations on the influences of process parameters in the single-stage SPIF baseline experiments conducted for this benchmark study

Process parameter	Observations
Tool diameter	The tool diameter has a very high influence on the geometric accuracy, with a larger tool (25 mm diameter instead of 10 mm diameter) performed significantly better. The larger tool resulted in a better surface finish and reduced bulging
Step size	• The surface finish improves when decreasing the step size, as the scallop width and height also decrease • However, a smaller step size also leads to longer forming times and may induce excessive strain hardening, which can lead to fracture • The absence of a universal trend in geometric accuracy suggests that the step size must be optimized in conjunction with other process parameters
Feed rate and spindle speed	• Both feed rate and spindle speed must be carefully selected to avoid extreme behavior • A feed rate of 1500 mm/s with a spindle speed of 3000 rpm showed improved dimensional accuracy and surface quality for this study by reducing friction and minimizing tool marks • Thermal effects were negligible in this study, but could become more significant in smaller parts or with different materials
Toolpath strategy	• Modified toolpath strategies are needed to ensure good surface finish in the areas with a very low wall angle, especially when applying a regular Z-level toolpath with constant vertical stepdown • Modifications include splitting up the toolpath and applying various step sizes based on the geometric features and wall angles of the part in that area • Other adaptations include applying a feature toolpath in (almost) flat areas. However, this also leads to corner folds

the need for additional processing steps, such as incorporating multi-stage strategies, which are discussed next, in Sect."Multi-stage SPIF", or alternative process variants, see Sect."Other ISF techniques", to achieve the desired level of accuracy and part quality.

Multi-stage SPIF

Even though multi-stage forming has been extensively discussed in literature, no clear definition of either single- or multi-stage forming has been established, as this was considered implicitly clear to most researchers and authors. However, in this study some strategies are proposed that cannot easily be allocated to either of the two categories, leading to the need for a non-ambiguous definition. Therefore, as stated in Sect."Multi-stage SPIF", we propose the definition of multi-stage forming as *incremental sheet forming where at least one area of the sheet is formed more than once*.

With such a definition in mind, this section examines multi-stage forming and its impact on the geometric accuracy of the proposed benchmark shape. It focuses on the effects observed in various zones of the benchmark shape, as illustrated in Fig. 1. The following sections, moreover, describe strategies that improve the effects described in Sect."Benchmark part"and address additional challenges encountered in multi-stage forming, such as expanding the process window and enhancing overall geometric accuracy. Lastly, all multi-stage experiments are compared to each other and to a single-stage strategy with a basic Z-level toolpath. While single-stage strategies are discussed in the previous section, some single-stage experiments are also revisited below as part of a comparison to a multi-stage variant. Lastly, recall that a best-fit approach was employed to ensure comparability of the results across institutes because not all institutes were able to align the measurements based on the clamping rig. Consequently, when comparing experiments across institutes, no conclusions can be drawn regarding process characteristics such as over- and underforming and springback.

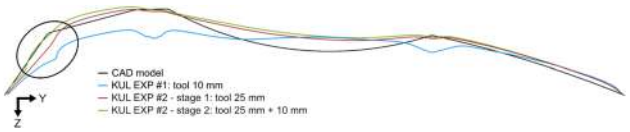

Fig. 34 Sectional comparison at x = 100 mm of the tent effect between zones B and C by investigating the influence of tool size. Three strategies are compared: forming the geometry with a single spiral toolpath using a ø10 mm tool (KUL EXP #1), the same toolpath with a ø25 mm tool (KUL EXP #2– stage 1), and a multi-stage combination with a ø25 mm tool in the first stage, followed by applying the same toolpath with a ø10 mm tool in the second stage (KUL EXP #2 – stage 2). The alignment is based on the clamping rig

Reducing the tent effect

As discussed in literature and in the corresponding section covering single-stage forming, the tent effect is highly influenced by the tool diameter and significantly decreases with increasing tool size. Figure 34 shows the influence of tool diameter on the tent effect, as well as the impact of multi-stage forming with a different tool size in each stage. Unexpectedly, the multi-stage combination of a spiral toolpath with a large tool, followed by a finishing toolpath with a smaller tool, leads to additional bulging in the middle of the flat wall of zone B (see KUL EXP #2 – stage 2 Fig. 34).

The tent effect can be further reduced by reprocessing the two walls using a workplane rotation, as shown in Fig. 35. However, this also leads to both more overforming in zone

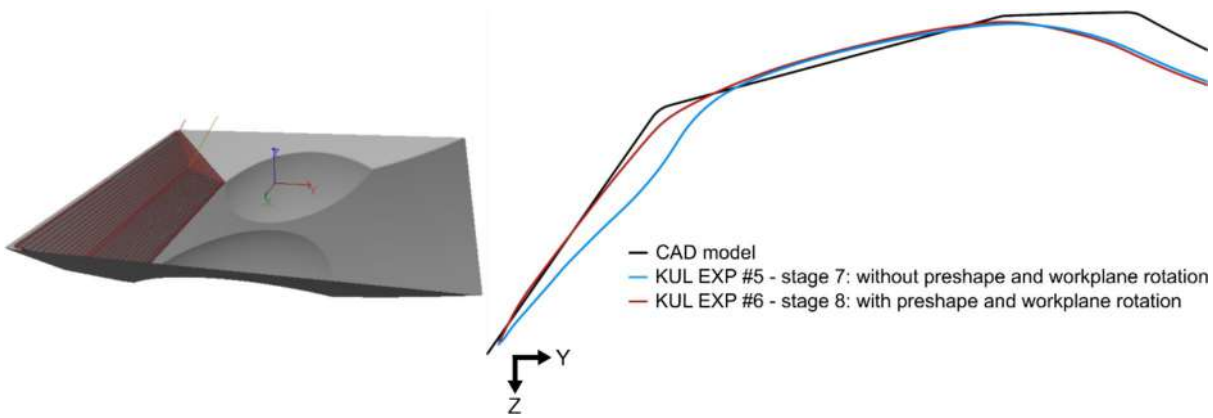

Fig. 35 Comparison of the tent effect between zones B and C without a preshape before forming zones B and C (KUL EXP #5 – stage 7) and with a preshape, after which these zones are processed again in a later step using workplane rotation (KUL EXP #6 – stage 8). The alignment is based on the clamping rig

B and a corner fold at the edge between the two walls, as this edge is now the final forming line of the additional toolpath.

Reducing the pillow effect

As discussed in Sects."Benchmark part"and"Geometric accuracy", the primary issue in the flat waist section (zone D) is the accumulation of material, leading to the pillow effect. The pillow effect is an unintended bulging of flat areas, typically at the bottom or base of a formed sheet part. The following sections explore various multi-stage strategies to mitigate these inaccuracies in zone D, focusing on process parameters, tool path strategies and intermediate shapes to achieve better geometric accuracy.

Increasing the tool diameter

As was described in conjunction with single-stage forming (Sect."Tool diameter"), a larger tool diameter reduces the pillowing or bulging effect. As can be seen in Fig. 36, a high deviation can be spotted in the middle of the waist section for KUL EXP #1 with a tool of 10 mm, where a corner fold at the edge between the concave and flat area propagated through the flat area. The experiments shown in this figure were conducted by means of a robotic arm, which has a lower stiffness than a typical CNC machining center frame. Due to this difference in stiffness, the propagation of the corner fold is more prominent with the less-stiff robotic arms than occurs with a CNC machining center frame.

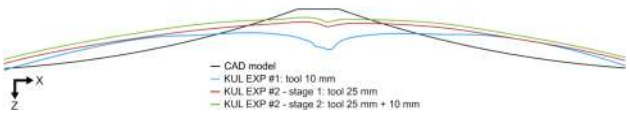

Fig. 36 Resulting deviations from the CAD geometry for KUL EXP #2 – stage 2, a multi-stage experiment using a spiral toolpath with a ø25 mm tool, followed by the same toolpath with a tool of ø10 mm, compared to the single-stage experiments that applied these two toolpaths separately (KUL EXP #1 and KUL EXP #2). The sections are taken at the location where the waist is the smallest, at y = −10 mm. The alignment is based on the clamping rig

While the 25 mm diameter tool (KUL EXP #2 – stage 1) improved geometric accuracy compared to the 10 mm tool (KUL EXP #1), it was too large for the edges and still resulted in underforming. Therefore, a second finishing pass with a smaller 10 mm diameter tool was applied after forming the part with a 25 mm diameter stylus (KUL EXP #2 – stage 2), as shown in Fig. 36. However, this approach of applying the same toolpath with a smaller tool in a second stage did not significantly reduce the pillow effect and even led to additional unwanted deviations due to rigid body motion.

Another approach, where an intermediate stage is added with a large diameter tool, was investigated by Fraunhofer IWU and Chemnitz University of Technology. In this experiment, the blank is pre-stretched by pushing it 22 mm in the negative Z-direction in the middle of the geometry (at x = 0 and y = 0), using a large 60 mm diameter tool with a rubber pad in the contact area between forming tool and sheet (see Online Resource 3). After this global pre-stretching stage, the measured depth in the middle of the sheet due to the stretching step was 5 mm. In the second stage, the geometry was formed with a 30 mm diameter tool, as illustrated in Online Resource 3. The results of this multi-stage experiment (Fraunhofer EXP #2, Fig. 37 (b)) were compared to a similar experiment without the pre-stretching stage (Fraunhofer EXP #1, Fig. 37 (a)). Figure 37 indicates that Fraunhofer EXP #2, the multi-stage strategy with a pre-stretching intermediate stage, which also involved changing the toolpath in zone D from a feature toolpath to a zig-zag toolpath (see Online Resource 3), enhanced geometric accuracy in zones D and E. The star-shaped deviations in zone D in Fig. 37 (a) are corner folds due to the feature toolpath and are discussed

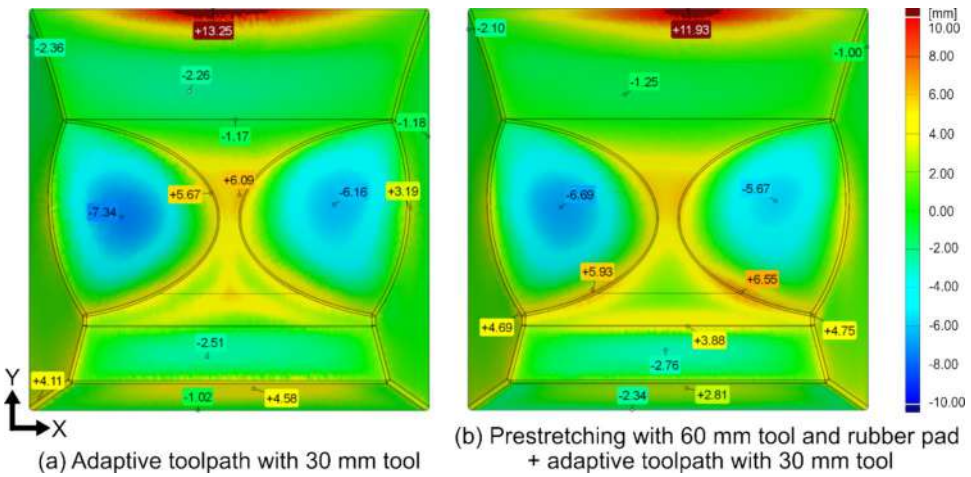

(a) Adaptive toolpath with 30 mm tool

(b) Prestretching with 60 mm tool and rubber pad + adaptive toolpath with 30 mm tool

Fig. 37 Resulting deviations from the CAD geometry for (a) the experiment with a ø30 mm tool following a spiral toolpath with different step sizes (Fraunhofer IWU EXP #1) and (b) the multi-stage experiment where, before forming the previous experiment, an intermediate stage is performed with a ø60 mm tool and a rubber pad (Fraunhofer IWU EXP #2). The alignment is done with a best-fit

in Sect."Reducing corner folds and inaccuracies at the edges", which addresses inaccuracies at the edges.

Adapting the toolpath

In conventional ISF, toolpaths typically follow the contours of the shape at each Z-level, gradually forming the part by tracing its outer edges. However, in the **area-filling Z-level toolpath**, the entire sheet surface within the shape boundary is progressively formed at each height level, rather than just the perimeter. This strategy treats the part as if it were a solid being milled, ensuring that both the outer edges and the internal regions are incrementally shaped within the XY-plane at each Z-level and leads to reduced forming forces compared to regular Z-level or spiral toolpaths. This approach was necessary, as the conventional Z-level or spiral toolpaths in a single-stage approach led to forming forces that were too large for the setup at Lucian Blaga University of Sibiu. Using this approach, instead of relying solely on the vertical stepdown to define the forming resolution, an additional horizontal step size, or scallop width, is used to control the spacing between adjacent tool passes in the XY-plane. By repeatedly forming the entire inner area multiple times at each Z-level, this approach can be considered a multi-stage forming process, where each Z-level pass represents an incremental forming stage. Figure 38 shows that, in this case, slightly larger values for the vertical stepdown and horizontal scallop resulted in a higher overall geometric accuracy.

Invoking segmentation for intermediate shapes

Another possibility to avoid the formation of corner folds caused by material accumulation and to eliminate the instabilities at the waist section is segmenting the part into left and right sides, thus avoiding the hourglass shape within a tool contour. The first intermediate shape is designed by cutting two planes through the shape, as shown in Fig. 39 and detailed in Online Resource 3. This method allows the corners to be easily formed using a workplane rotation, ensuring the toolpath starts from the already formed edges and maintains contact with the already formed sheet. A small overlap is chosen to ensure the sharp edges of the first intermediate shape are reprocessed. In these initial segmentation steps, a preshape with a lower wall angle between zones B and C is used to avoid formability issues when compensating the part in later experiments. After the segmentation (stages 1–5 in Fig. 39) and the additional step to form the two walls (step 6), backside forming of the concave areas (zone F) is applied to undo the overforming. Figure 40 shows the resulting deviations compared to the single-stage experiment with the same tool size. Measurements show that the proposed strategy significantly improves geometric accuracy at the waist section, primarily by reducing the bulging effect. By making the tool contours in the first forming step rectangular instead of the hourglass shape, the bulging or corner folds at the edges around the concave areas are no longer propagated to the waist section.

Multiple passes over specific areas

To improve the geometric accuracy at the waist section, the University of Palermo employed a multi-stage strategy

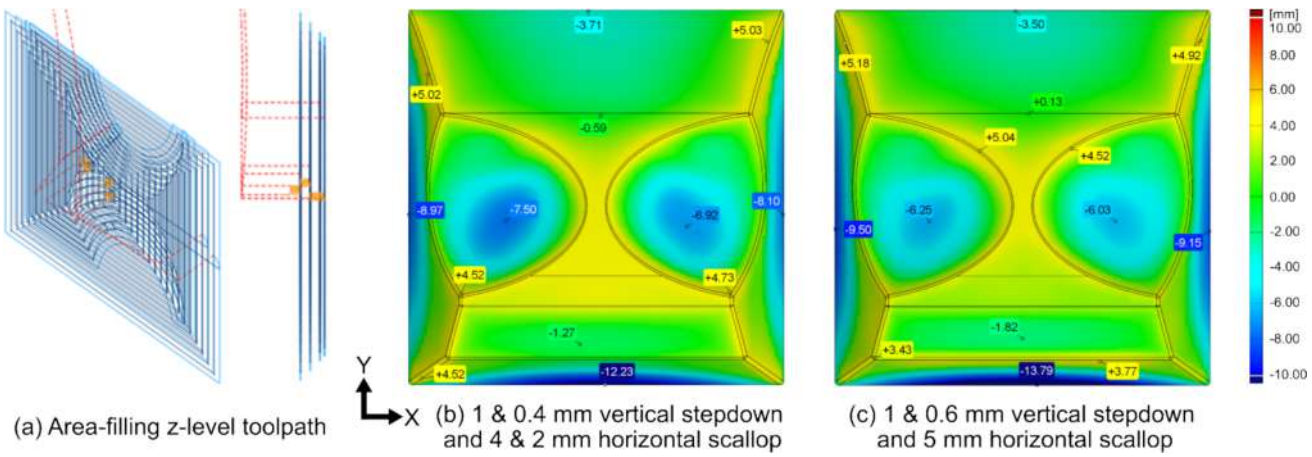

Fig. 38 (**a**) Area-filling Z-level toolpath and the resulting deviations from the CAD geometry after forming the sheet with (**b**) a vertical stepdown of 1 mm and horizontal stepover of 4 mm and respectively 0.4 and 2 mm in the flat area (LBUS EXP #1) and (**c**) a vertical stepdown of 1 mm and horizontal stepover of 5 mm up to half the full depth of the part and respectively 0.6 and 5 mm afterwards (LBUS EXP #2). The alignment is done with a best-fit

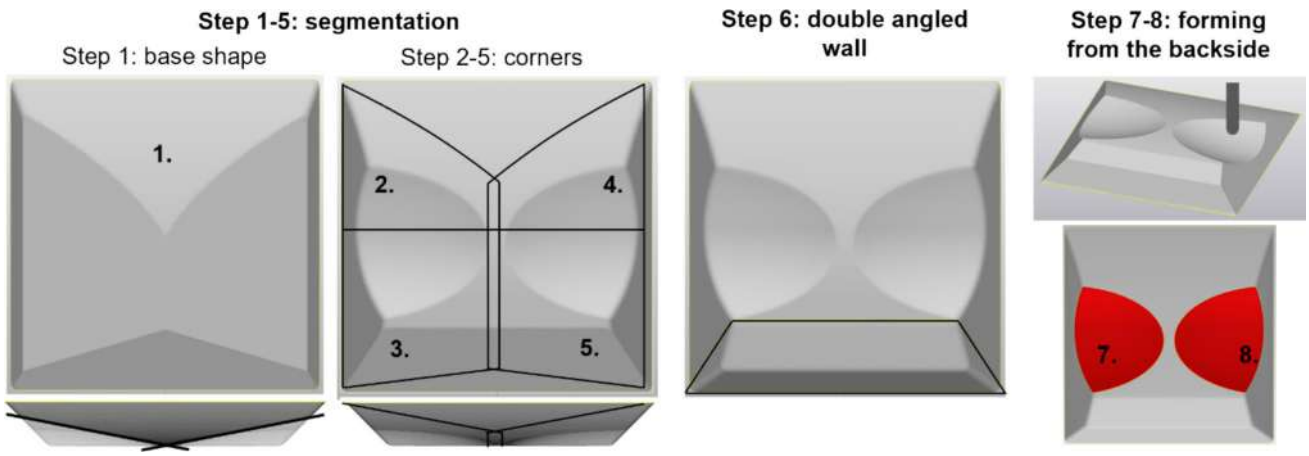

Fig. 39 Strategy for the experiment based on segmentation with backside forming (KUL EXP #6). All parameters and the toolpath strategies are further described in Online Resource 3

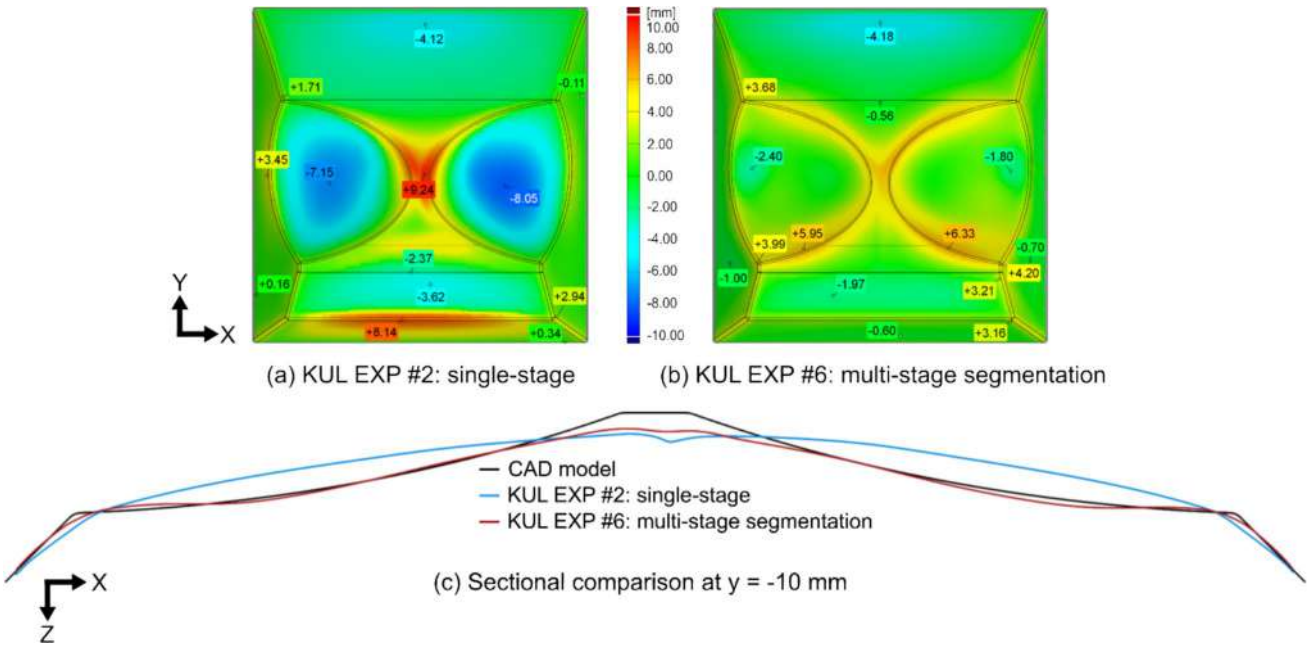

Fig. 40 Resulting deviations from the CAD geometry for (**a**) the single-stage experiment with a ø25 mm tool (KUL EXP #2 – stage 1) and (**b**) the multi-stage experiment based on segmentation with a ø25 mm tool (KUL EXP #6 – stage 8). The cross-sections are taken at the location where the waist is the smallest, at y = −10 mm and the alignment is based on the clamping rig

consisting of three stages: two spiral toolpaths and one projected spiral toolpath. The first stage involves a regular spiral toolpath. After that, a spiral toolpath with an offset in the negative Z-direction, applied only on zones D and E, and a **projected spiral toolpath** on zones B, C, D, and E are applied. This final, projected spiral toolpath is constructed as a spiral in the XY-plane, which is then projected along the Z-axis onto the 3D shape to be formed. This differs from the regular spiral toolpath as discussed in Sect."Toolpath strategies", as it is not a contouring toolpath based on Z-levels with interpolation, but a surface covering toolpath that also forms horizontal areas. Hence, a tool contour does not necessarily stay within a small Z-level interval, but follows the Z-heights of the shape. Two experiments were conducted to study this multi-stage strategy: both started with the same initial spiral toolpath, followed by the two stages described above, but for the second experiment, stages 2 and 3 were switched. In the first experiment, the stages were conducted as outlined above, with an offset of 4 mm in the second stage to compensate for the springback. In the second experiment,

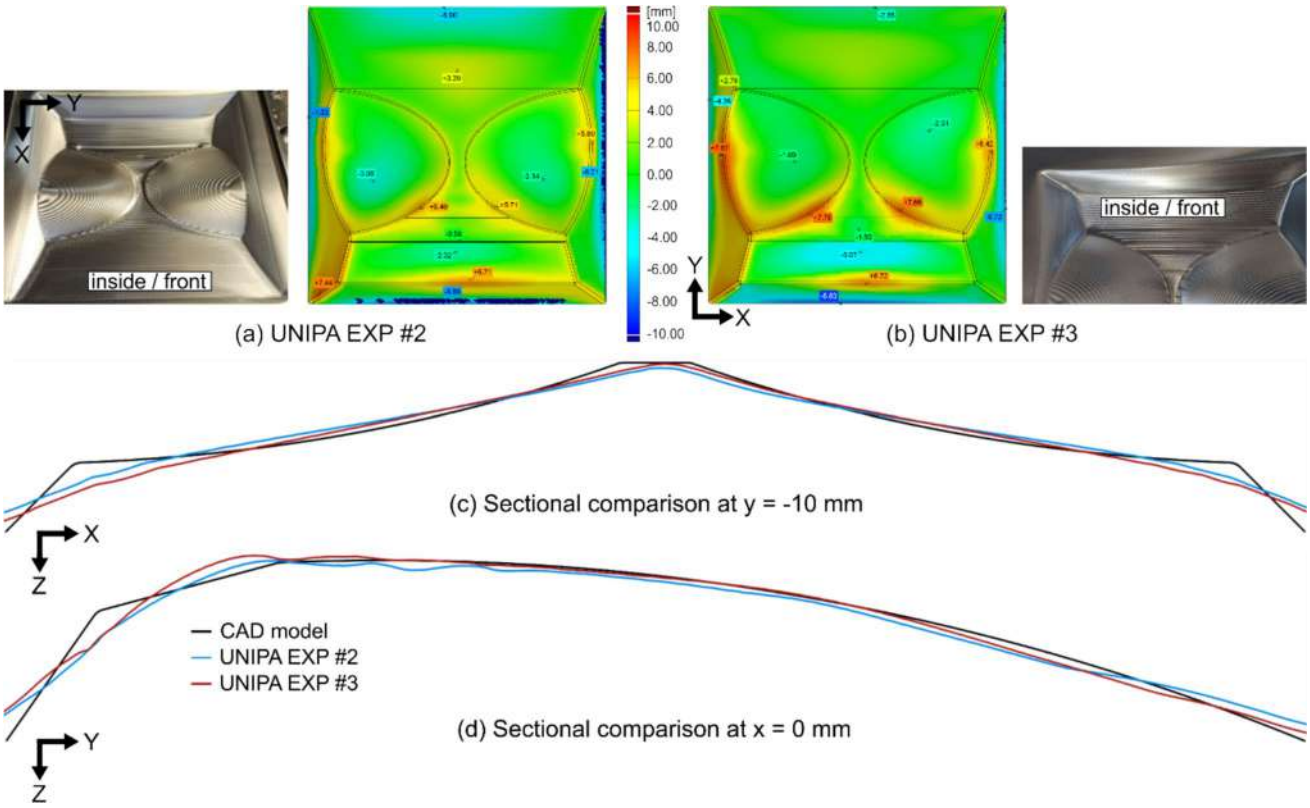

Fig. 41 Resulting deviations from the CAD geometry and surface finish for (**a**) the spiral – spiral – projected spiral (UNIPA EXP #2) and (**b**) the spiral – projected spiral – spiral strategy (UNIPA EXP #3) and (**c**) a sectional comparison at y = −10 mm. The alignment is done with a best-fit

steps 2 and 3 are switched and the offset of the spiral toolpath focusing on zones D and E was increased to 8 mm in the negative Z-direction based on the geometric accuracy (after a best-fit alignment) observed in the previous experiments. This strategy and the parameters are detailed in Online Resource 3. The deviations observed in Fig. 41 indicate improved geometric accuracy in the waist section but a much higher deviation at the edges of the concave areas.

Other strategies to minimize the pillow effect

Another common issue with flat areas is the high pillow between the tool contours (see Fig. 17) when using a conventional Z-level or spiral toolpath with constant vertical stepdown. To address this, a constant scallop width or height can be chosen instead, based on the smallest wall angle at each Z-level section. Other options include using a local zig-zag (e.g., Fraunhofer IWU EXP #2 and ULisboa EXP #8 and EXP #9) or a feature toolpath in the flat area. However, the latter may result in sharp direction changes within the flat area, leading to corner folds as a result of the pillow effect, as discussed later in Sect."Reducing corner folds and inaccuracies at the edges"on inaccuracies at the edges. To correct overforming, backside forming can be applied on specific areas. The University of Calabria, for example, used an additional backside forming stage to correct the overforming. Figure 42 shows the geometric deviations before and after this additional backside forming stage using a zig-zag toolpath on zones D and E. By this backside forming step, they managed to decrease the mean absolute deviation (after alignment with a best-fit) from 1.42 mm to 1.13 mm.

Additionally, a large overforming due to bulging was observed in all experiments in zone E, more specifically, the area with a low wall angle and a slight curvature, close to the clamping. A possible strategy to decrease the deviation is by applying an additional forming stage from the back. Figure 42 also shows that the backside forming step significantly increases the geometrical accuracy in the areas close to the edges of the benchmark shape. RWTH Aachen used zig-zag toolpaths to reduce the pillow effect and concluded that forming from flat to steep wall angles (from zone E towards zone B) helps to guide material distribution away from areas with low wall angles, which are prone to the pillow effect, as ISF tools push material in the forming direction. Their experiments are further described in Sect."Reducing overforming in concave areas".

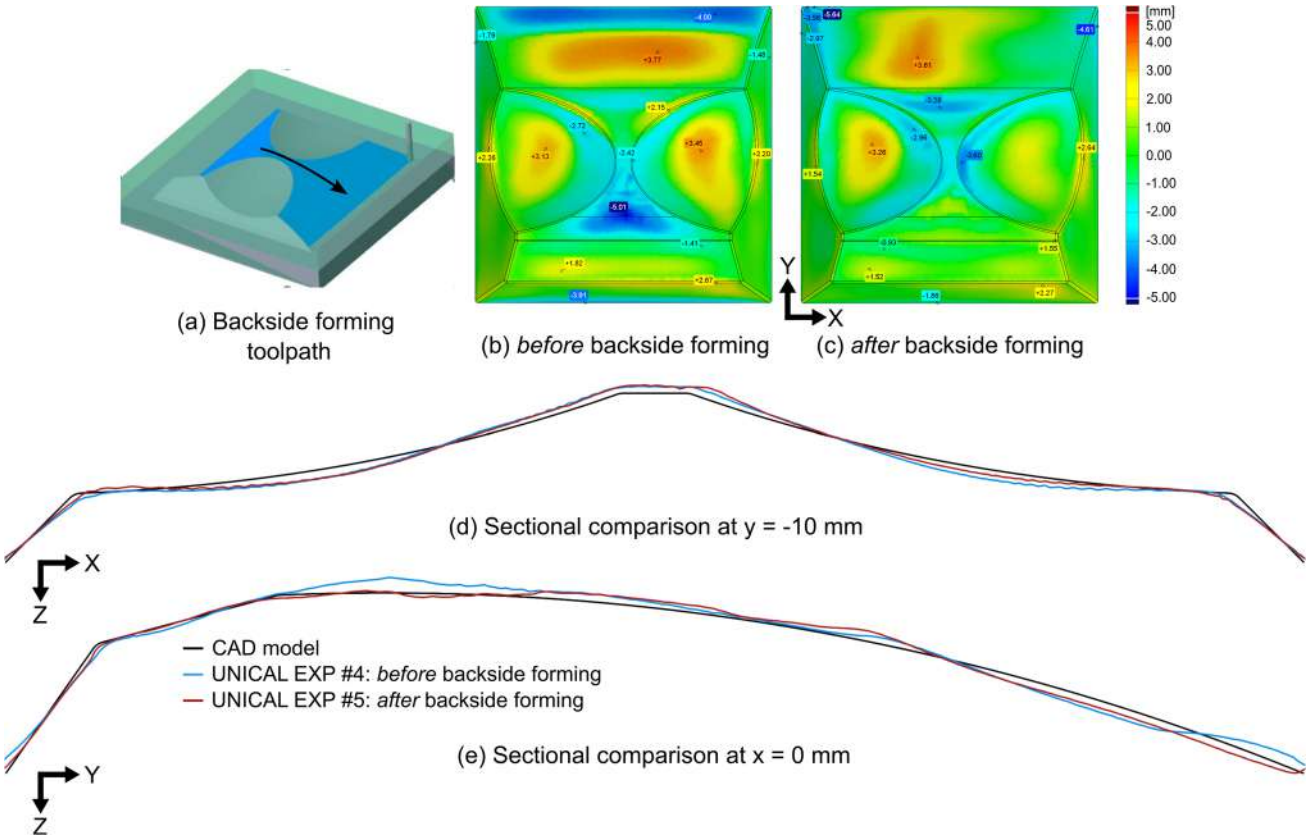

Fig. 42 (**a**) Zig-zag toolpath used for the backside forming stage and resulting deviations from the CAD geometry (**b**) before and (**c**) after applying an extra step of backside forming on zones D and E for, respectively, UNICAL EXP #4 and EXP #5. (**c**) and (**d**) show cross-sectional comparisons at y = −10 mm and x = 0 mm. The alignment is done with a best-fit

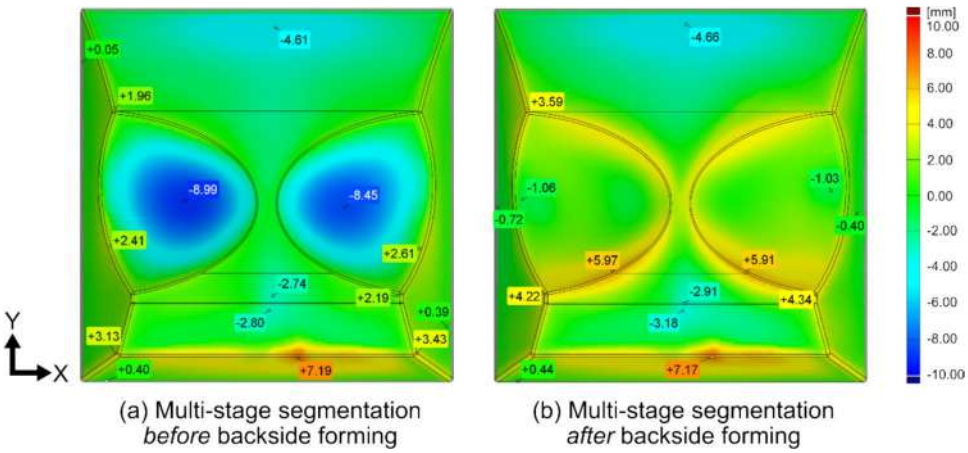

Fig. 43 Resulting deviations from the CAD geometry for (**a**) multi-stage experiment before the backside forming step on the concave areas, zone F (KUL EXP #4 – stage 5) and (**b**) the same experiment after backside forming (KUL EXP #4 – stage 7). The alignment is based on the clamping rig

Reducing overforming in concave areas

The highest overforming in the single-stage experiments was always observed in the concave zones and can be tackled using several strategies. One of the most straightforward options is adding an additional stage to form these areas from the backside, as discussed in Sect."Other strategies to minimize the pillow effect"and"Reducing overforming in concave areas". Figure 43 shows the deviations from the desired shape for KUL EXP #4 before and after backside forming (respectively stage 5 and 7). As the deviations are calculated after aligning the measured shape with the clamping rig instead of using a best-fit, the overforming (blue) and underforming (red) of the process can be studied. As

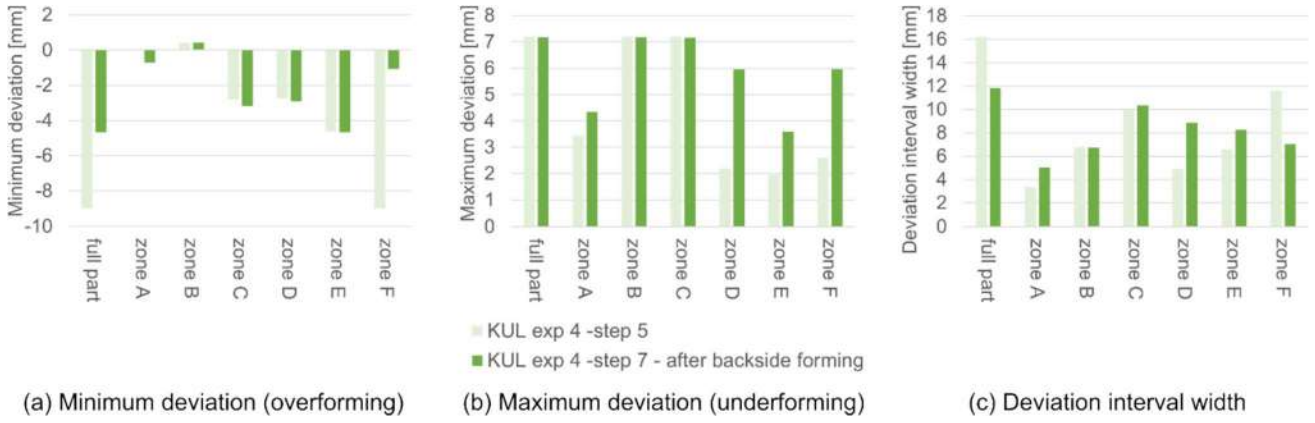

Fig. 44 Comparison of (**a**) the maximum overforming, (**b**) the maximum underforming, and (**c**) the interval range between the two maximum deviations for all zones, before (KUL EXP #4 stage 5, light green) and after (KUL EXP #4 stage 7, dark green) the backside forming stage on the concave areas (zone F). The alignment is based on the clamping rig

can be seen, the backside forming of the concave areas significantly reduces the overforming in these areas (zone F). However, this also leads to more underforming (red) at the edges of the concave areas. Figure 44 shows the maximal over- and underforming in each zone, as well as the difference between the two, the deviation width. These graphs clearly show a significant reduction of the maximal overforming in the affected concave areas, but also an increased maximal underforming in the formed area and surrounding areas (zones A, D, E, and F) due to rigid body motion. The difference between the maximal under- and overforming is shown as the deviation interval width in Fig. 44 (**c**), which also shows decreased deviations in the reprocessed concave areas (zone F) but an increase in the surrounding zones A, D, and E. However, the geometric accuracy of the full workpiece increases, with a lower deviation interval after backside forming.

One of the strategies in which the concave areas were formed from the back used a double-layer toolpath. This was done to avoid creasing or cracking in this step, as the maximum overforming before the backside forming stage was more than 4 mm for a 300×300 mm workpiece. After constructing a streamline toolpath that starts at the waist area and ends at the sides (zone A), the same path is added with an offset of 2 mm in the positive Z-direction (away from the sheet) and can be seen as an additional intermediate forming stage with an offset from the desired geometry, see Fig. 45. Other experiments also applied a backside forming step with more overforming than the experiment described above, but these did not experience the cracking or creasing that was observed here. This might be due to the difference in tooling or setup, as a larger tool reduces the effect and eliminates the need for this double-layer toolpath.

Backside forming shows to be an effective way to reduce the overforming in concave zones. However, not all setups allow for turning the sheet 180 degrees without unclamping the part. Another possibility to increase the geometric accuracy in the concave areas was investigated at RWTH Aachen. In one of their experiments, RWTH EXP #12, they formed the part using three intermediate shapes constructed by offsetting the geometry towards the inside with 30, 10, and 4 mm and applied a bidirectional Z-level toolpath to them. The fourth or final forming step was done on the desired benchmark geometry with a zig-zag toolpath. In a second experiment, RWTH EXP #13, a fifth finishing stage was added on top of the strategy of EXP #12 by reprocessing the edges, which is also discussed in the next section. A third experiment, RWTH EXP #15, was conducted with the addition

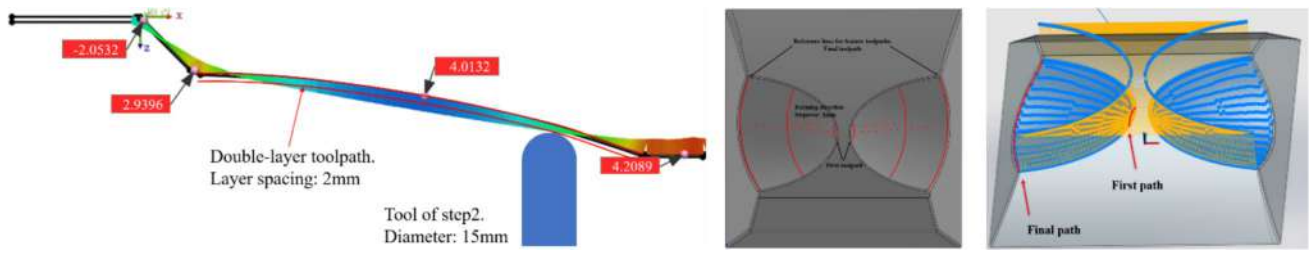

Fig. 45 Visualization of the double-layer toolpath for the backside forming stages of SDU EXP #1

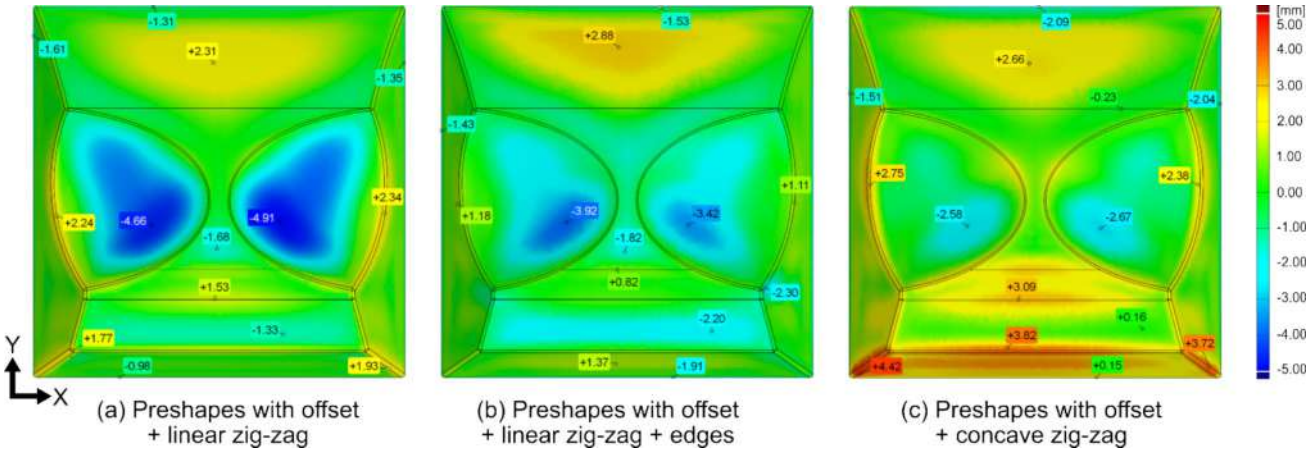

Fig. 46 Resulting deviations from the CAD geometry for (**a**) RWTH EXP #12, (**b**) RWTH EXP #13 (the same experiment with a finishing pass of the edges as a fifth step) and (**c**) RWTH EXP #15, a multi-stage experiment with part-stock in the first three steps and a concave zig-zag path in the fourth. The alignment is done with a best-fit

of a concave curvature on the zig-zag toolpath in the fourth forming step. The results after aligning the measurements using a best-fit can be seen in Fig. 46. With mean absolute deviations of 1.16 mm, 0.90 mm, and 1.53 mm, respectively, RWTH EXP #13 with an additional finishing step on the edges performs significantly better than the other two. Even though EXP #15 led to better results for the concave areas in zone F, a higher tent effect at the transition between zones B and C can be observed (Fig. 46 (c)).

Another institute, the University of Lisbon, reduced overforming in the concave areas by applying a 10 mm offset towards the inside of both concave areas (zone F). They applied this compensation in their first forming stage of ULisboa EXP #9, using a counterclockwise spiral toolpath. In the next stage, the desired geometry was formed with a spiral toolpath in the opposite direction (clockwise), followed by a reprocessing (third) stage of the flat area in zone D with a zig-zag toolpath. The final stage consisted of edge finishing with a smaller tool of 12 mm diameter. The effect of the offset in the concave areas is evident in the cross-section at x = 100 mm (Fig. 47). However, this approach also resulted in visible edges due to corner folds, a phenomenon that is discussed further in the next section.

Reducing corner folds and inaccuracies at the edges

This section closely examines two observed problems: edge inaccuracies and corner folds [14].

Increasing the geometric accuracy at the edges

As mentioned before, the geometric accuracy improves with increasing tool diameter. The downside, however, is that this reduces the accuracy at the edges, as the tool radius is larger than the desired edge rounding. As discussed in Sect."Reducing the tent effect"and shown in Fig. 34, adding

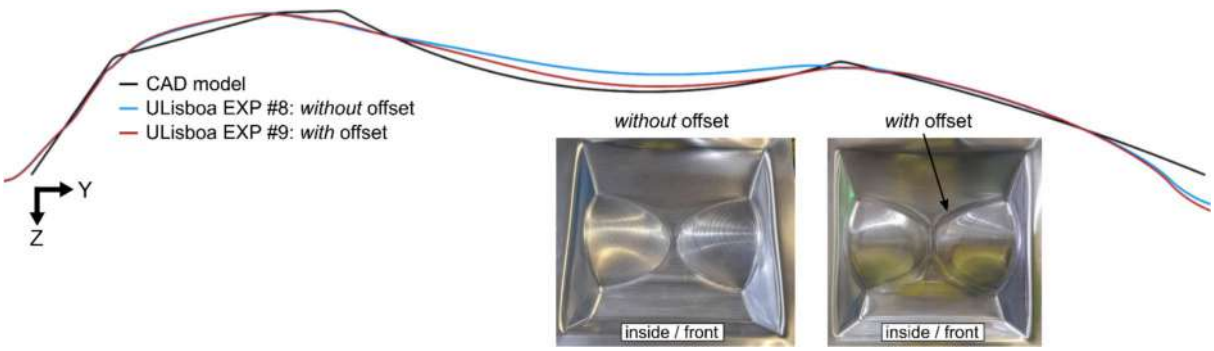

Fig. 47 Cross-sectional comparison at x = 100 mm and the surface finish of the final workpieces for the multi-stage experiment without (ULisboa EXP #8) and with (ULisboa EXP #9) an offset of 10 mm in the concave areas (zone F) in the first forming stage. The alignment is done with a best-fit

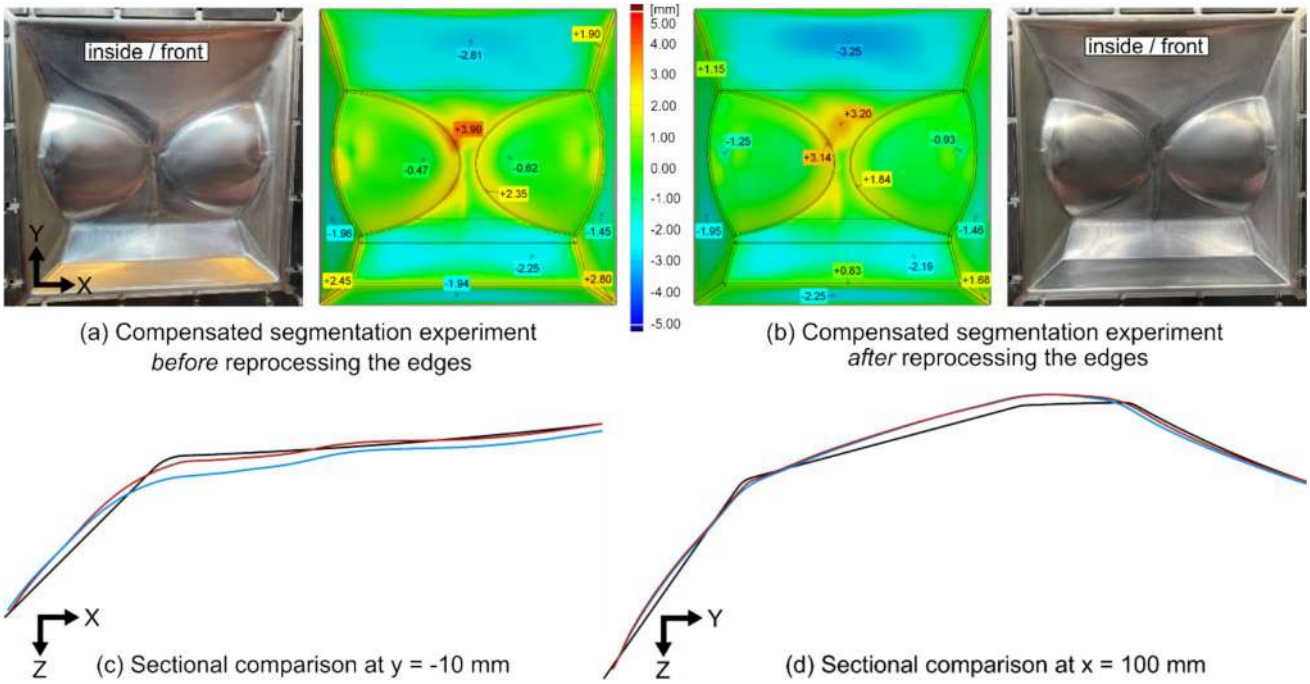

Fig. 48 Resulting deviations from the CAD geometry for the multi-stage segmentation experiment with compensation (KUL EXP #6 Compensated) (**a**) before (stage 8) and (**b**) after an edge finishing step with a ø10 mm tool (stage 9). The alignment is based on the clamping rig. (**c**) and (**d**) show cross-sectional comparisons at y = −10 mm and x = 100 mm. The alignment is done with a best-fit

a finishing step on the full shape with a tool of smaller diameter does not significantly improve the final geometry and even results in more rigid body motion. However, reprocessing only the edges with a smaller tool does help in achieving higher accuracy. This leads not only to a higher accuracy at the edges, as can be seen in Fig. 48, but also slightly less underforming and more overforming in other areas, due to rigid body motion.

Another creative solution to increase the accuracy of the edges is by first forming the edges in 2D to crease the sheet. This strategy is inspired by origami and cardboard forming, as a way to decrease the local stiffness and induce local deformations by applying the transition lines before forming the workpiece. The experiments were done on a smaller scale than the proposed one, with dimensions of 200 × 200 mm instead of the default 400 × 400 mm, as well as on a micro-scale of 20 × 20 mm. When comparing the single-stage spiral toolpath with the multi-stage experiment using 2D sheet creasing, the 2D edge tracing showed an increased geometric accuracy in the waist area (zone D) on the micro-scale level, see Fig. 49. On a larger scale of 200 × 200 mm, no significant effect between the single- and multi-stage experiments could be observed. Unfortunately, only the two-stage experiment with edge tracing before forming was repeated in full scale (400 × 400 mm), and no comparison to the single-stage experiment can be made on this larger scale. Hence, the micro-forming results show the potential of edge tracing before forming the part, but this effect should be further studied and optimized on a larger scale.

Reducing inaccuracies due to corner folds

As discussed before, this defect results from excessive material accumulation, resulting in extreme and localized bulging when systematic directional changes in feature toolpaths result in discontinuities in the material displacement. During the experimental campaign of this study, these corner fold effects were not only observed at the edges of the formed workpiece, but also at sharp direction changes of the toolpath in a relatively flat geometrical area, mostly in the feature toolpaths (Fig. 50 and Fig. 51). Hence, sharp direction changes induce material accumulation at these toolpath corners and result in a bulging effect, which shows as sharp corner folds in areas that have a very low curvature.

Unfortunately, even after applying toolpaths on top of the formed corner folds, the desired action of completely unforming them cannot be achieved. Even though the edges from previous steps are not always clear in the final deviation plots, they are still visible to the human eye (Fig. 52) and are clearly visible when comparing the thickness distributions (see Sect."Process window").

In conclusion, corner folds are very difficult to remove and should therefore be avoided. The key to this is

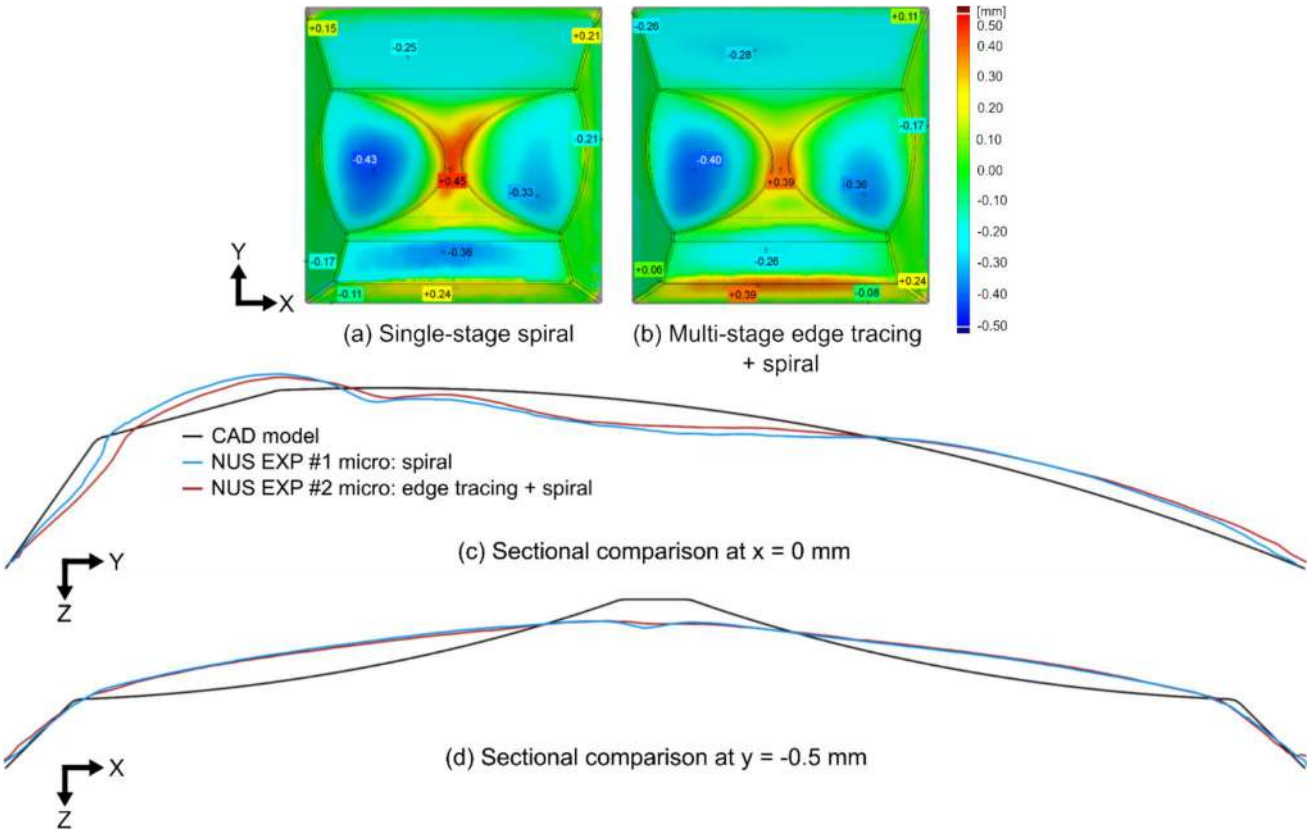

Fig. 49 Resulting deviations from the CAD geometry for the experiments at NUS on a micro-scale (20×20 mm) (**a**) without (NUS EXP #1 micro) and (**b**) with 2D edge tracing before applying a spiral toolpath (NUS EXP #2 micro). (**c**) and (**d**) show cross-sectional comparisons at x = 0 mm and y = −0.5 mm. The alignment is based on the clamping rig

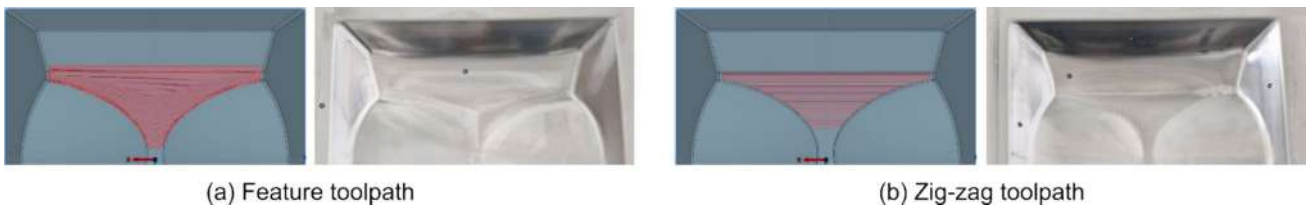

Fig. 50 Corner folds due to the pillow effect showing at sharp tool direction changes in the (**a**, **c**) feature toolpath strategy versus the (**b**, **d**) zig-zag toolpath for Fraunhofer IWU EXP #1 and #2

minimizing sharp changes of direction (mostly smaller than 90 degrees), both across tool contours and within one tool pass, as is often the case in feature toolpaths. Hence, alternative strategies, such as zig-zag toolpaths, should be used. In the first stage of the segmentation experiments from KU Leuven, the corner folds were significantly reduced by having a rectangular-shaped tool contour at a certain Z-level instead of an hourglass shape. By reducing the pillow effect, for example by increasing the tool size, the corner fold deviations also decrease.

Influence of the scale effect

As a promising experiment on a smaller scale, the strategy proposed by Shandong University showed successful results with a part size of 300×300 mm. However, when scaling up to the full dimensions of 400×400 mm – conducted at KU Leuven with the same tool size and machine type (a KUKA robot arm) – failure occurred during the fourth forming stage. This failure took place at the location of the inward fold formed in the first forming stage. In the second and third forming stages, the concave areas (zone F) were respectively

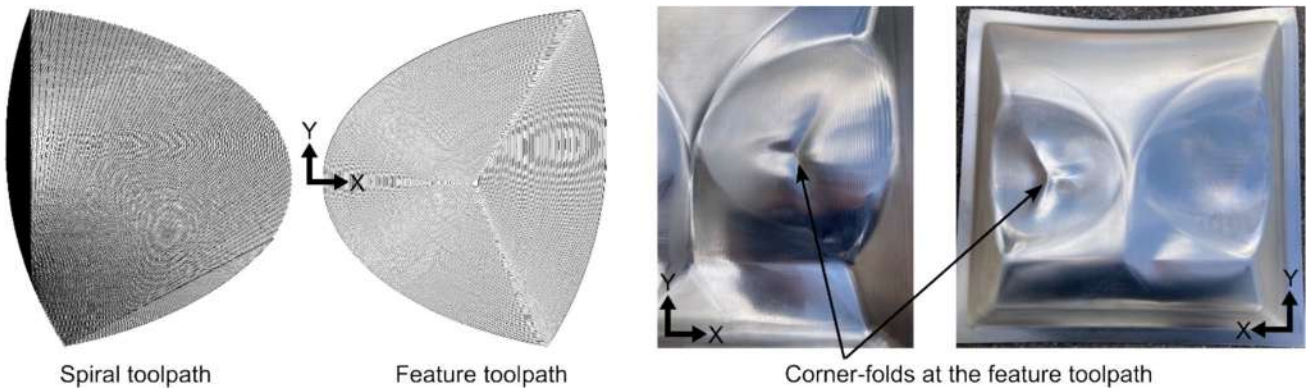

Fig. 51 Corner folds due to the pillow effect arise at sharp tool direction changes in the feature toolpath, compared to the regular spiral toolpath (KUL EXP #3 – stages 7 and 8)

Fig. 52 Edges formed in previous steps are, even after forming the area again, still visible in the final shape

formed from the backside and the waist area (zone D) was formed again with a zig-zag toolpath. However, in the fourth forming stage, the steep wall in zone B was also reprocessed with a zig-zag toolpath, moving from the edges of the CAD model toward zone C. This approach led to material accumulation and rigid body motion toward zone C, which was halted at the inward fold due to the stiffness of the already formed part (Fig. 53). As a result, failure occurred at this already formed fold.

This experiment highlights that, when scaling up, using the same toolpath and tool size can amplify unwanted effects, leading to failure. Therefore, further research is needed to determine appropriate scaling strategies for tool size and step size in relation to part dimensions.

Process window

As extensive material stretching results in failure of the part, a multi-stage approach can be used to enhance the process limits by improving the material distribution and thereby avoiding failure. In order to avoid failure in the steep wall of zone B, or increase the geometric accuracy as discussed in Sect."Reducing the tent effect"about the tent effect, an intermediate shape with a lower wall angle can be used. Multiple institutes did this independent of each other. The influence of this preshape on the wall angle is visualized in Fig. 54, where the part formed without a preshape showed the highest thinning at the wall of zone B, which leads to failure in this area when applying mirror compensation. When using an intermediate shape with a lower wall angle and applying a toolpath with workplane rotation to form the two walls of zones B and C, however, the thicknesses are much more uniformly distributed in these areas. Conversely, the two triangular areas at each side of zone A show a high decrease in material thickness when using the preshape.

Increasing the overall geometric accuracy with compensation

As described in Sect."Compensation strategies", the most commonly used compensation strategy, referred to as mirror compensation, is based on mirroring the deviations to determine a new, compensated shape on which a toolpath

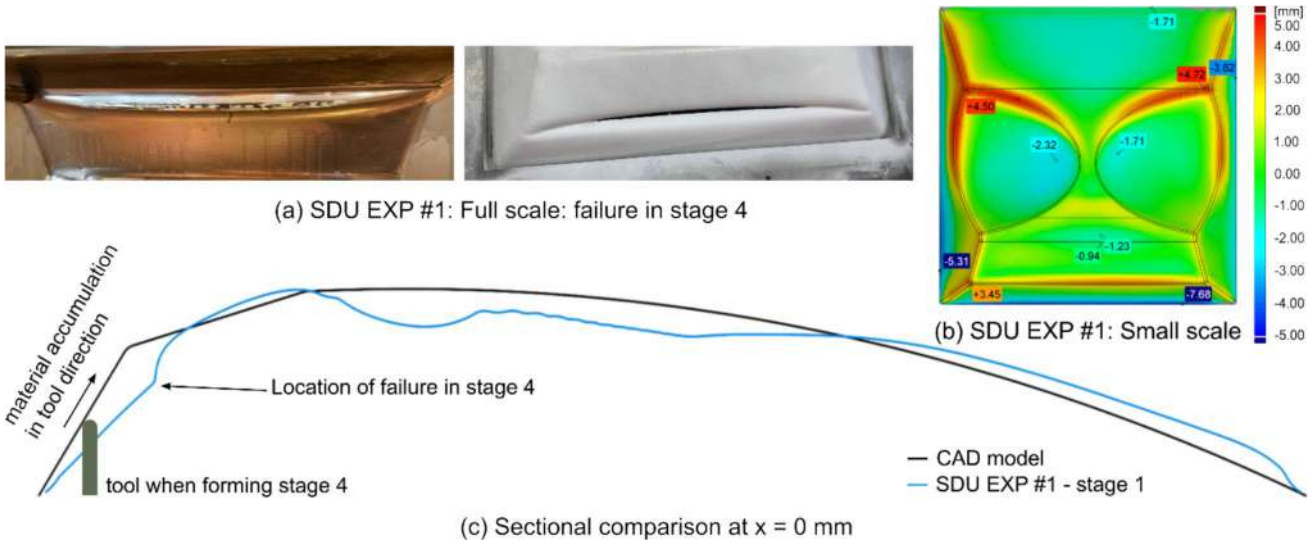

Fig. 53 (**a**) Failure after stage 4 when forming SDU EXP #1 on full scale and (**b**) Resulting deviations from the CAD geometry at smaller dimensions (300×300 mm). (**c**) Cross-section at x = 0 mm of the CAD model and stage 1 of the full-scale experiment and pictures of the location of failure after forming stage 4. The alignment is done with (**b**) a best-fit and (**c**) based on the clamping rig

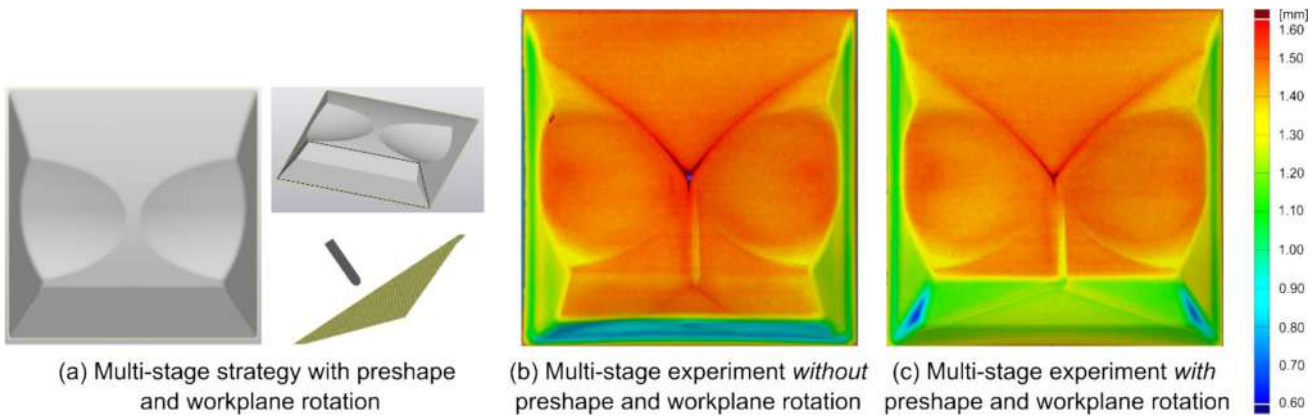

Fig. 54 (**a**) Twofold approach of preshape addition and workplane rotation, with resulting thickness distributions (**b**) without (KUL EXP #5 – stage 7) and (**c**) with using a preshape and applying a spiral toolpath with workplane rotation (KUL EXP #6 – stage 8)

can be applied. As an additional challenge in the benchmark design, applying mirror compensation in a single-stage approach does not work for the proposed benchmark shape, as this leads to exceeding the critical wall angle in some areas, resulting in excessive strains and failure. Given that compensation is a well-established method for improving geometric accuracy, it was applied in a multi-stage setting at KU Leuven. However, mirror compensation in a multi-stage process is less straightforward than in a single-stage approach. To ensure consistency, it is crucial to pursue the same toolpath strategies for the compensated part as those used in the original, uncompensated experiment that serves as the basis for the compensation calculations. The compensation experiment was conducted on the segmentation experiment KUL EXP #6, described in Sect."Invoking segmentation for intermediate shapes". In the first forming stage, mirror compensation was applied based on the measurements of the first stage of the uncompensated experiment. This approach ensured that (1) zone E was already compensated for in the first step, as it would not be formed again in later stages, and (2) the cutting planes used for segmentation remained as flat as possible after forming, ensuring proper tool contact when forming the next stages with a workplane rotation aligned with the cutting plane. For all subsequent forming stages, the final geometry of the uncompensated segmentation experiment was used and segmented with the same cutting planes. Figure 55 presents the resulting deviations for the two segmentation experiments, with and

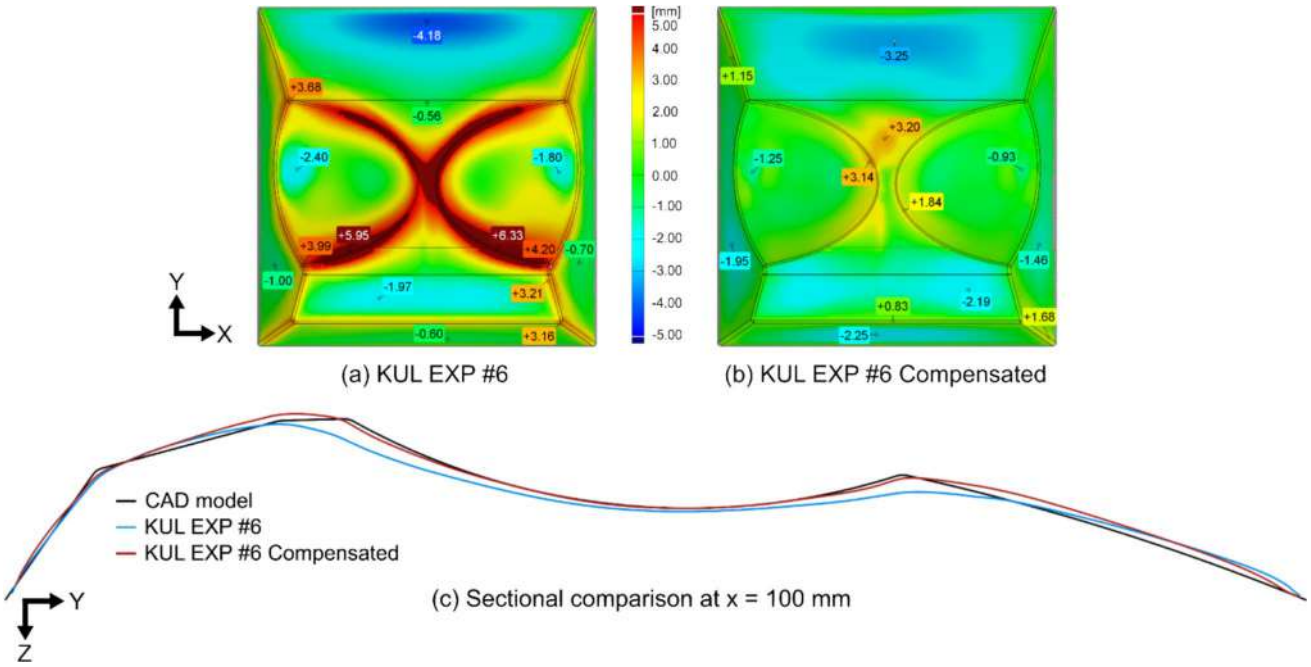

Fig. 55 Resulting deviations from the CAD geometry for the multi-stage experiment with a ø25 mm tool based on segmentation and backside forming (**a**) before (KUL EXP #6—step 8) and (**b**) after (KUL EXP #6 Compensated—step 8) applying mirror compensation. The sections are taken at x = 100 mm and the alignment is based on the clamping rig

without compensation, using the same tool and setup and after aligning the measured geometry based on the clamping rig. As shown, the compensated multi-stage experiment significantly enhances geometric accuracy, demonstrating the effectiveness of this approach.

Comparison of the multi-stage strategies

The comparison of experiments across institutes has been conducted after aligning the results using a best-fit approach in GOM Inspect 2019. Experiments conducted on a smaller scale or measured unclamped are not taken into account in this figure, as an unscaled comparison would be deceiving. The deviation distributions are presented in Fig. 56 as violin plots, illustrating significant differences between the various experiments.

Single-stage versus multi-stage forming. As discussed in Sect."Single-stage SPIF", the worst geometric accuracy was observed in the single-stage experiment with a 10 mm tool (KUL EXP #1). A noticeable improvement was achieved simply by using a larger tool diameter (KUL EXP #2). Overall, the multi-stage experiments generally outperformed the single-stage ones, demonstrating the benefits of using the versatility of incremental forming. However, multi-stage forming does not inherently guarantee better geometric accuracy. This is evident when comparing the UNIPA EXP #2, a multi-stage experiment with a 14 mm tool, to KUL EXP #2, a single-stage experiment using a 25 mm tool. In these two cases, the smaller tool used in the multi-stage experiment probably contributed to larger deviations.

Among all experiments, three showed the most compact deviation distributions, with their mean deviation close to 0 mm:

- *KUL EXP #6 Compensated*. This approach combined a segmentation strategy with backside forming and mirror compensation. A 25 mm tool was used for all stages, except for the final one, where a 10 mm tool was used to reprocess the edges, ensuring improved accuracy.
- *RWTH EXP #13*. This method did not include backside forming but utilized three intermediate geometries by offsetting the desired geometry, followed by a linear zig-zag toolpath from shallow to steep angles and a finishing stage to reprocess the edges. All stages were carried out with a 20 mm tool.
- *UNICAL EXP #5*. This strategy involved five forming stages with a 12 mm tool, focusing on reprocessing specific areas, backside forming, and a zig-zag toolpath to optimize material flow at low wall angles.

Figure 57 presents the geometric accuracy of these three experiments, showing similar deviation ranges, though the locations of deviations vary. Additionally, Fig. 58 provides images of the final geometries, where the edges from previous stages are still slightly visible in most of the experiments.

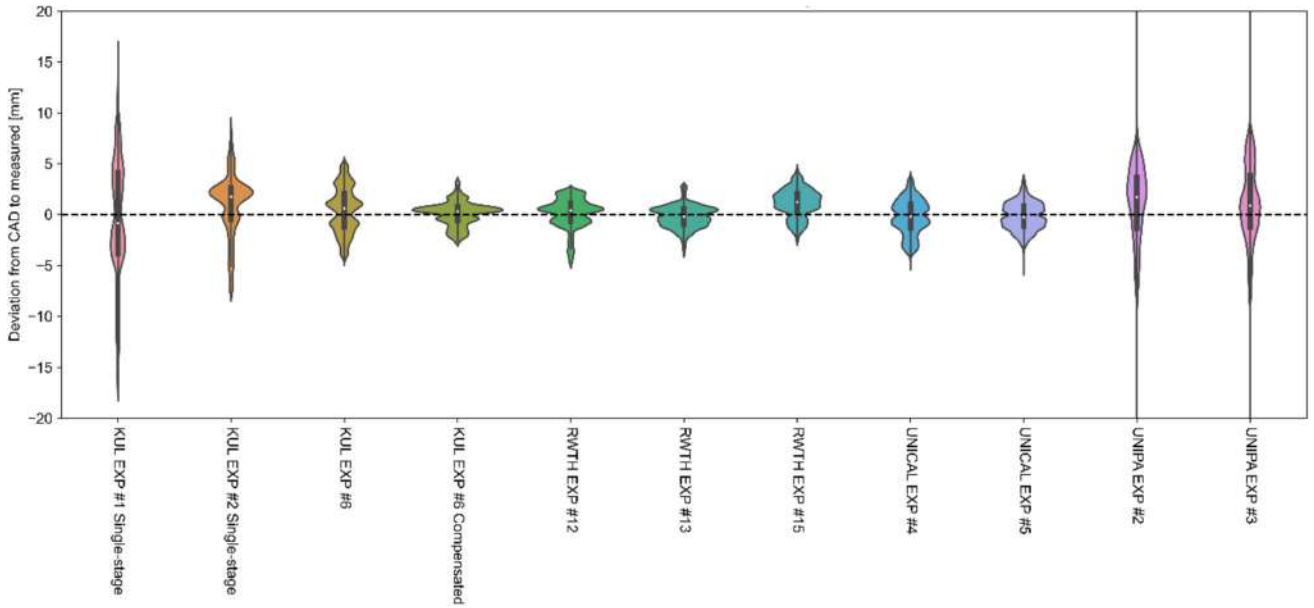

Fig. 56 Violin plots of the resulting deviations to the CAD for the discussed multi-stage SPIF experiments, compared to two single-stage experiments. All measurements are aligned with a best-fit in GOM Inspect 2019

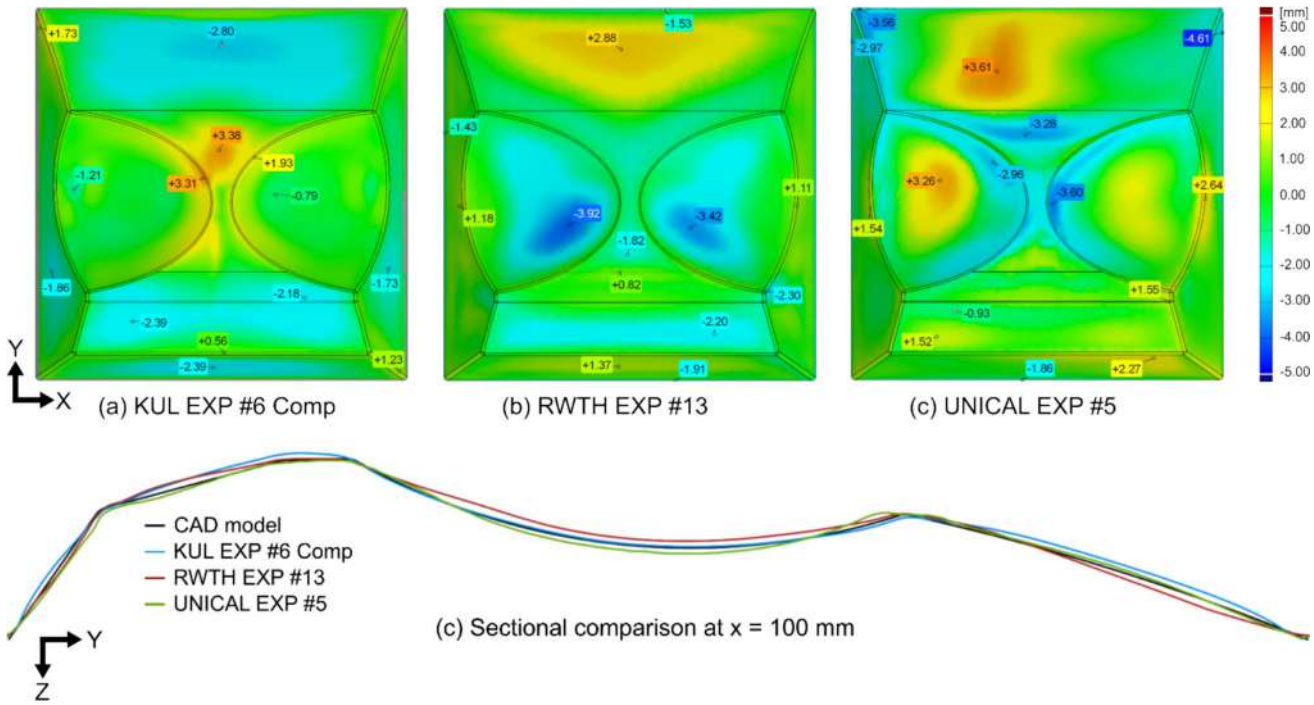

Fig. 57 Resulting deviations from the CAD geometry for the three multi-stage experiments with the narrowest error distributions: KUL EXP #6 Compensated, RWTH EXP #13, and UNICAL EXP #5. The alignment is done with a best-fit

Conclusion: multi-stage SPIF

This benchmark study demonstrates that multi-stage forming is essential for achieving high geometric accuracy in the proposed shape. The single-stage approach led to excessive deformations that require targeted solutions depending on the specific effect being mitigated. Multi-stage forming allows to effectively isolate and address individual

Fig. 58 Resulting workpieces for the three multi-stage experiments with the narrowest error distributions, illustrating the achieved surface quality: KUL EXP #6 Compensated, RWTH EXP #13, and UNICAL EXP #5

challenges, thereby significantly improving overall accuracy. Several key findings emerged from this multi-stage forming research and are summarized in Table 5.

Moreover, the impact of the different machines used and their corresponding stiffnesses on the obtained deviation distributions remains an open question. The observed differences suggest that some unwanted deformations may be linked to the machine setups used, such as an unstiff articulated robot versus a stiffer CNC machining center. Recent work by Simoncelli et al. [103] supports this, demonstrating that SPIF performed on a CNC machine yields higher geometric accuracy than when performed with a robotic system.

Finally, compensation strategies remain an area for further exploration. While mirror compensation has shown promising results in improving accuracy, more research is needed to refine these techniques and optimize their effectiveness in a multi-stage forming process.

Other ISF techniques

This section highlights other ISF techniques and provides a comparison to the SPIF experiments discussed above. The focus is on techniques with full support by die (TPIF) and partial support by using a pair of robots that form the part simultaneously on both sides (DSIF). The influence of using a full or partial support on geometric accuracy is investigated. For this, the deviations in the distinctive areas of the benchmark part will be discussed individually for each strategy and a general comparison with the SPIF results is presented.

Two point incremental forming

As discussed in Sect."ISF processes", Two Point Incremental Forming (TPIF) refers to the technique of using a die on the back side of the sheet. Partial or full support of the sheet reduces tensile stresses and increases compressive stresses in the part [104, 105]. The support reduces the tensile force needed to achieve the required plastic deformation. This often results in improved springback as the stress gradient across the sheet's thickness is reduced [106, 107]. Moreover, the support of the corners improves deviations in areas of curvature changes and reduces the tent effect. Unlike SPIF, which does not require dedicated 3D tooling, in TPIF the supporting die has to be designed and manufactured individually for each different part geometry, which compromises the flexibility of ISF and increases tooling costs.

The TPIF experiments in this work were conducted with a full die that follows the shape of the target geometry. The setup is shown in Fig. 59. In addition, the forming side is inverted. The clamping frame is mounted on a working table that moves downwards synchronized with the Z-steps of the ISF tool.

Four experiments were conducted, each with a different TPIF strategy, as listed in Table 6. Strategy 1 refers to single-stage forming with a Z-level toolpath. In Strategy 2 this single-stage forming is enhanced with stretching of the sheet. Therefore, the working table has a continuous lead of 10 mm over the sheet in Z-direction to increase the contact stiffness to the die and induce additional tension in the sheet. Strategies 3 and 4 are multi-stage ISF strategies. Here, after forming the sheet with a Z-level strategy similar to that used in TPIF #1, the sheet is reformed with either a linear or concave zig-zag forming path (Fig. 11). The aim of this is to reduce deviations that may remain after the first forming stage.

After the experiments, the specimens were 3D scanned and analyzed by comparing the surface to the target geometry as explained in the materials and method introduction and the measurement guidelines (Sect."Materials and methods"and Online Resource 4). In this case, however, the alignment of the measurements is done based on the highest point of the target part. The highest point of the target is chosen as the reference since it is bound by the die. It therefore takes the process into account and

Table 5 Summary of the conclusion on multi-stage SPIF experiments for this benchmark study

Effect to be reduced	Location	Strategy/observations
Tent effect	At discrete changes of wall angles (zones B and C)	• Increasing the tool diameter • Forming the double-angled wall with a preshape and workplane rotation
Pillow effect	At areas with low wall angles (zones D and E)	• Increasing the tool diameter. This can be combined with pre-stretching the sheet • Using an area-filling Z-level toolpath. However, this comes at the cost of a substantial increase in forming time • Segmenting the shape by cutting out the corners, to avoid an hourglass-shaped waist • Multiple passes over areas with low wall angles using adaptive, surface-covering toolpath strategies, such as zig-zag toolpaths • Forming from flat to steep wall angles helps guide material distribution
Overforming	Highest at concave areas (zone F) or close to the backing plate, at low curvatures and wall angles (zone E)	• Applying backside forming. However, this also leads to rigid body motion outside of the forming area • Using intermediate shapes with offset, formed with a bidirectional Z-level toolpath instead of a unidirectional one, and using a concave zig-zag toolpath to form the final geometry • Applying an offset in the first forming stage to avoid high overforming
Corner folds	At the edges of the geometry or at sharp changes of tool direction	• Avoiding toolpaths with sharp direction changes, such as feature toolpaths, that lead to ripples or folds in the material due to bulging. Alternative toolpath strategies include streamline or zig-zag toolpaths • Avoiding sharp edges in intermediate shapes, as once sharp edges or ripples are formed, they are challenging to eliminate and remain visible
Inaccuracies at the edges	At the edges	• Reprocessing the edges with a smaller tool in a final forming stage • Edge tracing in 2D before forming the final geometry. However, this only seemed to work at micro-scale (20 × 20 mm) and should be studied further
Scale effect	Full geometry	• Applying the same toolpath strategy with the same tool size when upscaling the part size can result in failure due to more pronounced unwanted effects • More research on the scale effect is needed to determine guidelines for adjusting process parameters such as the tool and step size
Failure due to low process window	At areas with high wall angles	Using an intermediate geometry with lower wall angles in this critical area
Increasing the overall geometric accuracy	Full geometry	• Applying (mirror) compensation • More research on additional, smart compensation can further increase the geometric accuracy of the full geometry

provides a better result than the best-fit for comparing the TPIF experiments to each other. The deviation measurements are shown in Fig. 60 in unclamped state. For greater clarity, only three experiments are shown because TPIF #3 and TPIF #4 did not show significant differences. Since the alignment is not based on a best-fit, this figure shows the deviations of the process, and not just the final shape, meaning that the negative deviations indicate underforming and the positive deviations indicate overforming. Note that this is the opposite of the representations in previous sections because the forming side has been changed compared to regular SPIF.

Fig. 59 Setup of TPIF experiments

Table 6 Overview of the four TPIF experiments and their strategies

Experiment	Strategy
RWTH TPIF #1	Single-stage forming: bidirectional Z-level
RWTH TPIF #2	10 mm pretension + bidirectional Z-level
RWTH TPIF #3	Two-stage forming: bidirectional Z-level + linear zig-zag toolpath
RWTH TPIF #4	Two-stage forming: bidirectional Z-level + concave zig-zag toolpath

In a first step of the analysis below, the TPIF experiments are compared with each other to investigate the influence of the different forming strategies. Then, a comparison between the best TPIF and an exemplary SPIF experiment is conducted to highlight the different characteristics of the two processes. Finally, a general deviation comparison of all TPIF experiments to a selection of the best SPIF experiments in this work is discussed using violin plots. For better comparability, moreover, the discussion of the results

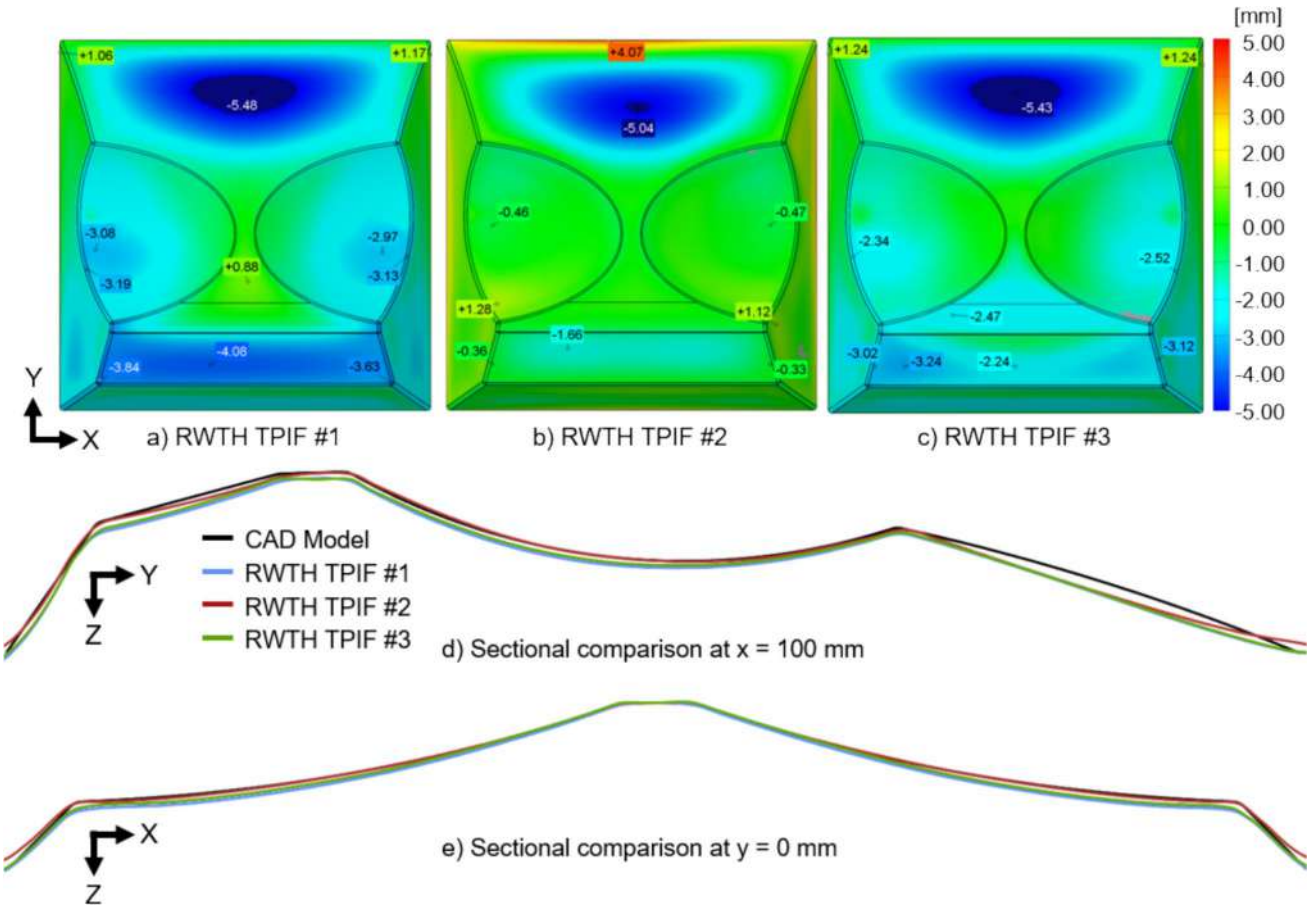

Fig. 60 Surface comparison of TPIF strategies to target CAD part in unclamped state: Blue indicates underforming, red overforming. (**d**) and (**e**) show cross-sectional comparisons at x = 100 mm and y = 0 mm. The alignment is based on the highest point of the geometry

focuses on the effects described in Sect."ISF Challenges"to discuss typical phenomena.

Reducing the tent effect

Recall that the concave areas (zone F) represent one of the most challenging areas to form in this benchmark part using SPIF. This difficulty arises from the transition between convex and concave surfaces. When forming the adjacent, lower regions of the part, the concave zones tend to flatten out. This can be counteracted by backside forming, if the setup allows for it, as addressed in Sect."Reducing overforming in concave areas". The situation is different with TPIF: Due to the full support on the opposite side of the ISF tool contact, the concave zones can be formed deeper without affecting the surrounding areas and vice versa. The tent effect is reduced (cf. Sect."Geometric accuracy"). Comparison of the presented TPIF strategies reveals that the deviations in zone F can be reduced by employing multi-stage strategies using linear or concave zig-zag toolpaths (see TPIF #3 and TPIF #4). Indeed, accuracies of approx. 2.5 mm can be achieved in this zone. However, the greatest improvement is seen with the pretension strategy (TPIF #2). The deviations in the zone F are in the range of −1 mm to 1 mm with an average of −0.13 mm.

The tent effect can also be observed for the discrete angle change (transition between zone B and C). This area is prone to underforming in TPIF. This is particularly true for the single-stage TPIF #1 strategy. Here, underforming of approximately 4 mm is observed. Due to the pretension in TPIF #2, the sheet is continuously stretched downwards over the die, thereby increasing the stiffness in this area and reducing the tent effect. As a result, underforming is reduced by this strategy as the sectional view Fig. 60 (**d**) indicates. The multi-stage strategies (TPIF #3 and TPIF #4) show slight influence in this area. The deviations are reduced from approximately 4 mm to 3.24 mm compared to the single-stage strategy (TPIF #1).

Reducing the pillow effect and underforming in shallow angled areas

Unlike in some single-stage SPIF strategies, TPIF produces no significant pillow effect in the flat waist area (zone D). This highest section of the part shows different deviations according to the different strategies, but it tends to underforming. This is also attributed to the way the die is designed: in this work, the die follows the form of the target part. Therefore, it is not possible to overform the sheet as the tool would penetrate the die in clamped state. When comparing the single-stage (TPIF #1) and two-stage (TPIF #3 and TPIF #4) forming, the first strategy achieves better geometric accuracy in zone D. The deviations there do not exceed 1 mm, compared to almost 2.5 mm underforming for the two-stage experiments. Again, forming with pretension (TPIF #2) results in the highest accuracy in this zone, with a slight overforming of 0.3 mm. Regarding the low wall angle area in zone E, all four TPIF experiments show the same tendencies. This area contains the highest deviation value of the full geometry, which is approx. 5.3 mm in all TPIF experiments. In the unclamped state, this region is lying below the target part with respect to the forming side and is therefore underformed. This bulging effect could not be significantly reduced with the strategies tested, although the strategy using pretension (TPIF #2) slightly mitigated the effect.

Increasing the geometric accuracy in areas with high wall angles

When comparing the regions of high wall angles (zones A and B), measurements indicate that all specimens except TPIF #2 achieve underforming with deviations of approximately 2.5 mm with the alignment described. The two-stage experiments (TPIF #3 and TPIF #4) have no significant effect on the areas with high wall angles in zones A and B compared to the single-stage experiment (TPIF #1). Applying a pretension before and during forming with a Z-level toolpath (TPIF #2), on the other hand, results in higher accuracies with a maximum deviation of 0.8 mm in these areas.

Comparison to SPIF

Figure 61 shows a direct comparison between one of the best SPIF experiments and TPIF #2 conducted at the same institutes. As discussed in the previous sections, the full support on the opposite side of the ISF tool contact results in higher accuracies in the zones C, D and F compared to one-sided SPIF Significant deviations remain in the shallow zone E. On the one hand, the deviations here were influenced by unclamping the parts before scanning them. On the other hand, this shallow yet wide area tends to bulge when being formed.

By using the die, the edges of the part are formed without any noticeable problems. The radii of the corners in the die help to perfectly define the corner shape of the sheet. As a result, the part contours appear sharper and more defined than most parts formed using SPIF strategies. Tent effect and other draw-in effects can be avoided by means of the support and the shape constraint imposed by the die.

The violin plots in Fig. 62 show the overall deviation distribution for all TPIF experiments and a selection of the most promising SPIF experiments, as discussed in Sect."Comparison of the multi-stage strategies". For better comparability across the experiments, the TPIF results have also been aligned by best-fit for this comparison. The KUL

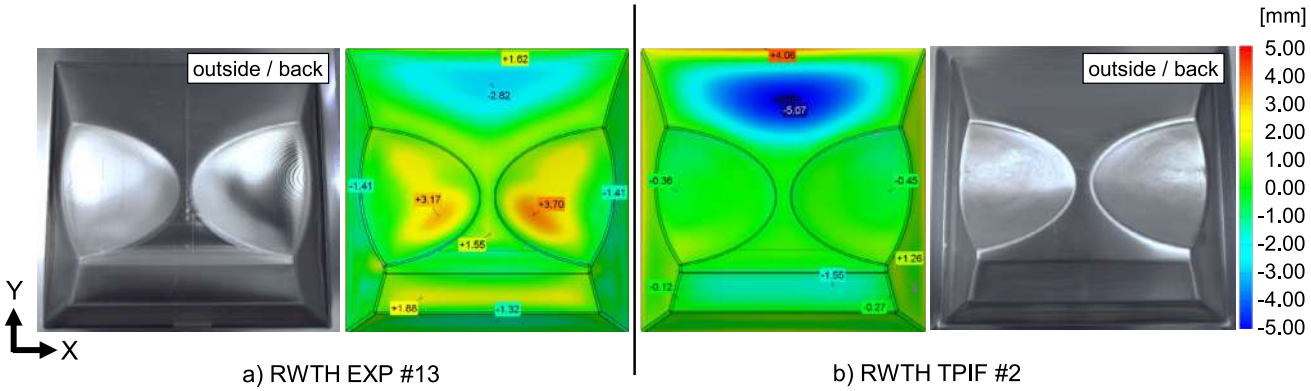

Fig. 61 Direct comparison of RWTH EXP #13 (SPIF) and RWTH TPIF #2. The alignment is done with a best-fit

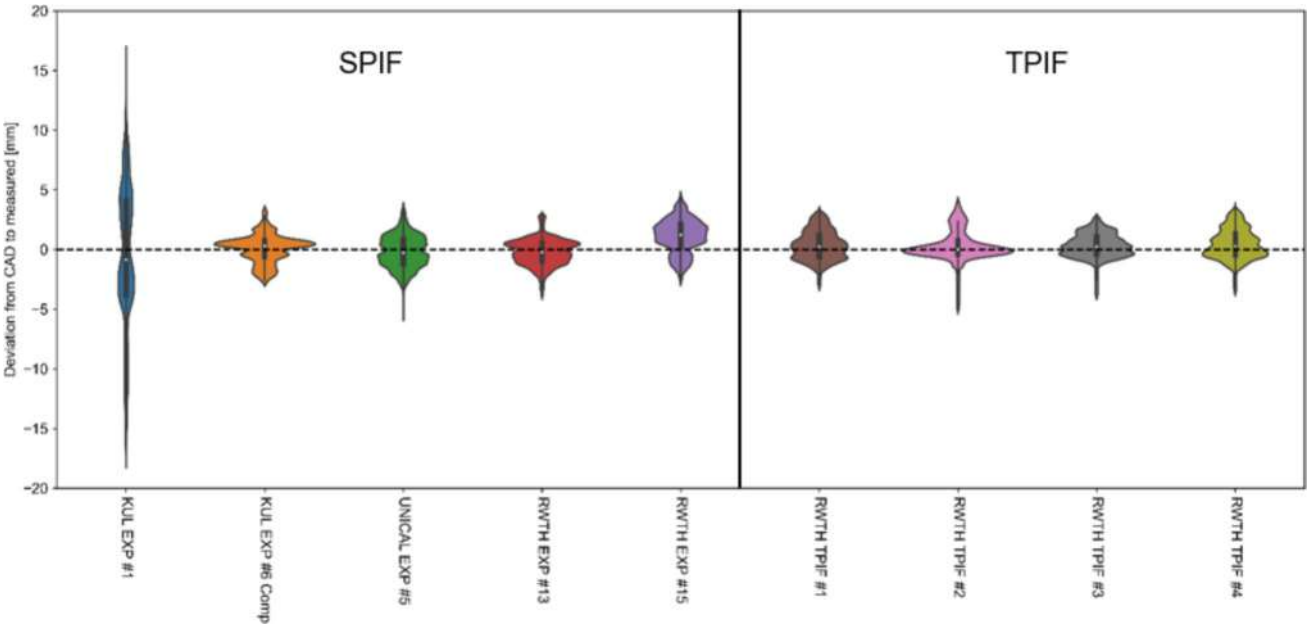

Fig. 62 Violin plots of the resulting deviations to the CAD for the discussed TPIF experiments, compared to the baseline and most promising SPIF experiments. The alignment is done with a best-fit

EXP #1 experiment is also shown as a reference, as this was the worst performing single-stage baseline experiment. The deviations indicate that TPIF performs well in direct comparison with the best SPIF experiments. Compared to SPIF, the greatest improvement in accuracy is in the lobes/bulges (zone F). Geometric features such as edges are formed more detailed and appear sharper and more precise. However, this comes at the cost of higher deviations due to bulging, as discussed in the beginning of this paragraph. Again, TPIF #2 shows the best results out of the four TPIF strategies, as the distribution is the most concentrated around a deviation of 0 mm, achieving similar deviations to KUL EXP #6 with compensation. The experiments and results illustrate one of the major differences between the SPIF and TPIF approaches: TPIF achieves relatively high levels of geometric accuracy with a smaller number of trials, at the cost of a more complex setup (e.g., a custom-made die), whereas the opposite is the case for SPIF. Several trials and compensation strategies are required when applying SPIF to achieve the same level of accuracy as the TPIF experiments, but the process itself is more versatile and requires less preparation of hardware.

Besides the comparison of deviations, more general observations can be addressed here. For example, surface quality is significantly improved with TPIF. The non-tool-contact side of the part reaches quality levels comparable to deep-drawn parts. Of course, the additional cost and effort required to manufacture the die must be considered. This

disadvantage especially accounts when applying compensation strategies to further increase the geometric accuracy, as a new, modified die is needed. This increases the lead time and costs for process iterations.

Double sided incremental forming

Double Sided Incremental Forming (DSIF) refers to a forming technique where, in addition to the usual SPIF tool, a second tool is introduced at the opposite side of the sheet metal. The first tool retains the role of forming the sheet, while the second tool traces the forming tool but acts as a local support. Therefore, the process maintains most of the advantages of SPIF while offering greater flexibility without the need for dedicated tooling such as dies. It offers a high degree of controllability of the geometric accuracy, as compensation strategies, for example, can be easily implemented. Of course, the machine setup and process planning are more complex, and the backside of the part must be accessible.

Only limited DSIF experiments were performed as part of this work. Due to machine range limitations, only tests with a reduced component size (150 mm × 150 mm) could be carried out. Therefore, reliable conclusions can only be drawn from the internal comparison of this DSIF test with a single-stage SPIF experiment on the same setup. A direct comparison with the other SPIF components of this work is therefore not provided. The DSIF setup used in this work is shown in Fig. 63.

The deviations for both SPIF and DSIF experiments are shown in Fig. 64. As for the results, the direct comparison of the part formed once with SPIF and once with DSIF is discussed according to the zones of the target part. Because no significant differences occurred in zones A, B, C, and E, the discussion focuses on the flat waist (zone D) and the concave regions (zone F).

Reducing the pillow effect

The largest underforming, due to the pillow effect, occurs in the flat waist area (zone D) for the single-stage SPIF experiment (Northwestern EXP #1). With the double-sided forming (Northwestern DSIF #1), the deviations were significantly improved from −2.44 mm to –0.88 mm. This can be attributed to the use of a supporting tool that allows forming of areas without flattening the adjacent sections. The same can be observed for the contours between zones D and F. With DSIF, these edges were less underformed, which implies they appear sharper and less flattened.

Reducing overforming in concave areas

The most obvious difference between the two strategies compared is found in the concave zones. When using SPIF, high overforming of approximately 4 mm occurred in these concave areas for a small-scale (150 × 150 mm) experiment at the same institute. This effect is also observed for multiple single-stage SPIF experiments on the full scale, as discussed in Sect."Reducing overforming in concave areas". The DSIF strategy prevents this flattening, as the pair of tools allows the concave zones to be formed deeper without flattening the unformed regions.

Conclusion TPIF and DSIF

Both alternatives to SPIF presented here, TPIF and DSIF, showed promising results for the specified benchmark part. In both cases, improved geometric accuracy in certain areas of the part was achieved compared to the corresponding

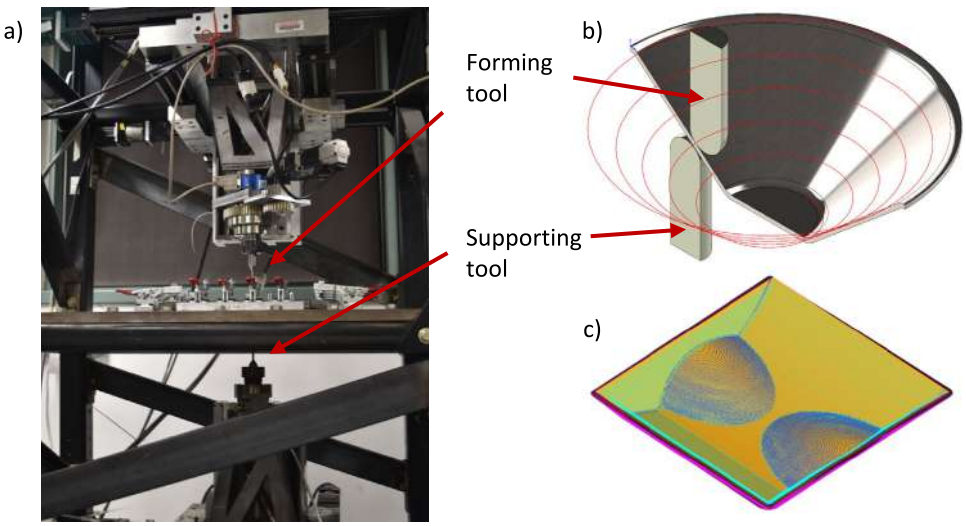

Fig. 63 (**a**) Setup for DSIF machine, (**b**) schematic of DSIF for forming a truncated cone, and (**c**) toolpath strategies for forming the benchmark geometry

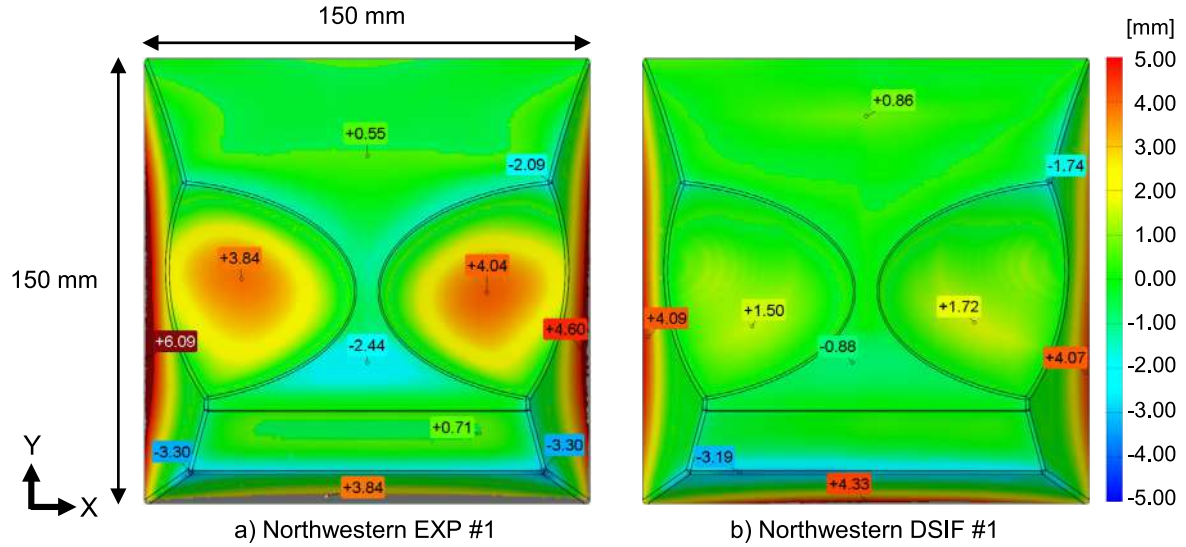

Fig. 64 Surface comparison of the smaller scale (150×150 mm) benchmark part formed with (**a**) SPIF and (**b**) DSIF in unclamped state. The alignment is done with a best-fit

Table 7 Summary of the TPIF experiments conducted in this benchmark study

Effect to be reduced	Location	Strategy
Tent effect	At discrete changes of wall angles (zones B and C)	• The tent effect is much less outspoken than in SPIF, as the die helps making the discrete change in angle • Underforming is an issue though, but can be reduced by adding an additional forming stage with a linear or concave zig-zag toolpath or by applying pretension • The single-stage TPIF experiment with pretension gave the best results
Pillow effect/bulging	At areas with low curvature and wall angles (zones D and E)	• Bulging is very high in the low wall angle area in zone E, showing severe underforming in all TPIF experiments • The proposed strategies did not manage to significantly reduce the underforming due to bulging, although the experiment with pretension led to a slight reduction
Inaccuracies at the concave areas	At concave areas (zone F)	All TPIF experiments led to increased accuracy in the concave areas. The strategy with pretension gave the best results
Underforming at high wall angles	At areas with high wall angles (zones A and B)	Applying pretension before and during forming helps to increase the geometric accuracy at areas with high wall angles
Inaccuracies at the edges	At the edges	The edges are formed without any noticeable problems, thanks to the support of the die. This results in sharper contours
Overforming	/	Not present in TPIF, as the die prevents the sheet from overforming

SPIF parts. A summary of the experimental outcomes is shown in Table 7 and Table 8. As mentioned above, DSIF was only compared on a smaller scale to a single-stage SPIF experiment, so its performance compared to an optimized, full-scale multi-stage SPIF approach remains uncertain. Overall, the benchmark experiments showed that TPIF, on the one hand, leads to higher accuracy in areas with changes in curvature. In addition, the contours are formed sharper and the surface quality on the backside of the sheet improves significantly. SPIF, as well as DSIF, on the other hand, allow

Table 8 Summary of the DSIF experiments conducted in this benchmark study

Effect to be reduced	Location	Strategy
Pillow effect	At areas with low wall angles (zones D and E)	The pillow effect is much less apparent than in the single-stage SPIF experiment
Inaccuracies at the concave areas	At concave areas (zone F)	A higher accuracy can be reached in the concave areas with a DSIF toolpath strategy, compared to single-stage SPIF
Inaccuracies at the edges	At the edges	The edges are formed more accurate than in the single-stage SPIF experiment, thanks to the supporting tool

for compensation strategies without the need of modifying a die. This way, these strategies can be further optimized to be more accurate, while TPIF does not offer this opportunity easily. With TPIF, iterations for improvement are more challenging and expensive due to new or modified dies. A conclusive statement as to whether TPIF and DSIF are fundamentally more accurate than SPIF cannot be made due to a high variety of influencing factors. However, the myriad experiments suggest that TPIF tends to result in greater underforming, while SPIF tends to more overforming. The effect of springback cannot be completely excluded, as the TPIF experiments were analyzed unclamped. Due to the die support, TPIF can achieve better results in the first trials and especially for geometries with curvature changes, but SPIF might utilize its flexibility and improve accuracy in further iteration steps using compensation strategies.

Simulations

Two institutes (the University of Michigan and the AGH University of Krakow) carried out numerical investigations based on finite element (FE) analysis to enhance the discussion for the ISF Benchmark study. The development of the SPIF numerical model was based on the guidelines already available in literature, e.g. [4]. As mentioned in Sect."Simulation of SPIF: Finite element modeling", FE modeling of ISF is well established. The 2021 ESAFORM Benchmark [108], as well as a review by Duflou et al. [2], provided guidelines for deep drawing and SPIF simulations with Hill 1948 yield functions, associated flow rule, and isotropic hardening for the accurate prediction of part shapes based on Lankford coefficients at 0°, 45°, and 90°. Additionally, the NUMISHEET SPIF benchmark [86] indicated no particular trend in result quality when using the implicit/explicit schemes during numerical approximation. The literature also suggests that classical shell-type FE meshes have limitations in accurate predictions of through-thickness 3D stress/strain fields during SPIF, and 3D solid elements should be applied if possible, although this is known to increase computational costs. The role of proper model discretization has been extensively investigated in literature as well: see e.g., [85].

Thus, given the complexity and scale of the ESAFORM 2024 benchmark part geometry, the current research paid particular attention to the evaluation of the possibility of developing a high-fidelity FE model to achieve optimal predictions of the geometric accuracy while balancing computational costs. Therefore, the research focused on comparative analysis of solid and shell elements and using high-performance computing center capabilities. Subsequent steps for developing such a high-fidelity FE model are presented in the following sections.

Material characterization

The AA5754 sheet behavior under the investigated process conditions was evaluated in the first step to adjust the complexity of subsequent material characterization and modelling techniques. The primary issue was the possibility of temperature increase due to deformation heating that could affect material flow characteristics. For that reason, the University of Sheffield carried out a single point forming operation under the observation of a thermal camera. A smaller sample size of 100×100 mm was used during the experiment to magnify the heat increase effect as presented in Fig. 65.

As presented, due to the nature of the process and the investigated material, the sample remains at near room temperature throughout the entire forming operation, which indicates that the effect of temperature on material hardening behavior can be neglected in this case.

Therefore, in the second step, the target material was characterized at the University of Michigan based on uniaxial tensile tests on flat sheet specimens at room temperature to provide sufficient data for the development of the numerical model. Specimens conforming to the ASTM E8 standard, with a 50 mm gauge length and 12.5 mm width, were utilized. The as-received sheet was cut at 45 ° intervals relative to the rolling direction (RD) and tested at a strain rate of 0.001 s^{-1} using an MTS Insight 10 Mechanical Tester at the University of Michigan. The orientation of the specimen relative to the RD is denoted here with the symbol of θ. Each orientation was tested three times to ensure repeatability, and the results were subsequently converted to true stress and true strain.

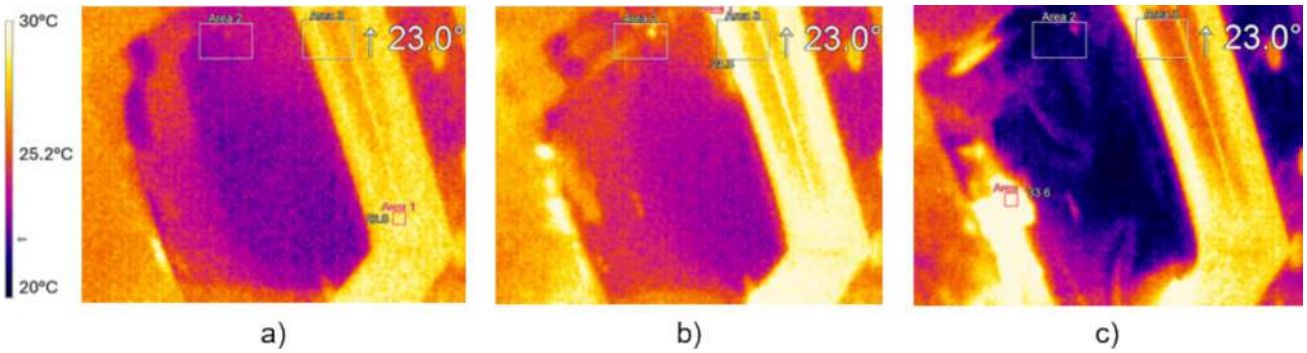

Fig. 65 Temperature field measured after (**a**) 5 min, (**b**) 10 min, and (**c**) 20 min of the 22-min forming process

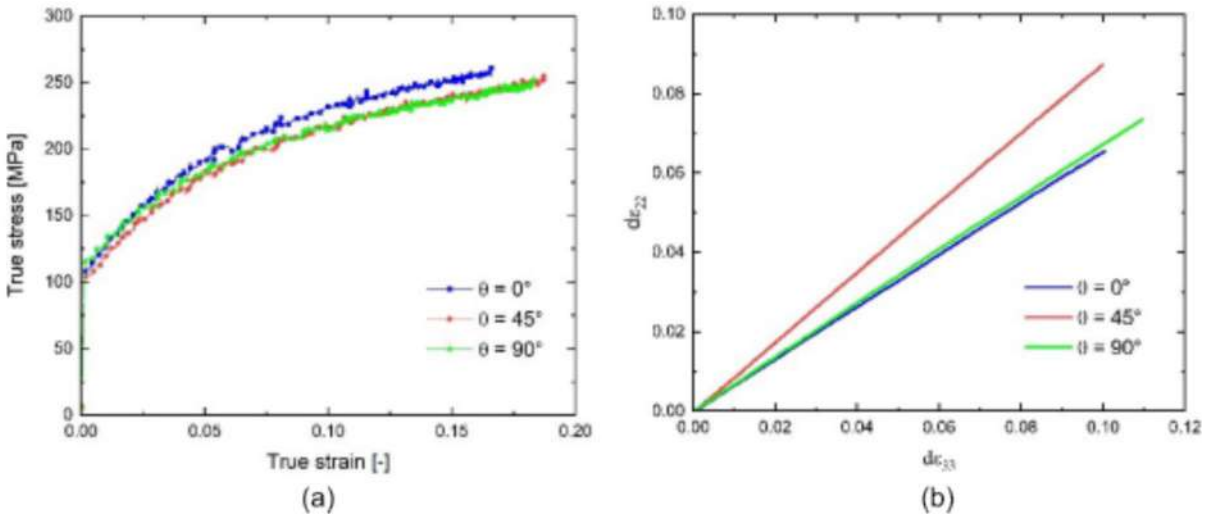

Fig. 66 Anisotropy of the AA5754 sheet tested at UM: (**a**) true stress – true strain curve of the sample in uniaxial tension in each direction; (**b**) width strain vs. thickness strain in uniaxial tension along each direction measured using DIC

A mechanical extensometer and 3-D Digital Image Correlation (DIC) system coupled with VIC 3D software were employed for accurate strain measurements (axial strain and width strain). With this approach, the stress–strain curve (Fig. 66 (a)) and Lankford coefficient r (the width-to-thickness strain ratio) were determined in each main loading direction. The Lankford coefficients were calculated in accordance with ISO 10113:2020. Based on material incompressibility, a plot of width strain (ε_{22}) versus thickness strain (ε_{33}) was created, as seen in Fig. 66(b).

A linear regression performed within a selected range was used to estimate the r-values. This analysis resulted in average r-values from the three repetitive tests in each main direction: $r_0 = 0.6539$, $r_{45} = 0.8799$, and $r_{90} = 0.6840$, which were further used in the material model development stage.

Material model development

The appropriate selection and identification of the material model are essential for accurately representing the material behavior in the numerical simulation of forming processes [109]. Importantly, the stress and strain distributions in SPIF are more complex and nonlinear than conventional sheet metal forming processes, such as deep drawing or hydroforming. While the constitutive equations in simpler processes can often be simplified for analytical solutions, the intricate deformation mechanisms in SPIF necessitate a more sophisticated approach to material modelling in FE modelling to ensure accurate predictions. As mentioned, different yield functions and hardening laws can be employed, ranging from simple von Mises yield criteria with isotropic hardening to more complex anisotropic

Table 9 Set of parameters for hardening law

Loading direction [°]	Swift isotropic hardening		
	K_0[MPa]	ε_0[-]	n[-]
0 (RD)	408.52	0.001	0.25

Table 10 Anisotropy coefficient for the Hill 1948 yield function obtained based on r-values

F	G	H	N	L	M
0.5780	0.6046	0.3953	1.6320	-	-

yield functions (e.g., Yld2004-18p [110]) with kinematic or distortional hardening laws [84].

Isotropic hardening was selected for this investigation as it is widely used to describe behavior in the plastic deformation regime under monotonic loading conditions or for processes that do not involve cyclic loading conditions. The isotropic hardening was described by the Swift law [111]:

$$Y\left(\overline{\varepsilon}^p\right) = K_0(\varepsilon_0 + \overline{\varepsilon}^p)^n \tag{1}$$

where K_0, ε_0, and n are material properties, and $\overline{\varepsilon}^p$ is the effective plastic strain. The parameters for the Swift hardening law, based on tensile test data at 0 °, are provided in Table 9.

The Hill 1948 yield function [87], an orthotropic extension of the isotropic von Mises yield criterion, was chosen due to material testing constraints, which is expressed as:

$$\sigma_{Hill} = \sqrt{F(\sigma_{22}-\sigma_{33})^2 + G(\sigma_{33}-\sigma_{11})^2 + H(\sigma_{11}-\sigma_{22})^2 + 2L\sigma_{23}^2 + 2M\sigma_{31}^2 + 2N\sigma_{12}^2} \tag{2}$$

Here, the material parameters F, G, H, L, M, and N are constants characterizing material anisotropy. These anisotropic parameters can be determined using either yield stresses from uniaxial loading along 0°, 45°, and 90° orientations or Lankford coefficients at the same orientations.

The Lankford coefficient is representative of sheet thinning during the forming process, and focusing data set identification on stress can generate Lankford prediction values that diverge significantly from experimental ones. The respective analytical formulas based on the associated flow rule are as follows:

$$\begin{aligned} F &= \frac{r_0}{r_{90}(1+r_0)} \\ G &= \frac{1}{1+r_0} \\ H &= \frac{r_0}{1+r_0} \\ N &= \frac{(r_0+r_{90})(r_{45}+0.5)}{r_{90}(1+r_0)} \end{aligned} \tag{3}$$

Table 10 provides the parameter values, where the L, M, and N values are assumed to be equal, as it is exceptionally challenging to perform experimental tests on sheet samples to measure through-thickness shear.

It is worth noting that the ability to introduce an objective function to determine parameters using numerical methods with both experimental r-values and yield stresses in more than three orientations was demonstrated in a previous study by the authors [90]. Finally, the experimental and predicted r-values in each direction are presented in Fig. 67 (a), while the Hill 1948 yield locus with experimental data is shown in Fig. 67 (b).

Initial and boundary conditions

After the material characterization stage, numerical simulations of SPIF were developed within the commercial FE software Abaqus, exploring the role of part discretization on the resulting accuracy and corresponding computational cost. The developed numerical models include three key components: a hemispherical tool, a clamping system with a stationary blank holder and a supporting frame, and a 1.5 mm thick aluminium sheet.

The ball nose tool represents the CNC tool, which follows a pre-programmed path used in the experimental setup. The clamping system prevents the free movement of the sheet

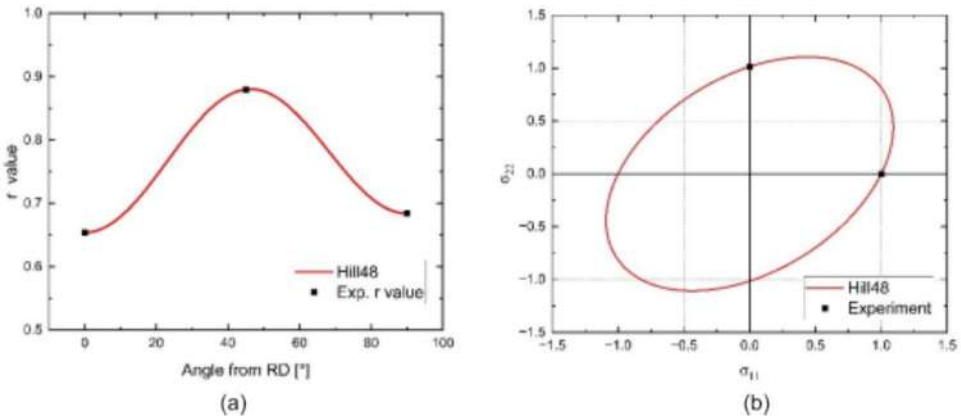

Fig. 67 Prediction of (**a**) Lanford coefficient values by Hill 1948 with the experimental data and (**b**) Hill 1948 yield locus in RD—TD orthotropic plane stress based on the obtained parameters

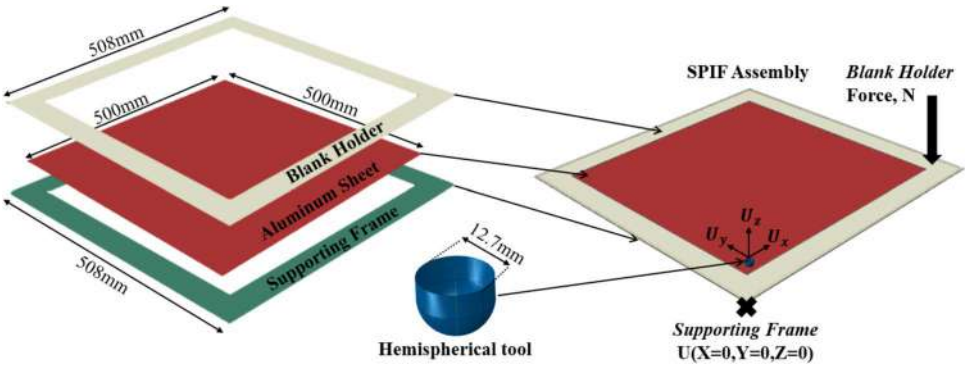

Fig. 68 Assembly and individual components of the developed SPIF model

during deformation. A clamping pressure was defined to match the experimental conditions according to the guidelines from [112]. The supporting frame is fully fixed in 3D space. The final assembly and individual components of the SPIF process model are illustrated in Fig. 68.

The material behavior was modelled using the Hill 1948 constitutive equation and isotropic Swift hardening model as described in Sect."Material model development". A Coulomb friction coefficient of 0.025 was used between the tools and the sheet. The Abaqus/Explicit solver, with properly selected mass scaling, was employed to ensure accurate results and avoid any potential unphysical artefacts. The analysis was conducted using shell elements with a different number of integration points and different sizes, as well as with solid FE elements of different sizes.

Model setup accuracy study

Classical shell elements are computationally less intensive than solid elements because they have fewer degrees of freedom, making them ideal for large-scale simulations where computational costs must be minimized. Shell elements are specifically designed for thin structures, making them more accurate in representing the bending and stretching behaviors typical in SPIF processes. However, as already pointed out, shell elements are less effective when the thickness of the sheet metal plays a significant role in the forming process. Also, detailed handling of complex tool-sheet interactions, especially at sharp part corners, is also a limitation.

On the contrary, solid elements are used to discretize the entire volume of a structure, allowing detailed stress state predictions throughout the thickness of the sheet. As result, solid elements can accurately represent complex part geometries or tool-part interactions and eventually identify potential failure events like thinning or tearing. However, solid elements are more computationally demanding than shell elements as they require more degrees of freedom to simulate the entire volume of the material. This leads to extensive simulation times and high memory usage.

The compromise between the two approaches may be the use of shell elements with multiple integration points called multi-layered shell elements. This type of FE element incorporates multiple integration points through the thickness of the element, allowing it to capture gradients in stress, strain, and other physical properties across the thickness of the sheet. The effect of increasing the number of integration points in shell elements for the investigated case study is shown in Fig. 69.

Figure 69 confirms that simulation accuracy based on a single-integration-point shell element provides the worst accuracy. At the same time, results obtained from meshes with three or more integration points are comparable. Therefore, shell elements with three integration points were selected for comparison with the solid FE mesh to limit the computational time.

A comparison between the accuracy of the obtained results with respect to the computational cost is presented in Fig. 70. For this comparison, four different FE element sizes were used to also evaluate the role of the mesh discretization level on the results accuracy.

These results indicate that the solid FE elements better reflect the experimental results than the shell elements. Interestingly, the results from shell elements are closer to the input CAD geometry. However, the differences between the two mesh types are generally insignificant. In both cases, slightly better predictions are obtained for finer meshes, however, with a significant increase in the simulation times, as shown in Fig. 71. Simulations were completed using 180 cores, each specified to be 3.0 GHz Intel Xeon Gold 6154 processors.

To summarize, in SPIF, where the sheet metal undergoes significant plastic deformation and thickness variations, using shell elements with multiple integration points allows for a quite accurate prediction of these phenomena while still maintaining a relatively low computational cost. This is especially useful in cases where the material's behavior across its thickness needs to be captured, but the full complexity of solid elements is not justified. However,

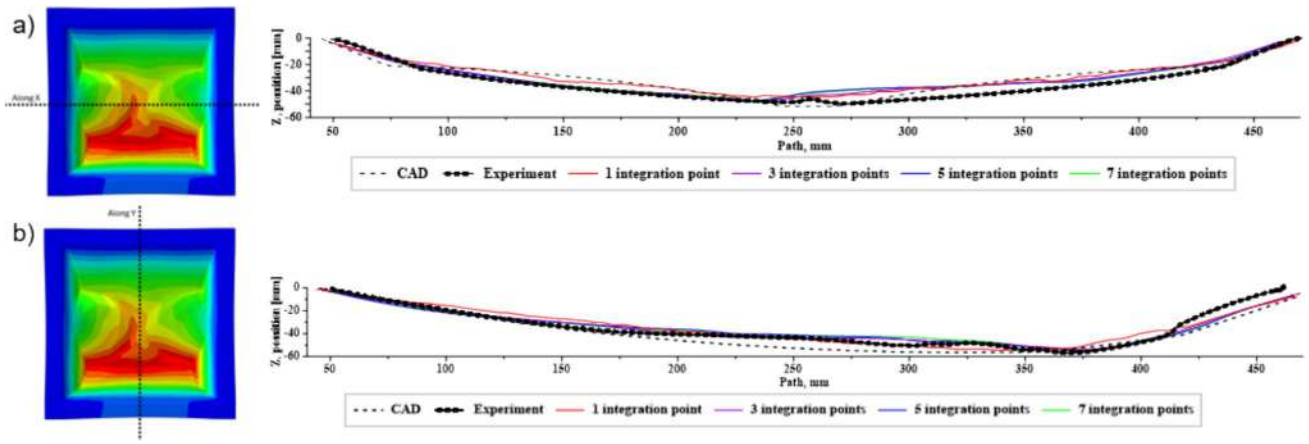

Fig. 69 Shape prediction accuracy with an increasing number of integration points in shell elements (**a**) horizontal and (**b**) vertical cross-section shape. The part (UMICH EXP #1) was scanned while clamped, and profiles were aligned using a best-fit

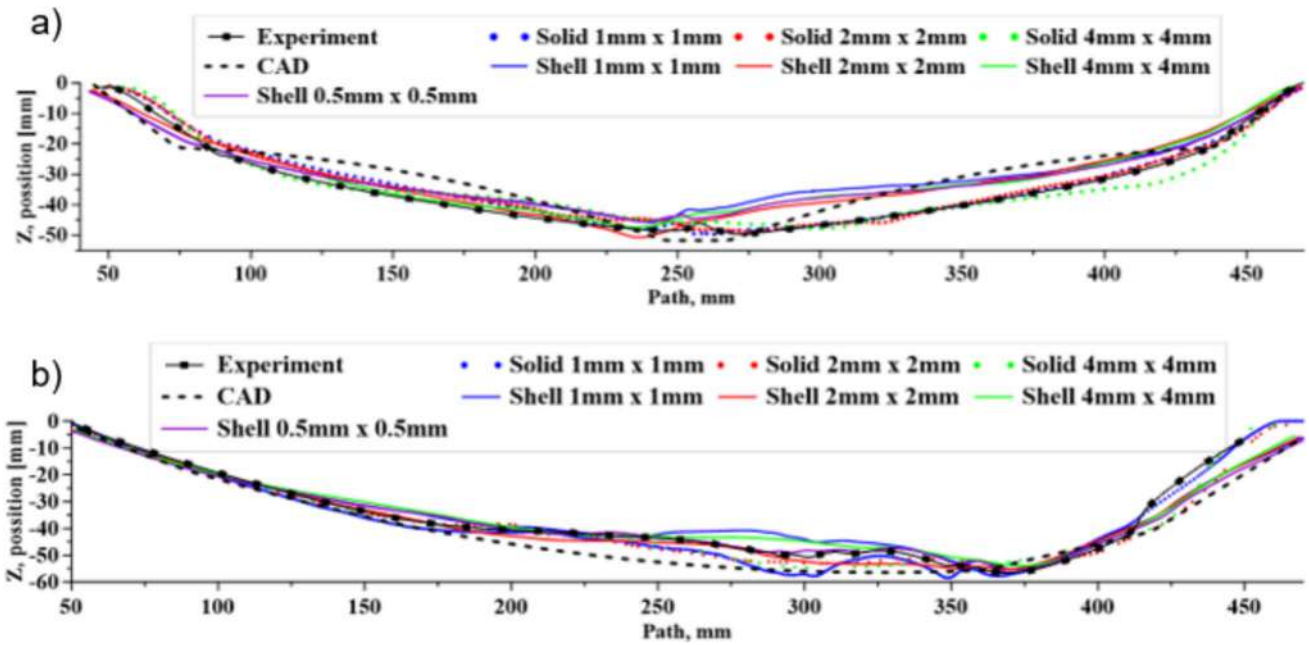

Fig. 70 Shape prediction accuracy with an increasing number of integration points in shell elements (**a**) horizontal and (**b**) vertical cross-section shape. The part (UMICH EXP #1) was scanned while clamped, and profiles were aligned using a best-fit

it must be emphasized that, although such shell elements improve accuracy over traditional shell elements, they still may not capture the detailed behavior that solid elements can, particularly in cases of extreme deformation or when very fine resolution is needed across the thickness.

Conclusion

As a collaboration among 15 research institutes, the ISF benchmark 2024 project, of which the results are presented in this paper, formed an excellent opportunity to compare experimental output obtained with different setups and

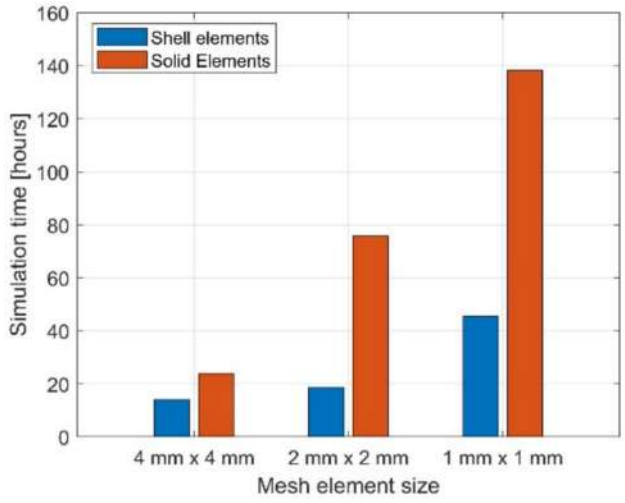

Fig. 71 Relation between the mesh element size and simulation times

using different process variants and processing strategies. Furthermore, the need to liaise between different benchmark partner institutes stimulated the participants to work towards:

1. uniform data exchange formats, as implemented in the ISF database platform.
2. non-ambiguous measurement guidelines that allow result comparison across institutes.
3. standardized nomenclature of the systems and phenomena observed in the studied processes.

By reporting these results in this paper, the participants hope to contribute to more efficient collaborative efforts in the domain of ISF in the years to come.

Besides these achievements with respect to facilitation of research exchange, the joint efforts led to some valuable knowledge development, which is summarized in the conclusions formulated below. More detailed conclusions with respect to the different phenomena observed in the ISF variants tested can be found at the end of the respective corresponding sections, specifically Sects."Single-stage SPIF"through"Simulations". A comparison between the studied process variants is provided in Table 11.

- Although a challenging, large scale geometry of 400×400 mm was chosen for this benchmark project, known to lead to typical unwanted deformation problems such as bulging in semi-flat features and tent effects in areas with changing slopes, qualitatively useful parts could be produced with good surface quality, while the absolute dimensional accuracy is still open for improvement, with maximal deviations of around 3 mm for the best experiments.

Table 11 Overview of the strengths and weaknesses of the ISF process variants, as observed in this study

	Incremental Sheet Forming			
	Single Point Incremental Forming (SPIF)		Other ISF techniques	
	Single-stage SPIF	Multi-stage SPIF	TPIF	DSIF
STRENGTHS	• Flexible setup • Eliminates the need for costly dies • Enables fast forming times	• Flexible setup • Eliminates the need for costly dies • Achieves higher geometric accuracy than single-stage forming • Can enhance forming limits for parts with high wall angles	• Achieves good geometric accuracy more easily, comparable to multi-stage experiments • Provides greater precision in concave areas when backside forming is not feasible • Produces sharper, more accurate edges • Well-suited for rapid prototyping	• More flexible setup compared to TPIF • Can reduce reliance on complex, multi-stage process plans • Delivers higher geometric accuracy in concave areas compared to single-stage SPIF
WEAKNESSES	• Unable to achieve sufficient geometric accuracy	• High process planning complexity • Longer forming times compared to single-stage forming • Maximum geometric deviations in this study remain around 3–4 mm	• Less flexible and more costly setup due to the need for a tailor-made die • Increased underforming • Limited flexibility for further improvement, as a new die is needed for each compensation iteration • Maximum geometric deviations in this study remain around 5 mm	• More complex setup requiring advanced hardware and powerful real-time control software • No conclusive results available at full-scale implementation

- The chosen comparison method plays a major role: absolute accuracy with respect to the clamping rig edges facilitates straightforward comparison based on the process variant used and allows unambiguous identification of over- and underforming, while a best-fit alignment results in a lower mean deviation.
- When comparing the results obtained with different ISF variants, a clear trade-off situation can be observed: the relative simplicity of a SPIF setup corresponds to substantial undesirable deformations that cannot be overcome with a single-stage toolpath strategy. However, more sophisticated multi-stage toolpaths allow to achieve qualitatively attractive parts using the limited degrees of freedom of a SPIF setup. On the other hand, alternative process variants that impose additional constraints on the sheet to be formed, typically produce parts that closely approximate the intended CAD geometry with relatively simple toolpaths, at the cost of a more complex setup. A more in-depth comparison across the ISF variants is available in Table 11.
- Process simulation could be a powerful tool to avoid excessive iterative experimental toolpath optimization procedures, but the heavy computational load of these simulations remains a major constraint for systematic use of simulations in replacement of iterative experimental procedures. Modelling styles reducing the computational load also reduce the accuracy of the simulation results, although multi-layered shell elements offer a promising trade-off option in this context.

While this benchmark study has provided valuable insights into the performance of ISF, several paths remain open for future exploration. Notably, the absolute accuracy of parts produced with SPIF is still open for improvement: although various toolpath strategies have been quite intensively explored in terms of toolpath types and processing sequence, the opportunities offered by dimensional compensation, using simulation, prediction, or feedback procedures, were not intensively investigated in this study.

The scalability of ISF experiments proved not to be straightforward and remains a critical challenge. Experimental results across different workpiece scales have demonstrated non-trivial variations, underscoring the importance and understanding of scale effects. An in-depth study of scale laws could facilitate more efficient use of small-scale experiments for optimizing process plans, ultimately contributing to more robust and cost-effective industrial applications.

Furthermore, the development of systematic, multi-stage process plans for complex and hard-to-form geometries, as targeted in this benchmark study, highlights the need for advanced, knowledge-based support tools. Future work should focus on the creation of computer-aided process planning systems that contain expert knowledge. These tools should be capable of feature recognition, prediction of undesirable deformations, and the generation of adaptive toolpaths that incorporate known mitigation strategies for problematic regions. Such advancements are a challenging task, but could significantly enhance the industrial applicability of ISF.

Additionally, further research should investigate the influence of different setup configurations on process performance and outcomes. Understanding how these setups affect forming behavior and geometric accuracy could guide more effective equipment selection and the choice of toolpath strategies. Moreover, assessing the repeatability of results across dissimilar setups would provide valuable insights into process robustness and reliability, which are essential for industrial adoption.

Supplementary Information The online version contains supplementary material available at https://doi.org/10.1007/s12289-025-01928-1.

Acknowledgements The Benchmark 2024 committee thanks ESAFORM for the supporting Benchmark Grant and the opportunity to conduct this in-depth benchmark study, fostering expertise sharing, knowledge transfer and collaboration with ISF research groups worldwide. Marthe Vanhulst thanks the Research Foundation – Flanders (FWO) for her support as a Predoctoral Strategic Basic Research Fellow with project 1S47624N. The work of IBF of RWTH Aachen University on the development of the database and exchange platform, used for the benchmark, has been funded by the Deutsche Forschungsgemeinschaft (DFG, German Research Foundation) under Germany's Excellence Strategy – EXC-2023 Internet of Production – 390621612. The AGH University of Krakow acknowledges the support by the program "Excellence initiative—research university" and the statutory research financed by the Ministry of Science and Higher Education Poland, Grant No. 16.16.110.663. Prof. M. Beatriz Silva acknowledges Fundação para a Ciência e a Tecnologia (FCT) for its financial support via the project LAETA Base Funding (https://doi.org/10.54499/UIDB/50022/2020). Fraunhofer IWU was funded by the Federal Ministry of Economics and Climate Protection via the AiF and DLR as part of the program for the promotion of joint industrial research on the basis of a resolution of the German Bundestag and performed their work on the IGF project 22860 BG 'µRoboForm' in cooperation with the Deutsche Forschungsvereinigung für Mess-, Regelungs- und Systemtechnik (DFMRS).

The authors would like to express their gratitude to João P. G. Magrinho from University of Lisbon, Carlos Saraiva, Daniel Bento and Pedro Dias from MCG company, Meenashisundaram Ganesh Kumar from National University of Singapore, Prof. Verena Kräusel from Fraunhofer IWU, Prof. Till Clausmeyer from Chemnitz University of Technology, Alex Ouyang, Jamie Booth and Daisy Bradley from University of Sheffield and Daniel Cooper and Prof. Alan I. Taub from University of Michigan, who are not part of the author list but also contributed to this work.

Author contribution M.V., Y.L., D.S., K.P., L.M. and J.R.D. wrote the main manuscript text. M.V., Y.L. and D.S. overviewed collection and analysis of data. M.V. coordinated the project. All authors contributed in the experimental campaign and reviewed the manuscript.

Data availability The data supporting the findings of this study are available within the supplementary information files and on the ISF database platform (https://www.isf-exchange.com/).

Declarations

Conflict of interest The authors declare no competing interests.

References

1. Jeswiet J, Micari F, Hirt G, Bramley A, Duflou J, Allwood J (2005) Asymmetric single point incremental forming of sheet metal. CIRP Ann Manuf Technol 54(2):88–114. https://doi.org/10.1016/s0007-8506(07)60021-3
2. Duflou JR, Habraken AM, Cao J, et al (2018) Single point incremental forming: state-of-the-art and prospects. Int J Mater Form 11:743–773. https://doi.org/10.1007/s12289-017-1387-y
3. Hirt G, Bremen T, Bailly D, Vanhulst M, Vanhove H, Duflou JR (2023) Development of a collaborative online knowledge management system for incremental sheet forming. Mater Res Proceed 25:45–52. https://doi.org/10.21741/9781644902417-6
4. Guzmán CF, Gu J, Duflou J, Vanhove H, Flores P, Habraken AM (2012) Study of the geometrical inaccuracy on a SPIF two-slope pyramid by finite element simulations. Int J Solids Struct 49(25):3594–3604. https://doi.org/10.1016/j.ijsolstr.2012.07.016
5. Ajay and Mittal RK (2020) Incremental sheet forming technologies: Principles, Merits, limitations and applications (1st ed). CRC Press. https://doi.org/10.1201/9780429298905
6. Gatea S, Ou H, McCartney G (2016) Review on the influence of process parameters in incremental sheet forming. Int J Adv Manuf Technol 87(1):479–499. https://doi.org/10.1007/S00170-016-8426-6
7. Peng W, Ou H, Becker A (2019) Double-sided incremental forming: a review. ASME J Manuf Sci Eng 141(5):050802. https://doi.org/10.1115/1.4043173
8. Lu B et al (2015) Investigation of material deformation mechanism in double side incremental sheet forming. Int J Mach Tools Manuf 93:37–48. https://doi.org/10.1016/j.ijmachtools.2015.03.007
9. Brosius A (2014) Incremental forming - CIRP encyclopedia of production engineering. Springer, Berlin Heidelberg, Berlin. https://doi.org/10.1007/978-3-642-20617-7
10. Li J, Geng P, Shen J (2013) Numerical simulation and experimental investigation of multistage incremental sheet forming. Int J Adv Manuf Technol 68(9–12):2637–2644. https://doi.org/10.1007/s00170-013-4870-8
11. Zhang Z et al (2016) Springback reduction by annealing for incremental sheet forming. Procedia Manuf 5:696–706. https://doi.org/10.1016/j.promfg.2016.08.057
12. Patel D, Gandhi A (2022) A review article on process parameters affecting incremental sheet forming (ISF). Mater Today Proc 63:368–375. https://doi.org/10.1016/j.matpr.2022.03.208
13. Oleksik V, Pascu A, Deac C, Fleaca R, Roman M, Bologa O (2010) The influence of geometrical parameters on the incremental forming process for knee implants analyzed by numerical simulation. AIP Conf Proc 1252:1208–1215. https://doi.org/10.1063/1.3457520
14. Isidore BBL, Hussain G, Shamchi SP, Khan WA (2016) Prediction and control of pillow defect in single point incremental forming using numerical simulations. J Mech Sci Technol 30(5):2151–2161. https://doi.org/10.1007/s12206-016-0422-0
15. Yan Z et al (2021) Multistage tool path optimisation of single-point incremental forming process. Materials 14(22):6794. https://doi.org/10.3390/MA14226794
16. Hussain G, Gao L, Hayat N (2011) Forming parameters and forming defects in incremental forming of an aluminum sheet: correlation, empirical modeling, and optimization: part A. Mater Manuf Processes 26(12):1546–1553. https://doi.org/10.1080/10426914.2011.552017
17. Behera AK, Vanhove H, Lauwers B, Duflou JR (2011) Accuracy improvement in single point incremental forming through systematic study of feature interactions. Key Eng Mater 473:881–888. https://doi.org/10.4028/www.scientific.net/KEM.473.881
18. Beltran M, Malhotra R, Nelson AJ, Bhattacharya A, Reddy NV, Cao J (2013) Experimental study of failure modes and scaling effects in micro-incremental forming. J Micro Nanomanuf 1(3):1–15. https://doi.org/10.1115/1.4025098
19. Peter I, Fracchia E, Canale I, Maiorano R (2019) Incremental sheet forming for prototyping automotive modules. Procedia Manuf 32:50–58. https://doi.org/10.1016/j.promfg.2019.02.182
20. Montanari L, Cristino VA, Silva MB, Martins PAF (2013) A new approach for deformation history of material elements in hole-flanging produced by single point incremental forming. Int J Adv Manuf Technol 69(5–8):1175–1183. https://doi.org/10.1007/s00170-013-5117-4
21. Duflou JR, Callebaut B, Verbert J, De Baerdemaeker H (2008) Improved SPIF performance through dynamic local heating. Int J Mach Tools Manuf. https://doi.org/10.1016/j.ijmachtools.2007.08.010
22. Vanhove H, Gu J, Sol H, Duflou J (2011) Process window extension for incremental forming through optimal work plane rotation. Accessed: Jan. 02, 2024. [Online]. Available: https://researchportal.vub.be/en/publications/process-window-extension-for-incremental-forming-through-optimal
23. Duflou JR et al (2008) Process window enhancement for single point incremental forming through multi-step toolpaths. CIRP Ann Manuf Technol. https://doi.org/10.1016/j.cirp.2008.03.030
24. Ham M, Jeswiet J (2007) Forming limit curves in single point incremental forming. CIRP Ann Manuf Technol 56(1):277–280. https://doi.org/10.1016/j.cirp.2007.05.064
25. Li Y et al (2017) A review on the recent development of incremental sheet-forming process. Int J Adv Manuf Technol 92(5–8):2439–2462. https://doi.org/10.1007/s00170-017-0251-z
26. Sevšek L, Pepelnjak T (2024) Optimisation of flexible forming processes using multilayer perceptron artificial neural networks and genetic algorithms: a generalised approach for advanced high-strength steels. Materials 17(22):5459. https://doi.org/10.3390/MA17225459
27. Kim YH and Park JJ (2022) Effect of process parameters on formability in incremental forming of sheet metal. Accessed: Dec. 12, 2018. [Online]. Available: https://ac.els-cdn.com/S0924013602007884/1-s2.0-S0924013602007884-main.pdf?_

tid=9a8b1581-2c23-4855-bf26-07f8d8d86f5b&acdnat=1544630324_db8d71de973b0f2841207d0b14f83234
28. Mirnia MJ, Dariani BM (2012) Analysis of incremental sheet metal forming using the upper-bound approach. Proc Inst Mech Eng B J Eng Manuf 226(8):1309–1320. https://doi.org/10.1177/0954405412445113
29. Echrif SBM, Hrairi M (2014) Significant parameters for the surface roughness in incremental forming process. Mater Manuf Processes 29(6):697–703. https://doi.org/10.1080/10426914.2014.901519
30. Li Y, Liu Z, Daniel WJT, Meehan PA (2014) Simulation and experimental observations of effect of different contact interfaces on the incremental sheet forming process. Mater Manuf Processes 29(2):121–128. https://doi.org/10.1080/10426914.2013.822977
31. Ben Said L (2022) The incremental sheet forming; technology, modeling and formability: a brief review. Proceed Inst Mech Eng Part E: J Process Mech Eng 236(6):2729–2755. https://doi.org/10.1177/09544089221093306
32. Fiorentino A, Ceretti E, Attanasio A, Mazzoni L, Giardini C (2009) Analysis of forces, accuracy and formability in positive die sheet incremental forming. Int J Mater Form 2(SUPPL. 1):805–808. https://doi.org/10.1007/S12289-009-0467-Z/METRICS
33. Malhotra R, Xue L, Belytschko T, Cao J (2012) Mechanics of fracture in single point incremental forming. J Mater Process Tech 212(7):1573–1590. https://doi.org/10.1016/j.jmatprotec.2012.02.021
34. Radu MC, Cristea I (2013) Processing metal sheets by SPIF and analysis of parts quality. Mater Manuf Processes 28(3):287–293. https://doi.org/10.1080/10426914.2012.746702
35. Honarpisheh M, Abdolhoseini MJ, Amini S (2016) Experimental and numerical investigation of the hot incremental forming of Ti-6Al-4V sheet using electrical current. Int J Adv Manuf Technol 83(9–12):2027–2037. https://doi.org/10.1007/S00170-015-7717-7/METRICS
36. Attanasio A, Ceretti E, Giardini C (2006) Optimization of tool path in two points incremental forming. J Mater Process Technol 177(1–3):409–412. https://doi.org/10.1016/j.jmatprotec.2006.04.047
37. Kumar A (2024) Critical state-of-the-art literature review of surface roughness in incremental sheet forming: a comparative analysis. Appl Surface Sci Adv 23:100625. https://doi.org/10.1016/j.apsadv.2024.100625
38. Van Sy L, Thanh Nam N (2013) Hot incremental forming of magnesium and aluminum alloy sheets by using direct heating system. Proceed Inst Mech Eng Part B: J Eng Manuf 227(8):1099–1110. https://doi.org/10.1177/0954405413484014
39. Vanhove H, Mohammadi A, Guo Y, Duflou JR (2014) High-speed single point incremental forming of an automotive aluminium alloy. Key Eng Mater 622–623:433–439. https://doi.org/10.4028/WWW.SCIENTIFIC.NET/KEM.622-623.433
40. Bârsan A, Popp MO, Rusu GP, Maroșan AI (2021) Robot-based incremental sheet forming–the tool path planning. IOP Conf Ser: Mater Sci Eng 1009:012004. https://doi.org/10.1088/1757-899X/1009/1/012004
41. Carette Y, Vanhove H, Duflou J (2019) Multi-step incremental forming using local feature based toolpaths. Procedia Manuf 29:28–35. https://doi.org/10.1016/J.PROMFG.2019.02.102
42. Lu B, Chen J, Ou H, Cao J (2013) Feature-based tool path generation approach for incremental sheet forming process. J Mater Process Technol 213(7):1221–1233. https://doi.org/10.1016/j.jmatprotec.2013.01.023
43. Bremen T, Bailly DB (2024) On the influence of wave-shaped tool path strategies on geometric accuracy in incremental sheet forming. J Mater Process Technol 8:27. https://doi.org/10.3390/jmmp8010027
44. Lu B et al (2014) Mechanism investigation of friction-related effects in single point incremental forming using a developed oblique roller-ball tool. Int J Mach Tools Manuf 85:14–29. https://doi.org/10.1016/j.ijmachtools.2014.04.007
45. Said LB, Mars J, Wali M, Dammak F (2016) Effects of the tool path strategies on incremental sheet metal forming process. Mech Ind 17(4):411. https://doi.org/10.1051/meca/2015094
46. Tanaka S, Hayakawa K, Nakamura T (2011) Incremental sheet forming with direction control of path planes. Special Edition: 10th International Conference on Technology of Plasticity. pp 503–507
47. Bambach M, Taleb Araghi B, Hirt G (2009) Strategies to improve the geometric accuracy in asymmetric single point incremental forming. Prod Eng 3(2):145–156. https://doi.org/10.1007/s11740-009-0150-8
48. Carette Y, Vanhulst M, Duflou JR (2021) Geometry compensation methods for increasing the accuracy of the spif process. Key Eng Mater 883 KEM:217–224. https://doi.org/10.4028/www.scientific.net/KEM.883.217
49. Khan MS et al (2015) An intelligent process model: predicting springback in single point incremental forming. Int J Adv Manuf Technol 76:2071–2082. https://doi.org/10.1007/s00170-014-6431-1
50. Behera AK, Verbert J, Lauwers B, Duflou JR (2013) Tool path compensation strategies for single point incremental sheet forming using multivariate adaptive regression splines. Comput Aided Des 45(3):575–590. https://doi.org/10.1016/j.cad.2012.10.045
51. Ren H, Xie J, Liao S, Leem D, Ehmann K, Cao J (2019) In-situ springback compensation in incremental sheet forming. CIRP Ann 68(1):317–320. https://doi.org/10.1016/j.cirp.2019.04.042
52. Möllensiep D, Kulessa P, Thyssen L, Kuhlenkötter B (2020) Regression-based compensation of part inaccuracies in incremental sheet forming at elevated temperatures. Int J Adv Manuf Technol 109(7–8):1917–1928. https://doi.org/10.1007/S00170-020-05625-Y/TABLES/9
53. Carette Y, Duflou JR (2022) Mastering the complexity of incremental forming: geometry-based accuracy prediction using machine learning. Eng Proceed 26(1):12. https://doi.org/10.3390/ENGPROC2022026012
54. Praveen K, Lingam R, Reddy NV (2020) Tool path design system to enhance accuracy during double sided incremental forming: an analytical model to predict compensations for small/large components. J Manuf Process 58:510–523. https://doi.org/10.1016/j.jmapro.2020.08.014
55. Bonnardot C, Malécot P, Thibaud S (2020) Shape accuracy improvement obtained by μ-SPIF by tool path compensation. Procedia Manuf 47:1399–1402. https://doi.org/10.1016/j.promfg.2020.04.293
56. Vanhulst M, Waumans S, Vanhove H, Duflou JR (2024) Investigating intermediate shapes for multi-stage forming of cranial implants. J Manuf Process 127:1–8. https://doi.org/10.1016/J.JMAPRO.2024.07.126
57. Verbert J et al (2008) Multi-Step toolpath approach to overcome forming limitations in single point incremental forming. IntJ Mater Form 1(S1):1203–1206. https://doi.org/10.1007/s12289-008-0157-2
58. Liu Z, Li Y, Meehan PA (2013) Vertical wall formation and material flow control for incremental sheet forming by revisiting multistage deformation path strategies. Mater Manuf Processes 28(5):562–571. https://doi.org/10.1080/10426914.2013.763964
59. Suresh K, Nasih HR, Jasti NVK, Dwivedy M (2017) Experimental studies in multi stage incremental forming of steel sheets.

Mater Today Proc 4(2):4116–4122. https://doi.org/10.1016/j.matpr.2017.02.316
60. Buffa G, Gucciardi M, Fratini L, Micari F (2020) Multi-directional vs. mono-directional multi-step strategies for single point incremental forming of non-axisymmetric components. J Manuf Process 55:22–30. https://doi.org/10.1016/j.jmapro.2020.03.055
61. Gonzalez MM, Lutes NA, Fischer JD, Woodside MR, Bristow DA, Landers RG (2019) Analysis of geometric accuracy and thickness reduction in multistage incremental sheet forming using digital image correlation. Procedia Manuf 34:950–960. https://doi.org/10.1016/j.promfg.2019.06.105
62. Mirnia MJ, Mollaei Dariani B, Vanhove H, Duflou JR (2014) Thickness improvement in single point incremental forming deduced by sequential limit analysis. Int J Adv Manuf Tech 70:2029–2041. https://doi.org/10.1007/S00170-013-5447-2
63. Skjødt M, Bay N, Endelt B, Ingarao G (2008) multi stage strategies for single point incremental forming of a cup. Int J Mater Form 1:1199–1202. https://doi.org/10.1007/S12289-008-0156-3
64. Tanaka S (2018) Incremental sheet metal formed square-cup obtained through multi-stepped process. Procedia Manuf 15:1170–1176. https://doi.org/10.1016/J.PROMFG.2018.07.372
65. Gupta P, Szekeres A, Jeswiet J (2019) Design and development of an aerospace component with single-point incremental forming. Int J Adv Manuf Technol 103(9–12):3683–3702. https://doi.org/10.1007/s00170-019-03622-4
66. Li J, Shen J, Wang B (2013) A multipass incremental sheet forming strategy of a car taillight bracket. Int J Adv Manuf Technol 69(9–12):2229–2236. https://doi.org/10.1007/S00170-013-5179-3/METRICS
67. Duflou JR, Behera AK, Vanhove H, Bertol LS (2013) Manufacture of accurate titanium cranio-facial implants with high forming angle using single point incremental forming. Key Eng Mater 549:223–230. https://doi.org/10.4028/www.scientific.net/KEM.549.223
68. Behera AK, Lauwers B, Duflou JR (2015) Tool path generation for single point incremental forming using intelligent sequencing and multi-step mesh morphing techniques. IntJ Mater Form 8(4):517–532. https://doi.org/10.1007/S12289-014-1174-Y/FIGURES/19
69. Dai P, Chang Z, Li M, Chen J (2019) Reduction of geometric deviation by multi-pass incremental forming combined with tool path compensation for non-axisymmetric aluminum alloy component with stepped feature. Int J Adv Manuf Technol 102(1–4):809–817. https://doi.org/10.1007/s00170-018-3194-0
70. Malhotra R, Bhattacharya A, Kumar A, Reddy NV, Cao J (2011) A new methodology for multi-pass single point incremental forming with mixed toolpaths. CIRP annals 60(1):323–326. https://doi.org/10.1016/J.CIRP.2011.03.145
71. Yanagimoto J, Banabic D, Banu M, Madej L (2022) Simulation of metal forming – visualization of invisible phenomena in the digital era. CIRP Ann 71(2):599–622. https://doi.org/10.1016/j.cirp.2022.05.007
72. Surech K, Regalla SP (2014) Effect of time scaling and mass scaling in numerical simulation of incremental forming. Applied Mechanics and Materials 612:105–110. Trans Tech Publications, Ltd. https://doi.org/10.4028/www.scientific.net/AMM.612.105
73. Pepelnjak T, Sevšek L, Lužanin O, Milutinović M (2022) Finite element simplifications and simulation reliability in single point incremental forming. Materials 15(10):3707. https://doi.org/10.3390/ma15103707
74. Li Y, Daniel WJT, Meehan PA (2017) Deformation analysis in single-point incremental forming through finite element simulation. Int J Adv Manuf Technol 88(1–4):255–267. https://doi.org/10.1007/s00170-016-8727-9
75. Robert C, Dal Santo P, Delamézière A, Potiron A, Batoz JL (2008) On some computational aspects for incremental sheet metal forming simulations. IntJ Mater Form 1(SUPPL. 1):1195–1198. https://doi.org/10.1007/s12289-008-0155-4
76. Yue ZM, Chu XR, Gao J (2017) Numerical simulation of incremental sheet forming with considering yield surface distortion. Int J Adv Manuf Technol 92(5–8):1761–1768. https://doi.org/10.1007/s00170-017-0269-2
77. Esmaeilpour R, Kim H, Park T, Pourboghrat F, Mohammed B (2017) Comparison of 3D yield functions for finite element simulation of single point incremental forming (SPIF) of aluminum 7075. Int J Mech Sci 133:544–554. https://doi.org/10.1016/J.IJMECSCI.2017.09.019
78. Hirt G, Ames J, Bambach M, Kopp R, Kopp R (2004) Forming strategies and process modelling for CNC incremental sheet forming. CIRP Ann 53(1):203–206. https://doi.org/10.1016/S0007-8506(07)60679-9
79. Ayed LB, Robert C, Delamézière A, Nouari M, Batoz JL (2014) Simplified numerical approach for incremental sheet metal forming process. Eng Struct 62:75–86. https://doi.org/10.1016/J.ENGSTRUCT.2014.01.033
80. Henrard C et al (2011) Forming forces in single point incremental forming: prediction by finite element simulations, validation and sensitivity. Comput Mech 47(5):573–590. https://doi.org/10.1007/s00466-010-0563-4
81. Bouffioux C et al (2011) Experimental and numerical study of an AlMgSc sheet formed by an incremental process. J Mater Process Technol 211(11):1684–1693. https://doi.org/10.1016/J.JMATPROTEC.2011.05.010
82. Eyckens P et al (2011) Strain evolution in the single point incremental forming process: digital image correlation measurement and finite element prediction. IntJ Mater Form 4(1):55–71. https://doi.org/10.1007/s12289-010-0995-6
83. Malhotra R, Huang Y, Xue L, Cao J, Belytschko T (2010) An investigation on the accuracy of numerical simulations for single point incremental forming with continuum elements. AIP Conf Proc 1252(1):221–227. https://doi.org/10.1063/1.3457555
84. Flores P et al (2007) Model identification and FE simulations: effect of different yield loci and hardening laws in sheet forming. Int J Plast 23: 420–449. Accessed: Dec. 02, 2024. [Online]. Available: https://lirias.kuleuven.be/1092108
85. De Sena JIV et al (2016) Simulation of a two-slope pyramid made by spif using an adaptive remeshing method with solid-shell finite element. Int J Mater Form 9:383–394. https://doi.org/10.1007/s12289-014-1213-8
86. Elford M, Saha P, Seong D, Haque MD, Yoon JW (2013) Benchmark 3 - incremental sheet forming. AIP Conf Proc 1567:227–261. https://doi.org/10.1063/1.4849983
87. Hill R (1948) A theory of the yielding and plastic flow of anisotropic metals. Royal Soc. https://doi.org/10.1098/RSPA.1948.0045
88. Barlat F, Aretz H, Yoon JW, Karabin ME, Brem JC, Dick RE (2005) Linear transfomation-based anisotropic yield functions. Int J Plast 21(5):1009–1039. https://doi.org/10.1016/j.ijplas.2004.06.004
89. Esmaeilpour R et al (2018) Calibration of Barlat Yld 2004–18P yield function using CPFEM and 3D RVE for the simulation of single point incremental forming (SPIF) of 7075-O aluminum sheet. Int J Mech Sci 145:24–41. https://doi.org/10.1016/J.IJMECSCI.2018.05.015
90. Betaieb E et al (2024) Influence of the identification procedures of the material model in accurate prediction of incremental sheet forming forces. Proceedings of the 14th international conference on the technology of plasticity - current trends in the technology of plasticity. pp 591–602. https://doi.org/10.1007/978-3-031-40920-2_61

91. Hockett JE, Sherby OD (1975) Large strain deformation of polycrystalline metals at low homologous temperatures. J Mech Phys Solids 23(2):87–98
92. Lievers WB, Pilkey AK, Lloyd DJ (2004) Using incremental forming to calibrate a void nucleation model for automotive aluminum sheet alloys. Acta Mater 52(10):3001–3007. https://doi.org/10.1016/j.actamat.2004.03.002
93. Belchior J, Guillo M, Courteille E, Maurine P, Leotoing L, Guines D (2013) Off-line compensation of the tool path deviations on robotic machining: application to incremental sheet forming. Robot Comput Integr Manuf 29(4):58–69. https://doi.org/10.1016/j.rcim.2012.10.008
94. Seong DY, Haque MZ, Kim JB, Stoughton TB, Yoon JW (2014) Suppression of necking in incremental sheet forming. Int J Solids Struct 51(15–16):2840–2849. https://doi.org/10.1016/j.ijsolstr.2014.04.007
95. Lee HR, Lee MG, Park N (2023) Effect of evolutionary anisotropic hardening on the prediction of deformation and forming load in incremental sheet forming simulation. Thin-Walled Struct 193:111231. https://doi.org/10.1016/j.tws.2023.111231
96. Esmaeilpour R, Kim H, Park T, Pourboghrat F, Agha A, Abu-Farha F (2020) Effect of hardening law and process parameters on finite element simulation of single point incremental forming (SPIF) of 7075 aluminum alloy sheet. Mech Ind 21(3):302. https://doi.org/10.1051/meca/2020019
97. Duchêne L, Guzmán CF, Behera AK, Duflou JR, Habraken AM (2013) Numerical simulation of a pyramid steel sheet formed by single point incremental forming using solid-shell finite elements. Key Eng Mater 549:180–188. https://doi.org/10.4028/www.scientific.net/KEM.549.180
98. Tuninetti V, Yuan S, Gilles G, Guzmán CF, Habraken AM, Duchêne L (2016) Modeling the ductile fracture and the plastic anisotropy of DC01 steel at room temperature and low strain rates. J Phys Conf Ser 734:032075. https://doi.org/10.1088/1742-6596/734/3/032075
99. Hadoush A, van den Boogaard AH (2008) Time reduction in implicit single point incremental sheet forming simulation by refinement - derefinement. Int J Mater Form 1(1):1167–1170
100. Lequesne C, Henrard C, Bouffioux C, Duflou J, Habraken AM (2008) Adaptive remeshing for incremental forming simulations. Proceedings of the 7th international conference and workshop on numerical simulation of 3D sheet metal forming processes 7:399–403
101. Hussain G, Lin G, Hayat N (2011) Improving profile accuracy in SPIF process through statistical optimization of forming parameters. J Mech Sci Technol 25(1):177–182. https://doi.org/10.1007/s12206-010-1018-8
102. Hussain G, Al-Ghamdi KA, Khalatbari H, Iqbal A, Hashemipour M (2014) Forming parameters and forming defects in incremental forming process: Part b. Mater Manuf Processes 29(4):454–460. https://doi.org/10.1080/10426914.2014.880457
103. Simoncelli A, Buglioni L, Martínez Krahmer D, Sánchez Egea A (2025) Effects of machine compliance on forming accuracy and forces in SPIF of AISI 430. Int J Adv Manuf Tech 1–14. https://doi.org/10.1007/s00170-025-15854-8
104. Maqbool F et al (2021) Targeted residual stress generation in single and two point incremental sheet forming (ISF). Arch Appl Mech 91(8):3465–3487. https://doi.org/10.1007/s00419-021-01935-z
105. Wang C, Daniel WJT, Lu H, Liu S, Meehan PA (2017) FEM investigation of ductile fracture prediction in two-point incremental sheet metal forming process. Procedia Eng 207:836–841. https://doi.org/10.1016/j.proeng.2017.10.838
106. Peng W, Ou H (2023) Deformation mechanisms and fracture in tension under cyclic bending plus compression, single point and double-sided incremental sheet forming processes. Int J Mach Tools Manuf 184:103980. https://doi.org/10.1016/j.ijmachtools.2022.103980
107. Zhao X, Ou H (2024) A new hybrid stretch forming and double-layer two-point incremental sheet forming process. J Market Res 30(April):3485–3509. https://doi.org/10.1016/j.jmrt.2024.04.093
108. Habraken AM et al (2022) Analysis of ESAFORM 2021 cup drawing benchmark of an Al alloy, critical factors for accuracy and efficiency of FE simulations. IntJ Mater Form 15(5):1–96. https://doi.org/10.1007/S12289-022-01672-W/FIGURES/6
109. Volk W et al (2019) CIRP annals - manufacturing technology models and modelling for process limits in metal forming. CIRP Ann Manuf Technol 68(2):775–798. https://doi.org/10.1016/j.cirp.2019.05.007
110. van den Boogaard T, Havinga J, Belin A, Barlat F (2016) Parameter reduction for the Yld 2004–18p yield criterion. IntJ Mater Form 9(2):175–178. https://doi.org/10.1007/S12289-015-1221-3/FIGURES/1
111. Swift HW (1952) Plastic instability under plane stress. J Mech Phys Solids 1(1):1–18. https://doi.org/10.1016/0022-5096(52)90002-1
112. Duflou JR et al (2018) Single point incremental forming: state-of-the-art and prospects. IntJ Mater Form 11(6):743–773. https://doi.org/10.1007/S12289-017-1387-Y

Authors and Affiliations

Marthe Vanhulst[1] · Youngrok Lee[2] · Dennis Steinfels[3] · Thomas Bremen[3] · Konrad Perzyński[4] · Hans Vanhove[1] · Giuseppina Ambrogio[5] · Radu-Eugen Breaz[6] · Gianluca Buffa[7] · Romina Conte[5] · Liugi De Napoli[5] · Livan Fratini[7] · Xiao Da Terrence Fu[9] · Francesco Gagliardi[5] · Margarida Gralha[10] · Putong Kang[8] · Łukasz Kuczek[11] · A. Senthil Kumar[9] · Andreas Kunke[12] · André Leonhardt[12] · Yanle Li[13] · Zhuoer Li[2] · Roberto Licari[7] · Hui Long[14] · Darren Wei Wen Low[9] · Sever-Gabriel Racz[6] · Peter Scholz[15] · M. Beatriz Silva[10] · Shaoqi Song[13] · Dieter Weise[15] · Krzysztof Żaba[11] · Hui Zhu[14] · David Bailly[3] · Mihaela Banu[2] · Lukasz Madej[4] · Joost R. Duflou[1]

✉ Joost R. Duflou
joost.duflou@kuleuven.be

[1] Department of Mechanical Engineering, KU Leuven/ Flanders Make, Celestijnenlaan 300B, 3001 Leuven, Belgium

[2] Department of Mechanical Engineering, University of Michigan, 2350 Hayward Street, Ann Arbor, MI 48109, USA

[3] Institute of Metal Forming (IBF), RWTH Aachen University, Intzestr. 10, 52072 Aachen, Germany

[4] Faculty of Metals Engineering and Industrial Computer Science, AGH University of Krakow, Mickiewicza 30 Av. 30-59, Krakow, Poland

[5] Department of Mechanical, Energy and Management Engineering (DIMEG), University of Calabria, Arcavacata Di Rende (CS), 87036 Calabria, Italy

[6] Department of Industrial Machines and Equipment, Lucian Blaga University of Sibiu, Victoriei 10, Sibiu, Romania

[7] Department of Engineering, University of Palermo, Viale Delle Scienze, 90128 Palermo, Italy

[8] McCormick School of Engineering and Applied Science, Department of Mechanical Engineering, Northwestern University, 2145 Sheridan Road, Evanston, IL 60208, USA

[9] Department of Mechanical Engineering, National University of Singapore, 9 Engineering Drive 1, Block EA, Singapore 117576, Singapore

[10] IDMEC, Instituto Superior Técnico, University of Lisbon, Av. Rovisco Pais, 1, 1049-001 Lisbon, Portugal

[11] Faculty of Non-Ferrous Metals, AGH University of Krakow, Mickiewicza 30 Av. 30-059, Krakow, Poland

[12] Professorship Forming Technology, Chemnitz University of Technology, Reichenhainer Str. 70, 09126 Chemnitz, Germany

[13] School of Mechanical Engineering, Shandong University, Jinan 250061, People's Republic of China

[14] School of Mechanical, Aerospace and Civil Engineering, The University of Sheffield, Sheffield S1 3JD, UK

[15] Department of Sheet Metal Processing, Fraunhofer Institute for Machine Tools and Forming Technology IWU, Reichenhainer Str. 88, 09126 Chemnitz, Germany